AGSO

Landsat-5-Thematic Mapper spectral-lithological correlations, Northern Pilbara Craton, Western Australia

ANDREW Y. GLIKSON

RECORD 1998/22

AGSO

AUSTRALIAN
GEOLOGICAL SURVEY
ORGANISATION

AUSTRALIAN GEOLOGICAL SURVEY ORGANISATION
DEPARTMENT OF PRIMARY INDUSTRIES & ENERGY

AGSO RECORD 1998/22

Landsat-5-Thematic Mapper spectral-lithological correlations, Northern Pilbara Craton, Western Australia

ANDREW Y. GLIKSON

Minerals Division, Australian Geological Survey Organisation, GPO Box 378, Canberra, ACT 2601

CANBERRA 1998

Department of Primary Industries & Energy

Minister for Primary Industries & Energy: The Hon. J. Anderson, MP
Minister for Resources & Energy: Senator the Hon. W.R. Parer
Secretary: Ken Matthews

Australian Geological Survey Organisation

Executive Director: Neil Williams

ISSN 1039–0073
ISBN 0 642 27358 8

Bibliographic reference: Glikson A.Y., 1998. Landsat-5-Thematic Mapper spectral-lithological correlations, Northern Pilbara Craton, Western Australia. Australian Geological Survey Organisation, Record 1998/22

Contents

Figures

Abstract

This report documents the correlation of field-tested Landsat-5-Thematic Mapper multispectral 7-bands scanner data, and to a lesser extent gamma ray spectrometric data, with lithological and stratigraphic units in the northern Pilbara Craton, conducted as a part of the North Pilbara AGSO-GSWA NGMA project. Reflectance values and band ratios of a range of weathered surface types provide indirect diagnostic signatures for the underlying fresh rock types. Mean reflectance values for <36 pixel-large test areas, which consist of relatively uniform lithological surface types, yield distinct spectral profiles for different materials. Mathematical treatment of the spectral data, including band ratios, log residuals, principal components and directed principal components, combined with gamma ray spectrometer K-Th-U data, allow identification of several material types, including (1) clay and/or other hydrosilicates (OH molecule - high 5/7 band ratios); (2) carbonates, characterised by high 5/7 band ratio and distinguished from clay by principal component analysis; (3) iron oxide-rich weathering crusts of mafic igneous rocks and of laterite (high 5/4 and 3/2 band ratios), which can be distinguished from each other using principal component analysis; (4) plutonic granite-derived quartz and eroded abraded alluvial sediments (high combined 1+7 reflectance, as contrasted to clay or iron oxides); (5) chert and vein quartz, characterised by high 5/7 band ratio due to their contained water inclusions; (6) green vegetation (high 4/3 band ratios). The 2nd PC of the combined band ratio file [4/3;5/7] selects clay, hydrosilicates and carbonates and deselects green vegetation, due to the low correlation of 4/3-5/7 band ratios in clays and the high correlation of 4/3-5/7 band ratios in green vegetation. This results in negative expression of gum-fringed creeks which outline drainage patterns. The RGB algorithm pc2(4/3;5/7):5/4:1+7 combines the above criteria and enables interpolations of ground observations and ground navigation.

Combination of the above methods allow discrimination between several rock types characteristic of different stratigraphic units. For example (1) Tectonised early to mid-Archaean tholeiitic to high-Mg basalts (Warrawoona Group and Gorge Creek Group) are dominated by ferruginous weathering crusts (high 5/4 band ratios) whereas the little-deformed outliers of late Archaean Fortescue Group basalts - which include high-K basalts with high radiometric counts (Kylena Basalt) - display clay alteration (higher 5/7 band ratios); (2) Advanced alteration of tholeiitic to high-Mg basalts of the upper Warrawoona Group effects an increase in the 5/7 band ratios and in radiometric K-Th-U counts. Such alteration patterns in andesitic volcanics associated with Cu-Zn sulphide mineralisation in the Strelley area facilitate alteration mapping and exploration for base metals; (3) Progressive increase in the importance of K-rich rhyolites with higher stratigraphic levels in the Duffer Formation is manifest by the increase in radiometric counts; (4) Post-tectonic granitoids (Moolyella Granite, Cooglegong Granite, southern Corruna Downs batholith) display higher clay weathering (high 5/7) and low 1+7 reflectance due to clay coating of quartz.

The little-deformed late Archaean Fortescue Group and early Proterozoic Hamersley Group volcanic and sedimentary rocks of the Hamersley Basin and its outliers over the north Pilbara Craton are particularly amenable to spectral characterisation. These sequences, which unlike the older greenstones are of mostly pumpelyite-prehnite metamorphic facies and are less affected by the shearing and attendant silicification and carbonatisation which resulted in various degrees of lithological homogenisation of the older greenstones, can be mapped in great detail with the aid of enhanced Landsat-5-TM images. In view of the poor accessibility of large parts of the Hamersley Basin, this method allows rapid and accurate interpolation and extrapolation of field traverses.

Chapter 1. Introduction

The northern Pilbara Craton (Hickman, 1983) (Figs 1.1), constitutes an Archaean (3.5-2.7 Ga) greenstone-granite terrain exposed over an area about 50 000 km^2, and is fringed by the 2.77-2.45 Ga Hamersley Basin to the south, 2.77-1.8 Myr Patterson province to the east, and late Palaeozoic to Mesozoic Canning Basin to the north (Fig. 1.1). The age of the rocks, the good outcrop, the weathering crusts which enhance spectral contrasts render the Pilbara Craton ideal for correlations between remotely sensed data and a wide range of lithological characteristic. This report is concerned with a study of 7-band Landsat-5-TM multispectral image data, covering the visible to short wave infrared (Appendix 1). In some areas monochromatic Spot image data and 13-bands Geoscan Mark-I airborne scanner data (Honey and Daniels, 1987) were studied. The work was conducted as a part of the GSWA-AGSO North Pilbara NGMA project, which encompasses systematic 1:100 000 scale mapping and associated geophysical, structural, mineralisation, geochemical, and isotopic age studies.

The principal aim of the multispectral study was to identify suitable methods for lithological correlations relevant to the 1:100 000 geological mapping program. A directed principal components of band ratios method (DPCRM), specifically the algorithm RGB pc2[4/3;5/7]: 5/4: 1+7, has been identified as particularly suitable for the correlation of a wide range of surface materials as well as capable of delineating morphological drainage features (Glikson, 1997a,b). This study benefited from experience gained during earlier Landsat-5-TM correlations with a range of rock types and surface deposits in the western Musgrave Block, central Australia (Glikson and Creasey, 1995; Feeken, 1991, 1992). Discriminations allowed by this method include (1) separation of tholeiitic basalts and high-Mg to peridotitic komatiites within greenstone sequences; (2) separation of foliated mafic volcanics from and outliers of younger little-deformed basalts; (3) identification of felsic volcanic and sedimentary units within greenstone sequences; (4) identification of alteration zones within volcanics of the greenstone belts; (6) differentiation between intrusive units within granitic batholiths; (7) tracing of faults, shear zones and dykes; (8) identification of the composition and thereby the source of alluvial and creek bed deposits; (9) delineation of lateritic zones; (10) charting of calcrete deposits, with implications to ground water.

The following Landsat-5-TM scenes (185x185 km) were processed (Fig 1.1): Dampier (path 114 row 74); Yarraloola (p114r75); Roebourne (p113r74); Pyramid (p113r75); Port Hedland (p112r74); Marble Bar (p112r75); southern part of Yarrie (p111r74); Nullagine (p111r75). Gridding of these images to the Australian Metric Grid (AMG), using between 10 and 23 control points for each Landsat scene, was carried out by M. Peljo and P. Upward, AGSO, with RMS errors of <50 metres and in some instances sub-pixel (<30 m) errors. A series of enhanced image maps has been designed and released as both hard copies and as digital files. The data are also available as ERmapper bil-format data files (.ers file) and algorithms (.alg file) for processed Landsat scenes and for individual gridded 1:100 000 sheets, including location diagrams and explanatory surrounds (Glikson, 1997b).

Chapter 2. Methodology

The application of remotely sensed multispectral imagery to regional mapping of little-metamorphosed to greenschist facies metamorphic terrains, such as in the Pilbara Craton, utilizes the characteristic absorption/reflectance spectra of hydrosilicates (amphibole, mica, chlorite, serpentine), iron oxides and alteration and weathering products (clay minerals, carbonates, hydrated iron oxides). The varying proportions of these components in the weathering crusts provide diagnostic fingerprints of the primary lithologies. The remotely sensed data in the visible (VIS), near-infrared (NIR) and shortwave infrared (SWIR) range correlates with a range of surface materials, green vegetation and dry vegetation, and highlights fireburn/regrowth patterns (Simpson, 1978). The following correlations generally hold:

The visible range (bands 1-3). The high reflectance of OH molecule-bearing materials (clays, hydrosilicates, carbonates and fluid inclusion-rich silcrete and chert) and the strong absorption of iron oxide in the VIS range (bands 1-3), allow useful distinctions between materials of different clay/iron oxide proportions (Fig. 2.1). Coarse grained plutonic quartz reflects strongly in all spectral bands and can be identified by combination (addition) of bands 1+7, an effective discriminant from iron oxide and clay since only one of these bands is strongly reflected by these materials. The quartz and clay-rich weathering products of granitic rocks result in generally marked radiance of batholiths in the VIS range (Fig. 1.2). Clay-rich weathering crusts of felsic volcanics and felsic-derived sediments also display radiance in the VIS range. Mafic volcanic rocks, doleritic dykes and lateritic caps show strong absorption in the VIS range due to their iron oxide-rich composition (Fig. 2.1). Ultramafic rocks show high reflectance in the VIS range due to their chlorite and other Mg hydrosilicates-rich alteration products. Chert and silicified units show high radiance attributed tp the abundance of fluid inclusions. Banded iron formations (BIF) display an important clay signature due to the abundance of silt-rich inter-laminae which coat flat BIF slabs in the associated colluvium. Band 2 displays a small radiance peak compared to bands 1 and 3 for green vegetation (Fig. 2.1).

The infrared range (bands 4-5,7). The near-infrared (band 4) is characterized by strong radiance of green vegetation and to a lesser extent dry vegetation, and a fairly high radiance of clay and carbonates relative to iron oxides (Fig. 2.1). The short wave infrared (SWIR) range (bands 5 and 7) show high radiance of iron oxides, allowing the effective discrmination of ferruginous materials (mafic volcanics and hypabyssal intrusions, laterite) from clay-rich weathering crusts of felsic volcanic rocks and derived sediments.

The broad spectral windows of Landsat-5-TM bands allows only first order approximations of the finer spectral patterns within each pixel (Fig. 2.1). However, although the 30x30 metre pixel size of Landsat-5-TM images

(120x120 metre for the thermal band 6) exceeds the scale of individual outcrops, sub-pixel discriminations of spectrally distinct materials are discernable. This occurs where contiguous linear lithological units - such as =>10 metre thick dykes, sills, or layered units - straddle adjacent pixels. Smaller-scale absorption features may be identified by multispectral scanners such as MK-II (37 channels), Geris-band (69 channels) or Aviris (224 channels).

Comparisons between raw spectra, dark pixel-corrected spectra and field/laboratory measured end member spectra are complicated by differences in the conditions under which each spectral set has been scanned. For this reason, whereas comparisons of spectra *within* any particular dataset have a relative meaning, comparisons *between* different sets must take measurment conditions into account. A potential source of error are spectral variations related to differences in the grain size of otherwise similar materials, complicating direct correlations between laboratory-measured end members and remotely sensed pixel data.

Landsat-5-TM data are affected by (1) additive factors, including atmospheric path radiance and scatter, and (2) multiplicative factors, including atmospheric transmittance of solar radiation, solar illumination variations, reflected radiation at specific solar zenith, satellite nadir view angles and sensor gains. Ideally, calibration to compositionally uniform pixel consisting of field-measured material/s is required. In this procedure, relatively homogeneous pixels are selected, e.g. water, uniform green vegetation cover, exposures of monomineralic material or known uniform rock/weathering crust composition, and compared with available mineral or rock spectra. In practice, overall corrections can be applied which involve subtraction of these influences from the minimum-radiance pixel - ie. dark pixel subtraction (DPS). In this study, the DPS method coupled with empirical correlations between the spectral features of pixels and the usually heterogeneous ground materials are applied.

The need for calibration is reduced where band ratioing is applied, including log residuals and principal components of band ratio methods. These methods are relatively independent from overall atmospheric and gain corrections that apply uniformly to all the pixels and bands of any particular scene. This hinges on the uniformity of correction factors for different spectral bands within any individual scene scanned at a particular time. The log-residual enhancement procedure represents the within-scene relationships of the pixel data, namely for each spectral reading it represents the ratio of this DN value to the within-pixel 7 bands average DN value, to the between-pixel average DN value for the entire scene. Band ratio and log residual images are less affected by topographic shade component, which in-principle does not alter the within-pixel band ratios. On the other hand, the loss of the albedo brightness/shadow effect in band ratio images render them difficult to use in the field. Further, spectral mixing of components, such as dry vegetation and clay in the 5/7 BR, complicates correlations.

Image processing was conducted using both the IIS and ERmapper software. Radiance data were converted to reflectance values by means of the two following methods (1) DPS - namely subtraction in each band of the minimum pixel DN value in the entire scene, assuming that minimum DN values represent additive atmospheric scatter; (2) empirical comparisons of measured DN values with those of pixels consisting of known materials, and (3) pixel-unmixing and de-vegetation analysis (Bierwirth, 1990) which involves corrections for illumination, atmospheric transmittance, incidence/reflectance angles, global ground radiance, additive atmospheric scatter, sensor gains and sensor offset into account (Forster, 1984; Richards, 1986). The method uses band means and an inferred reflectance mean, and estimates the pixel reflectance (R) for any particular wavelength interval on the basis of corrections for dark pixel radiance, sensor gains and the average solar spectrum. Spectral-lithological fingerprinting were performed by examination of the average DN radiance values for sub-image training areas (<=36 pixel-large), representing relatively uniform lithological surface types as identified in the field. Mean reflectance values for selected training areas in the central Pilbara Craton are listed in Appendix 2 and plotted in Fig. 3.1.

Chapter 3. Landsat-5-TM spectral profiles

In this report the Marble Bar and Nullagine 1:250 000 Sheet areas (Fig 1.1) form the framework within which training pixels and test areas have been selected. The Soanesville-Tambourah area (119°2'-119°13'E; 21°24-21°33'S), mapped in part by the author in 1986, was selected for correlations between Landsat imagery with different rock units (Figs 4.1, 5.1, 6.1, 8.1-3). Other type areas include the Marble Bar-Camel Creek area (119°57'-120 25'E;21°2'-21°26'S) (Fig. 8.4-6) and Meentheena syncline area (21°12-21°31'S;120°13'-120°33'E) (Fig. 8.7-9). The mean spectra of 54 pixel groups from lithologically and stratigraphically distinct test pixels within the Central Pilbara block are listed in Appendix 2 and plotted in Fig. 3.1. In the following, the spectral features of ground-correlated test pixels are described:

3.1 Mafic and ultramafic rocks

Foliated meta-basalts of the Archaean Warrawoona Group show high 5/4 band ratios (BR) (mainly >2.4) and low 5/7 BRs (~1.3-1.7) compared to the little-deformed basalts of the Fortescue Group (5/4 ~ 2.0-3.1; 5/7 ~ 1.6-1.8), representing relatively high iron oxide and low clay in weathering surfaces of the older foliated basalts (Figs 3.3A). The 4/3 BR is generally higher in the younger Fortescue Group basalts, representing the relative abundance of green vegetation on the moisture-sustaining clay-high weathering surfaces of these volcanics (Fig. 3.2A). Carbonated meta-basalts of the Warrawoona Group show in some instances very high 5/7 BRs (Fig. 3.2A, 3.3A). As expected, clay-altered basalts of the Strelley succession (Gorge Creek Group) show high 5/7 BRs, while the less altered equivalents show lower 5/7 and higher 5/4 BRs (Fig. 3.3A). In the Sulphur Springs area altered clay-rich Strelley succession basalts contain numerous small sulphide-bearing gossans. This allows the detection of possibly mineralised sectors in the basalt through delineation of clay and vegetation-rich zones.

Gabbro sills and dykes correspond to the general range of basalts in terms of their 5/4 BRs (iron oxide) but tend to have high 5/7 BRs (clay), probably representing weathering of coarse grained plagioclase, as noted in weathering surfaces of gabbro in the Musgrave Block (Glikson and Creasey, 1995). Peridotitic ultramafic rocks show wide variations, with some units noted by high 5/7

BRs (1.8-2.0) and very low 5/4 BRs (1.4-1.6) of their weathering surfaces, which are dominated by Mg-hydrosilicates (Fig. 3.3A). The distinctions between mafic and ultramafic rocks are well represented on the 1+7:5/7:5/4 ternary diagram (Fig. 3.5A), where the iron oxide rich composition of weathering surfaces of Warrawoona Group basalts relative to Fortescue Group basalts, and the clay-rich composition of some ultramafic weathering crusts is evident. Overall positive relations pertain between the 5/4 and 3/2 BRs (Fig. 3.4A).

3.2 Felsic igneous rocks

The spectral features of felsic volcanic rocks, granitoid gneisses and post-kinematic adamellites are capable of being distinguished on Landsat-5-TM images. Felsic volcanic rocks of the Warrawoona Group and Fortescue Group display 5/7 BRs in the range of 1.8-2.3, and 5/4 BRs in the range of 1.6-1.9, while granitoids display a 5/7 BR range of 1.7-1.8 and 5/4 BR range of 1.7-1.85, due to enhanced clay alteration of the felsic volcanics and relative iron oxide enrichment on weathering surfaces of the granitoids (Fig. 3.3B). However, differentiated post-kinematic adamellites, represented by the Cooglegong Granite and to a much lesser extent by the Strelley Granite, show higher 5/7 BRs than older foliated granodiorite gneiss. This may be attributed to the lesser stability of K-feldspar and its greater alteration to clay. Little or no variation in vegetation is observed between these granitoids. The foliated gneiss display higher 1+7 band total reflectances than felsic volcanics, as shown on the ternary 1+7:5/7:5/4 diagram (Fig. 3.5B), representing the high total reflectance of coarse-grained quartz of the gneisses. Post-kinematic granitoids are distinct from both foliated gneisses and felsic volcanics due to their low total 1+7 DN values relative to the gneisses and low 5/7 BR relative to the volcanics (Fig. 3.5B).

3.3 Clastic sediments

The spectral features of Archaean sandstones and Fortescue Group sandstones overlap within the 5/7 BR range of 1.9-2.1 and a wider 5/4 BR range of 1.6-2.2 (Figs 3.3C, 3.4C, 3.5C). As represented on the ternary plot 1+7:5/7:5/4, Fortescue Group sandstones show somewhat higher reflecance values, represented by higher total 1+7 band totals (Fig. 3.5C), probably related to the higher contents of plutonic quartz in these sediments as compared to older feldspathic sandstones and greywackes. Recent alluvial sands, notably in creek beds, show very high total 1+7 DN values (Fig. 3.5C), due to high content of coarse grained detrital quartz, and commonly show high 5/4 ratios. By contrast, siltstones have the lowest total reflectance values (Fig. 3.5C). Laterites show uniquely high 5/4 BRs (>3.0) and high 5/7 BRs (≥2.3), in accord with their high iron oxide and clay abundance (Figs 3.3C, 3.5C).

3.4 Chemical sediments

Banded iron formations (BIF) display low 5/7 BRs (1.5-1.75) relative to sandstones, moderate to high 5/4 BRs (1.65-2.45) and high 3/2 BRs (1.8-2.3). However, in many instances the dominant reflectance of BIF is in the high 5/7 BRs due to the abundance of siltstone intercalations, the well layered structure of the BIF and the abundance of flat-lying silt-coated flaggy scree around outcrops. Cherts display a wide variation (Appendix 2), attributed to the rugged and broken, an therefore heterogeneous, nature of narrow ridge outcrops. The common dominance of high 5/7 BRs is thought to represent the abundance of water inclusions in cherts and thereby adsrbtion in the short wave-infrared range (band 7). Sedimentary carbonates, represented by the Carawine Dolomite, show spectral features intermediate between those of BIF and sandstone (Fig. 3.3C). Calcrete crusts display very high 5/7 BRs, attributed in part to their water inclusion contents.

3.5 Green vegetation

Two pixel groups were measured were the density of green vegetation was observed to be over 90 percent: (1) dense river gums along the Coongan River, Marble Bar area, and (2) dense green shrubs in a creek junction, Chinaman Creek, west of Marble Bar. In the first area the 4/3 BR is high (1.56) and in the second very high (1.77, 1.91) relative to other materials (Appendix 2).

3.6 Significance of the short wave infrared radiation (Landsat-5-TM band 6)

Correlations of the thermal signature allowed by band 6 of Landsat-5-TM (thermal infrared 10.4-12.5 μ) suffer from spurious variations in reflectance due to temperature differences effected by moisture in the atmosphere, rocks, soils and vegetation. Correlation of single pixels or small groups of pixels are complicated by the larger pixel size (120x120 m) of band 6 readings. However, under the dry conditions of inland Australia, the variations locally correlate with blackbody thermal radiation. In principle the stronger the absorption of materials in the visible and near-infrared bands the stronger the radiation in the thermal infrared band 6 This is generally supported by the relationships between the 5/4 BR, 5/7 BR and thermal radiance in band 6. Thus, iron oxide-rich weathering crusts and laterites (high 5/4 and 3/2 BRs) display relatively high radiation in the thermal band. By contrast, due to their strong reflectance in the visible and near-infrared bands (high 5/7 BRs), and possibly the cooling effect of their combined water molecules, clays are characterized by relatively low thermal infrared radiation in band 6. This effect is enhanced by the general tendency toward richer vegetation on clay-high material (Fig. 3.2), which lowers thermal radiation due to the evaporation effect.

The above considerations are generally supported by thermal infrared radiation values of test areas. The mean band 6 reflectance values (MR) and mean log residual (LR) values of lithologically relatively uniform test areas, in declining order of the mean values (MR), are as folows (values in DN)

1. Laterites - mean of 2 test areas: 18MR, 48LR;
2. Banded ironstones of the Brockman Iron Formation (17MR) and the Marra Mamba Member of the Hamesley Group (15MR). The base of the both formations is characterised by very high band 6 log residual values (57LR), thought to be related to the generally low reflectance values in the visible, near infrared and short wave infrared (Appendix 3.L);
3. Warrawoona Group basalts - mean of 8 test areas: 16MR, 38LR;
4. Deformed felsic volcanics - mean of 8 test areas: 15MR, 31LR;
5. Peridotites - mean of 4 test areas: 14MR, 36LR;
6. Granitoids - mean of 14 test areas: 14MR, 26LR;

7. Ferruginous siltstones - mean of 2 test areas: 13MR, 41LR;
8. Deformed Archaean sandstones - mean of 6 test areas: 13MR, 32LR;
9. Siltstone/banded iron formations - mean of 6 test areas: 13MR, 28LR;
10. Gabbro sills (plagioclase-rich) - mean of 5 test areas: 13MR, 27LR;
11. Little deformed Fortescue Group sandstones - mean of 8 test areas: 13MR, 25LR;
12. Forescue basalts - mean of 14 test areas: 12MR, 29LR;
13. Dolerite dykes - mean of 2 test areas: 10MR, 39LR;
14. Carbonated ultramafics - mean of 4 test areas: 10MR, 24LR;
15. Little-deformed Fortescue felsic volcanics - mean of 4 test areas: 9MR, 23LR;
16. Sedimentary carbonates - mean of 2 test areas: 8MR, 20LR.

The high band 6 radiance of Warrawoona Group basalts relative to Fortescue Group basalts is consistent with the higher iron oxide contents of weathering crusts of the former (Appendix 2; Figs 3.3). The thermal radiance of clay-altered basalts can be significancly less than the ferruginous-crusted basalts (Appendix 2.B), with implications to the identification of clay-altered mineralised volcanic rocks. The relatively high thermal infrared radiance of peridotites, which have high 5/7 BR (Appendix 2), suggests that the magnesian phyllosilicates which dominate the weathering surfaces of these rocks are mixed with fine grained iron oxides. By contrast, carbonated ultramafics and sedimentary carbonates show significantly lower thermal radiation. The relatively high thermal infrared radiance of felsic igneous rocks is probably related to their ferruginous weathering crusts. The moderate thermal radiance of hypabyssal gabbro and of sandstones is attributable to the disintegration of feldspar into clay minerals. Field spectometer measurements of the weathering crusts are required in order to test these relationships further.

Band combination 1+7. Since the expression of clay hinges on strong reflectance in the visible bands and absorption in the near-infrared bands, whereas the reverse applies to iron oxides, high combined reflecance in the visible and near-infrared is diagnostic of materials such as quartz, cherts, silcrete and calcrete. However, plutonic quartz in granites and derived alluvial deposits can be distinguished from fine grained silica and carbonates thanks to the general abundance of water inclusions in the latter and thereby their high 5/7 band ratios (Fig. 3.7).

Chapter 4. Log residual images

Log residual (LR) images (Green and Craig, 1985) help to identify the significance of any single within-pixel reflectance value (R_{bp}), which is normalised through its division by the within-pixel mean value (R_{bmp}), further divided by the mean of the multispectral radiance of the entire image or subimage (R_{mmi}):

$$\text{LR DN value} = R_{bp} / R_{bmp} / R_{mmi}$$

This normalization procedure cancels out multiplicative effects such as atmospheric adsorption, solar illumination and sensor gains which effect all the pixels of any particular scene. Furthermore, the log residual procedure identifies an albedo/shade component as a separate band, which can be subsequently recombined with spectral LR bands in order to enhance topography and structure. Inverted log residuals (ILR) assign high DN values to absorption features. Thus, clays and/or carbonates are represented by either high LR-1 values or high ILR-7 values, green vegetation is represented by high LR-4 values or by high ILR-3 values, and iron oxides are represented either by high LR-7 values or by high ILR-1 values. In the present study the log residual digital number values (LRDN) of lithologically relatively uniform training areas (Appendix 3) were calculated and were used to examine the significance and correlations made for non-normalised spectral data (section 3).

4.1 Single log residual (LR) band images

LR1 (Fig. 4.1A) - The effect of hydrosilicates and carbonates is enhanced in this band. Chlorite and other hydromagnesian silicates are strongly expressed in LR1 (log residual of band 1), as manifested for example in peridotite units of the composite Soanesville sill [SP] (Fig. 4.1A). Deformed carbonated (magnesite-coated) ultramafic rocks [CU] located along the faulted western contact of the Soanesville greenstone belt are likewise expressed strongly in LR1. Sericitic phyllites (meta-siltstones)[SP] north of the Tambina Granite [TG] and arkosic sandstones such as a Llala Rookh Sandstone outlier west of the Tambina Granite [LR] are well manifest in LR1. A criss-cross of high-DN LR1 zones coincide with clay and carbonate alteration commonly related to faults, cf. west Soanesville fault - [SF]. Patchy high-LR1 distribution represents heterogeneous clay and carbonate alteration, clay pans and calcrete deposits along creeks [CA] and gullies. Low-LR1 zones commonly correspond to granitoids [TG], winnowed alluvial sands and sandy creeks [WS], and iron oxide-rich units, including laterites [LA], banded iron oxide [BF] and andesite/basalt [AB]. Fireburns patterns are manifest by variations between dry vegetation (high 5/7 signature) in old-growth areas and young green regrowth following more recent fireburn areas. These variations are capable of masking primary lithological variations, particularly in granitic terrains.

LR2 (Fig. 4.1B) - Similar correlations as shown by LR1 images apply to LR2 images. However, while the contrast between high albedo areas (clay, carbonate) and low albedo areas (iron oxide-rich) is stronger in LR2 images, the definition of detail is somewhat weaker.

LR3 (Fig. 4.1C) - The strong absorption of band 3 by green vegetation results in a good expression of drainage/creek patterns as dark lineaments, which renders this image morphologically useful. Calcrete and magnesite-encrusted areas [CA] are well pronounced by high DN values. Clay and chlorite-rich surfaces of ultramafic rocks [UM] show high DN values, whereas mafic volcanics [AB] show very low DN values, due to the strong absorption of iron oxide in band 3.

LR4 (Fig. 4.1D) - Images in this band display opposite characteristics to the LR3 image with respect to green vegetation and thereby gum-straddled drainage surfaces,

showing strong reflectance in band 4. Clay and hydrosilicates show higher reflectance than iron oxides, as in lower band images.

LR5 (Fig. 4.1E) - This image shows little contrast, and shows the reverse relations as compared to the lower band images, ie. clay and hydrosilicate display low albedo due to absorption whereas iron oxides show high albedo. Calcrete surfaces display low reflectance, laterites show in shades of white, while the Soanesville sill peridotite sill is subdued due to absorption by chlorite and other magnesian hydrosilicates which dominate its weathering surface.

LR6 (Fig. 4.1F) - The log residual of the thermal short wave infrared band 6 accentuates the expression of black body radiation, ie. in particular lateritic materials (which absorb strongly in the visible and short wave lengths) display high band 6 DN values, whereas high-reflectance granitic materials show little or no radiance in band 6. Otherwise, only poor differentation is shown between mafic and felsic materials.

LR7 (Fig. 4.1G) - This image shows excellent discrimination between high-reflectance iron oxide-rich materials (laterites, basalts, banded iron formations) and clay and hydrosilicate-rich materials (chlorite-coated ultramafic units).

LR8 (Fig. 4.1H) - This additional band corresponds to the total reflectance in all bands, thus expressing sun-illuminated and shadow areas, which results in good manifestation of the morphology.

4.2 Ratios of log residual bands

RGB images combining log residual ratios, for example RGB LR5/LR4 : LR4/LR3 : LR5/LR7 result in images very similar to the equivalent unenhanced BRs, confirming the preservation or original inter-band relationships in log residual ratio plots.

Warrawoona Group metabasalts diplay generally lower LR5/LR7 ratios (<0.9) and high LR5/LR4 ratios (mostly >1.6) than basalts of the Fortescue Group (LR5/LR7 = 0.85-1.0; LR5/4 = 1.3-2.1), accentuating the lower clay component of weathering surfaces of the Warrawoona rocks (Fig. 4.2A). Clay-altered, carbonated basalts and coarse grained plagioclase-rich hypabyssal mafic rocks are clearly manifest by high 5/7 ratios (>1.05). Ultramafic rocks generally exhibit high LR5/LR7 ratios, due to chlorite alteration, and low iron oxide (LR5/LR4 ratios mostly <1.3) in their weathering surfaces.

The high LR5/LR7 log residual ratios (>1.0) and low LR5/LR4 log residual ratios (<1.3) of felsic volcanics distinguish them from most granitic rocks (LR5/LR7≤1.1; LR5/LR4>1.2), and in particular banded gneisses (LR5/LR7 <1.0; LR5/LR4≥1.4)(Fig. 4.2B). Late high level differentiated granites, represented by the Cooglegong Granite, show moderately high LR5/LR7 (>1.05) and high LR5/LR4 (>1.5).

Deformed and undeformed sandstones and siltlstones fall into the same general field of high LR5/LR7 ratio (>1.0) and low LR5/LR4 ratio (<1.5), due to the abundant clay trapped in these immature clastic sediments (Fig. 4.2C). By contrast, iron-oxide coated winowed alluvial creek sands display far lower LR5/LR7 (≤0.9). Banded iron formations display low LR5/LR7 and a wide range of LR5/LR4. Laterite display very high LR5/LR4 ratios (≥1.7). Carbonates fall into a distinct intermediate field.

Chapter 5. Band ratio images

Although the identification of surface types by Landsat-5-TM images is limited by the small number and the broad wavelength of spectral windows, some of the essential components can be defined by band ratios (BR) and band combinations, including (1) iron oxide (high 3/2, 5/4, 5/3 BR); (2) clays/hydrosilicates/fluid inclusion-bearing materials and dry vegetation (high 5/7 BR); (3) green vegetation (high 4/3 BR), and (4) quartz (bands 1+7). BRs 5/4 and 7/4 are uniquely suited for discrimination of iron oxides, since BR 3/2 closely coincides with and are therefore partly masked by green and dry vegetation. BR 5/4 images highlights most iron oxide-rich surfaces (mafic volcanics, laterites and banded iron formations - containing both menatite and goethite), whereas BR 3/2 images appear to (weakly) express only laterite and banded iron formations (goethite-bearing) surfaces. The combination of band 54 and 3/2 images thus allows an effective discrimination between iron oxide species. RGB 5/4:4/3:5/7 images are useful for distinction of the relationships between iron oxides, green vegetation and clay, respectively. Although discrimination of clay from carbonate poses a problem, it is assisted by textural/morphological patterns such as layering, joint systems and juxtaposition of calcrete deposits with creek beds. As distinct from quartz, chert and silcrete display high 5/7 ratios - a likely consequence of the abundance of water inclusions in fine-grained siliceous rocks and the absorpiton effect of the OH molcules in band 7 (T. Cudahy, pers. comm., 1997). In the following, the characteristics of individual BR images are described:

Band ratio 5/7 images. This BR (Fig. 5.1A) is diagnostic of clays and hydrosilicate minerals, of sedimentary carbonate and calcrete, and of water inclusions in opaline silica/chert units (T. Cudahy, pers. comm., 1997). Lithological correlations are partly masked by the 5/7 BR of dry vegetation. Felsic sedimentary rocks (sandstone, conglomerate) and ultramafic rocks show high 5/7 BRs, due to their clay and chlorite alteration, respectively. By contrast, ferruginous weathering crusts of basalts and laterites show low to very low ratios.

Band ratio 5/4 image. This BR (Fig. 5.1B) is uniquely sutable for the identification of iron oxide-rich materials, including hematite and goethite, since the other common components - clay, carbonate, green and dry vegetation - have significantly lower 5/4 band ratios. High 5/4 DN values are typical of iron-rich weathering crusts of basalt, pyroxenite and oxidized mafic-derived colluvium. Creeks appear dark due to the very low 5/4 band ratio of accompanying green vegetation. The hydromagnesian silicate weathering coatings of ultramafic rocks shows in black due to very low 5/4 band ratio.

Band ratio 3/2 image. The 3/2 BR images (Fig. 5.1C) is also useful for identification of iron oxide but are markedly affected by the masking effects of dry vegetation, which also yield high 3/2 band ratios. Consequently, the images are strongly affeted by fireburns. Comparisons between 5/4 and 3/2 images can be useful for

discrimination between the dominant forms of iron oxide in the weathering crusts of mafic volcanics (probably hematite) and in laterites (probably goethite).

Band ratio 4/3 images. DN values of this ratio are diagnostic of green vegetation, and represent the commonly better vegetated gullies, creeks, strike depressions, and southern shaded and vegetated slopes (Fig. 5.1D). High 4/3 BR zones commonly represent young regrowth of green vegetation in recent fireburns areas.

Chapter 6. Principal component analysis of single bands and band ratios

6.1 Single bands

The, generally high correlation between spectral bands of common natural components requires a method of discriminating spectral patterns which departs from the general norm. Principal components (PC) analysis measures the degree of correlation between band reflectance values in each pixel and the mean spectral pattern of the total pixel array, and quantifies the proximity of each DN value to best-fit variance axes in N-dimensional space - the number of axes equaling the number of spectral channels. The highest PC (PC1) represents best correlated band DN values, whereas lower PCs represent decreasingly correlated spectra of potential interest. Each PC is influenced by all the Landsat-5-TM bands, each band being represented by an Eigen vector which weighs the influence of this band on the relevant principal component. Commonly, individual PCs are influenced by particular surface types, although such correlations may vary between images scanned unde different conditions. Whereas RGB images of the 1st, 2nd and 3rd PCs commonly outline the geological and structural elements, RGB images of the lower order PCs tend to reflect the distribution of vegetation and fireburn areas (Glikson and Creasey, 1995).

It is emphasised that the characteristic of principal components depend inherently on the statistics of each scene or subscene, and thus may be inconsistent between scenes. For this reason, in interpreting the lithological significance of principal component images correlations with known surface types are required in each case. Below the main characteristics displayed by principal component images of the central Pilbara test areas (21°2'-21°26'S;119°32'-119°54'E) are described:

PC1 (Fig. 6.1A) - The 1st PC represents the strong correlations between bands in materials characterised by high total reflectance, ie. plutonic quartz in granitoids, abraded alluvial granitoid-derived quartz in creeks and valleys, and silcrete/calcrete evaporative surface crusts commonly associated with creeks. PC1 images also allow distinctions between high-correlation sandstone/conglomerate units, low-correlation mafic volcanics and very low correlation ultramafic rocks. PC1 images are useful for identifying the relative age of fireburns, which show increasing albedo with younger age, and are useful for definition of roads and tracks.

PC2 (Fig. 6.1B) - The 2nd PC show a high correlation by iron oxide-rich surfaces such as basalts, dolerite dykes, and in particular laterites, whereas clay-rich weathering surfaces, such as occur on siltstones, granitoids and sandstones, generally show low correlations. Fireburn areas display generally higher correlations than old growth. Green vegetation, in particular gum corridors along creeks, display low correlations, rendering the 2nd PC useful for the expression of the drainage patterns.

PC3 (Fig. 6.1C) - Felsic materials, in particular granites, yield higher (although patchy) correlations than mafic materials. An exception are iron oxide-rich laterites, which display high correlations. This feature can be useful for distinctions between the weathering crusts of mafic volcanics (?hematite-rich) and laterites (?goethite-rich). Green vegetation displays a high correlation in the 3rd PC, whereas high-albedo materials such as abraded alluvial quartz have very low DN values.

PC4 (Fig. 6.1D) - The 4th PC offers a general, although poorly defined, discrimination between mafic and felsic volcanic rocks, where the latter display very low correlations as compared to the latter. Granitic rocks display intermediate correlations. This principal component is useful in depicting laterites due to their very low correlations. Fireburns display low correlations relative to old growth areas, with recent fireburn displaying extremely low correlations.

PC5 (Fig. 6.1E) - 5th PC images are stripy and show a generally high correlation for mafic rocks and laterites as compared to felsic rocks. Fireburns stand out due to their higher correlation in this PC, whereas green vegetation shows very low correlations.

PC6 (Fig. 6.1F) - 6th PC images are stripy but offer an excellent distinction of green vegetation, which can be usefully combined with other images in order to outline the drainage system accurately. Distinctions between mafic and felsic rocks are very poor, the latter displaying somewhat lower correlations. Laterites display significantly high correlations.

PC7 (Fig. 6.1G) - The image is extermely banded, showing mainly the large creek, due to high correlation of high-reflectance material such as abraded quartz. Recent fireburn areas can be vaguely discerned by their higher albedo.

In summary, PC images are extremely useful where used in combination with single band or band ratio images, in that they allow the following discriminations:

(1) between clay-rich and carbonate-rich materials with similar 5/7 BR values.
(2) between laterites and the iron oxide-rich weathering surfaces of mafic volcanic and hypabyssal rocks.

6.2 Principal components of band ratios

Application of principal component analysis to band ratios allows discriminations between materials with partly overlapping spectral patterns (Fraser and Green, 1987). Thus, high 4/3 ratios pertain to both iron oxide and green vegetation, and high 5/7 ratios pertain to both clay and vegetation. However, iron oxide can be distinguished from vegetation by lower 5/7 ratio, and clay can be distinguished from vegetation by lower 4/3 ratios. These discriminations are achieved using principal component analysis of pairs of

ratios. For vegetation and clay the difference is expressed by principal components analysis of band ratios 4/3 and 5/7, where vegetation-rich materials will show a high correlation between these ratios (PC1) while clay-rich materials will display a low correlation between these ratios (PC2).

In line with the above considerations, the image RGB PC2(4/3; 5/7): 5/4 : 1+7 was found to allow direct comparisons between the ratios of clay/carbonate, iron oxide and green vegetation. In this type of image the visually-sensitive red and green colours represent lithological variations and the visually less senstive blue colour represents vegetation. As green vegation is also represented by the removal of its signature in the expression PC2(4/3; 5/7), the third channel is chosen as the sum of the bands 1+7, shown to enable the idenitifation of materials with highest reflectance in all bands, as follows:

Red channel - pc2(4/3;5/7): Clay/hydrosilicate materials and fluid inclusion rich materials (carbonate, chert, silcrete) are selcted. The de-selection of green vegetation provides excellent morphological control, due to removal of Eucalypt-rich drainage arteries. Consequently, the drainage system is markedly manifested by dark to black outlines.

Green channel - 5/4 band ratio: The discrimination of iron oxide components is often achieved by reference to the high 3/2 BRs of haematite and goethite - components difficult to discriminate from each other by Landsat-5-TM. However, the similarly high 3/2 BR of dry vegetation somewhat obscures this signature. In this study the 5/4 BR is chosen as representative of the role of iron oxide, since haematite - the normally dominant iron oxide - displays uniquely high 5/4 BRs.

Blue channel - bands (1+7): Materials yielding highest reflectance in all bands include quartz and silcrete. In particular, coarse grained quartz grains within granitoid rocks, and abraded clastic quartz in mature arenite and in alluvial sands in creek beds reflect strongly in all bands, as confirmed by field correlations. The sum of reflectance values of any two or more bands can be used in this regard.

Throughout the Pilbara region outcrops are variously covered by dry spinifex and grass vegetation and in the more humid areas, particularly near to the coast, also by lichen. Depending on the density of the vegetation cover, the effect is to partially mask the rocks with the 5/7 BR signature of dry vegetation and to a lesser extent the 4/3 signature of green chlorophyll-rich vegetation. However, under the semi-arid conditions of the Pilbara a high proportion of rock weathering surfaces is normally exposed, allowing excellent spectral/lithological correlations. This is demonstrated by the expression of unique lithological signatures in the Landsat-5-TM spectra, including for example (1) the 5/4 BR which characterises iron oxides of laterites and weathered magnetite-rich gabbro, dolerite and pyroxenite, and is distinct from the spectral signature of spinifex and lichen vegetation, and (2) quartz-rich rock types such as granitoids whose strong reflectance is normally masked by vegetation signature only to a minor extent. Consequently, RGB pc2(4/3; 5/7):5/4:1+7 images allow expression of four factors, namely clay, iron oxide, quartz and drainage patterns. Advantages of this method include (1) discrimination of visually sensitive red-green (clay-iron oxide) mixtures which, along with minor silica and carbonate, dominate weathering crusts in the Pilbara region; (2) good expression of drainage systems, and (3) the consequent direct lithological and morphological information allowed by these images. In the following, spectral/lithological correlations of individual rock types are considered.

Chapter 7. Spectral-lithological correlations

Precise calibrations of Landsat spectra to distinct surface types require identification of pure test pixels in each scene in order to account for the additive and multiplicative atmospheric factors. In this study, as no such pure pixels were found, Landsat-5-TM lithological correlations depend on empirical field observations. Ideally such correlations need to be examined using field spectrometers, x-ray spectrometric analysis and thin section studies of weathering crusts and their parental materials. The present correlations are based on the single band, log residual, band ratio, principal components and directed principal components of band ratio methods. Correlations with gamma ray spectrometric K-Th-U data are included to test the Landsat data. Stratigraphic classifications of unit terms referred to below are given in Appendix 4.

Based on the RGB pc2(4/3;5/7):5/4:1+7 formula, a series of enhanced geo-referenced Landsat scenes and algorithm files defining the geographic coordinates of individual 1:100 000 sheet areas have been prepared (Glikson, 1997a, 1997b). The image data cover seven and one half Landsat-5-TM (185x185 km) scenes covering a total area of c. 240 000 km^2, and algorithms for 46 1:100 000 sheet areas covering a total area of c. 115 000 km^2 defined by longitudes 116°00-121°00E and latitudes 20°00-22°00S. Scenes include Dampier (path114row74), Yarraloola (p114r75), Roebourne (p113r74), Pyramid (p113r75), Port Hedland (p112r74), Marble Bar (p112r75), Nullagine (p111r75) and the southern part of Yarrie (p111r74). The enhanced Landsat-5-TM image 1:100 000 data sets, when used in conjunction with geological maps on the same scale, allow detailed comparisons between stratigraphic interpretations and lithological indicators. This should facilitate further focusing of observations in the field on details not generally allowed by cartographic map presentation standards.

Some of the lithological correlations indicated by Landsat-5-TM correlations can be tested with reference to gamma-ray spectrometric data. In particular, clay alteration of volcanic rocks and sediments, and the composition of clays formed by weathering of granitoids, can be expected be reflected by variations in the potassium (K) abundances in the weathering crusts. Examination of K-Th-U distribution patterns observed on 90 metre pixel gamma-ray spectrometric RGB images combined with Landsat-5-TM band ratios 5/7, representing clay and dry vegetation, are outlined below.

In the following, lithological expressions on RGB pc2(4/3;5/7):5/4:1+7 images are summarised:

7.1 Ultramafic and mafic intrusive rocks

The Mg-hydrosilicate (chlorite, serpentine, talc, brucite) dominated weathering crusts of peridotites show high 5/7 BRs. Examples of peridotites include a dunite-peridotite

sill located above cherts across Camel Creek north of Corruna Downs batholith (119°51'E; 21°21'S), the Soanesville layered sill (119°5.3'E; 21°29.1'S), serpentinite coated extensively by magnesite in the western part of the Soanesville belt, the eastern part of the Andover intrusion (117°13'E; 20°50'S) and the northern part of the Munni Munni intrusion (116°51E; 21°6'S). Pyroxenites show weathering crusts dominated by phyllosilicate (high 5/7 BRs) and iron oxide (high 5/4 and 3/2). crusts show in green. Gabbro shows a greater role of clay, weathered from coarse grained plagioclase, relative to pyroxenites.

7.2 Mafic volcanics and dykes

High-Mg to peridotitic komatiitic volcanics show different degrees of mixture of iron oxide and lesser clay bearing weathering crusts, with high 5/4 and 3/2 BRs. Tholeiitic to high-Mg basalts of the Warrawoona Group (Appendix 4) yield little or no radiometric counts for K, Th and U.

7.3 Felsic volcanics

Felsic volcanics show clay to iron oxide-dominated weathering crusts, expressed by 5/7 and 5/4 BRs, respectively. Felsic volcanics of the Duffer Formation display a general increase in the radiogenic elements with higher stratigraphic level, in accord with the increase in the role of K-rhyolites toward the top of this sequence (Glikson and Hickman, 1981a,b). Very high levels of radiogenic elements also pertain to K-rich rhyolites of the Wyman Formation. Dacitic volcanics which underlie the Panorama Cu-Zn prospects, central Pilbara, display general enrichment in potassium, which may be of both primary and hydrothermal origin. Sectors of clay-altered pillowed andesites which underlie the dacites tend to show patches of high 5/7 BRs and high potassium.

7.4 Sandstones

Sandstones of the Gorge Creek Group - the oldest major sandstone sequences in the Pilbara - show only low radiometric counts, whereas outliers of Fortescue Group sediments (Hardy Sandstone) have very high radiogenic element levels, a difference representing the increase in granitoid-derived detritus with time. Calcrete deposits along creeks are typically very rich in radiogenic elements.

7.5 Granitoids

Granitoids dominated by quartz and clay-rich arkose weathering, typically show high total 1+7 reflectance, particularly marked in fireburn areas, and feature as 1st principal component values. Hickman (1983) discriminated between several major units within Pilbara granitoid batholiths, including syntectonic granodiorite to adamellite gneisses, which in places display concentric zonation, and post-tectonic potassium-rich granites. The latter type include the Moolyella (119°58'E; 21°7'S) and Cooglegong (119°27'E; 21°36'S) granites, which stand up on RGB K-Th-U images due to their very high abundance in all the three elements. Areas underlain by these granites are also characterised by high 5/7 BR on Landsat-5-TM images, suggesting that potassium feldspar is more prone to weathering into clay than the plagioclase in the surrounding granodioritic gneisses. Similar characteristics are shown by the south Corruna Downs adamellite (119°51'E; 21°44'S). At least in the case of the Moolyela granite, the enrichment in clays may also be related to hydrothermal alteration of pegmatitic veins which abound in these K-rich tin-bearing graniotids. The total 1+7 bands, expressing the effect of quartz, is markedly lower in the Moolyella K-rich granite and in parts of the Cooglegong granite, probably due to clay-coatings of quartz grains. K-rich granites have a tendency for higher 5/4 BRs, suggesting relatively ferruginous weathering crusts.

Potassium enrichment is also shown by distinct concentric high-K rings within the main granodiorite-adamellite gneiss zones of the Mount Edgar, Corruna Downs and Shaw Batholiths (Fig 7.1). Some of these zones display high 5/7 BRs, although less consistently than the post-tectonic K-rich granites. Possibly, much of the potassium in these rocks is tied in solid solution in the relatively stable sodic plagioclase.

An outer aureole of clay alteration occurs at the peripheries of the Strelley Granite (119°9'E; 21°15'S) and is likely related to the hydrothermal clay alteration associated with sulphide mineralisation of overlying dacites of the Panorama Cu-Zn prospect. Such alteration zones in granitic batholiths, expressed by both clay and high-K readings, form potential targets for mineralisation.

7.9 Chert units, vein quartz and banded iron formations (BIF)

In contrast to the high total reflectance (bands 1+7) shown by plutonic quartz and its alluvial derivatives, cryptocrystalline opaline silica of chert units and quartz veins feature high 5/7 BRs, apparently due to the absorption of band 7 by the OH molecule vibration effect of water inclusions (T. Cudahy, pers. comm., 1997). Due to the universal interbanding of banded iron formations with siltstone units, and the abundance of flat lying silt-coated slabs around outcrops, these rocks display dominant clay signature mixed with iron oxide. Landsat identifications of BIFs are aided by the strong positive signature of these rocks on airborne magnetic images.

7.10 Alluvial deposits and laterites

Mafic source-derived detritus and creek deposits display iron oxide and clay signatures, showing mixtures of 5/4 and 5/7 BRs. Alluvial quartz-rich felsic source-derived detritus and creek bed sand markedly represented in high 1+7 band reflectance. Major creeks display strongly in combined 1+7 bands forming corridors fringed by green vegetation, which on directed principal component pc2(4/3;5/7):5/4:1+7 images show in dark to black due to the removal of the green vegetation signature of fringing Eucalypts. Laterites commonly occur as relic plateau and flat hill tops (mesa), displaying in deep apple green.

7.13 Alteration patterns

Geological mapping during 1995-1996 has allowed identification of clay alteration patterns within mafic volcanic rocks, displayed as high 5/7 BR anomalies within host basalts of high 5/4 BR. Examples occur in mafic volcanics of the Gorge Creek Group which underlie volcanogenic massive sulphides flanking the Strelley Granite. Clay alteration zones are associated with pods of sulphide, facilitating field and remote scanner-based economically oriented alteration mapping.

Chapter 8. Landsat-5-TM lithological/stratigraphic correlations: Pilbara Supergroup

Type areas dominated by the Archaean Warrawoona Group and Gorge Creek Group described below include (1) early Archaean Warrawoona Group and the boundaries with intrusive and faulted granitoids in the Marble Bar-Camel Creek area (Fig. 8.4-6); (2) middle Archaean Gorge Creek Group and intrusive or faulted granitoids in the Soanesville area (Fig. 8.1-3). For stratigraphic nomenclature refer to Appendix 4.

8.1 Soanesville-Tambourah area

The Soanesville-Tambourah area (119°2'-119°13'E; 21°24-21°33'S) (Fig. 8.1-3) includes a downfaulted zone of c. 3.0 Myr old Gorge Creek Group volcanic and clastic sediments. The northern block of this zone consists of a sequence of mafic-felsic volcanics, chert, sandstone and banded iron formation intruded by voluminous ultramafic sills in the north. A southern block of a yet undetermined age includes sequences of sheared mafic volcanics, pyroxenites, felsic schists and cherts intruded by the Tambourah Granite and faulted against the Shaw batholith in the south (Fig. 8.1-3). The two zones are separated by a major strike fault (Van Kranendonk, 1997). Surface deposits include laterite capping of a major chert unit northeast of the Tambina Granite, magnesite crusts on deformed serpentinised ultramafic rocks, and calcrete mostly along creeks. A combination of Landsat-5-TM images and K-Th-U data (Fig. 8.3) allow the following correlations around the Soanesville syncline area. Peridotitic component of ultramafic sills displays a strong 5/7 BR signature due to their chlorite and serpentinite alteration. Resolution of the peridotitic components of the sills by Geoscan Mark-I image indicate internal zonation of the sills, including thin chilled zones of pyroxenite which display strong iron oxide signature (high 5/4 BR). Mafic and andesitic volcanics occur both below the Soanesville main sill and in the core of the syncline typically display high 5/4 BRs and contain chert intercalations showing high 5/7 BRs. Overlying patches of calcrete and magnesite show very high 5/7 BRs. Sandstone units are recognised by their typical dendritic drainage morphology, moderately high 5/7 BRs and radiogenic element signatures. Unconformably overlying Fortescue Group mafic volcanics show somewhat higher radiogenic element counts that the older Strelley basalts and andesites. This is an important criteria which, along with the typical rectangular fracture pattern which distinguishes the Fortescue Group basalts from the tectonic fabric of the Warrawoona and Strelley basalts, allows their discrimination. The overlying Hardy Sandstone displays particularly high counts.

8.2 Marble Bar-Camel Creek area

The Marble Bar-Camel Creek area (21°2'-21°26'S;119°32'-119°54'E) (Fig. 8.4-6) contains the classic successions of the c. 3.47 Myr old Warrawoona Group. The oldest supracrustal sequence is represented by tholeiitic to high-Mg basalts of the Talga-Talga Subgroup, which includes an intercalation of dacite-andesite porphyry (McPhee Formation) and is overlain by a thick lense of andesite-dacite-rhyolite of the Duffer Formation. The latter is in turn overlain by dominantly ultramafic volcanic and hypabyssal rocks with chert intercalations. Unconformable late Archaean Fortescue Group outliers in the area include the Mount Roe Basalt and Hardy Sandstone. Granitoids include granodioritic to trondhjemitic gneisses of Warrawoona Group age and the post-tectonic Moolyella Granite. Talga Talga Subroup mafic volcanics display iron oxide-rich weathering crusts (high 5/4 BR) with very low to nil radiometric counts. The Duffer Formation displays a mottled zone consisting of mixtures of clay (high 5/7 BR) and iron oxide (high 5/4 BR) signatures - the latter in part due to the abundance of mafic dykes. Radiometric counts increase within the felsic volcanic sequence upward, representing concentration of rhyolites at the top (Glikson and Hickman, 1981). Lower sections of the mafic-ultramafic volcanic Salgash Supbgroup display very low radiometric counts, whereas extensive carbonate alteration of this sequence upward is characterised by high K and U counts. Wyman Formation K-rich rhyolites and sandstones of the Gorge Creek Group in the Camel Creek and Coongan belt, respectively, are strongly manifest. Unconformably overlying near-flat units of Mount Roe Basalt show patchy radiometric highs. Gneisses of the Mount Edgar batholith display a dominant 1+7 signature of plutonic quartz, cris-crossed by clay-rich (high 5/7 BR) lineaments representing alteration zones accompanied by green vegetation related to higher moisture levels. High 5/4 BR patches represent surficial enrichment of iron oxide in soils. The post-tectonic Moolyella Granite is characterised by generally lower reflectance in most bands, interpreted in terms of clay-coating of plutonic quartz grains. It shows strong clay enrichment (5/7 BR), high radiometric counts and a general but weak increase in density of green vegetation (high 4/3 BR).

Chapter 9. Landsat-5-TM lithological/stratigraphic correlations: Fortescue Group and Hamersley Group

Type areas for the late Archaean Fortescue Group and early Proterozoic Hamersley Group include (1) A late Archaean outlier of the Meentheena syncline, southeast of the Mount Edgar batholith (Fig. 8.7-9), and (2) the Fortescue Group and Hamersley Group sections in the southern flank of the Mingar Dome and the Robe River areas.

9.1 Meentheena syncline, east Pilbara

The Meentheena Syncline (21°12-21°31'S;120°13'-120°33'E) (Fig. 9.1-3) includes a little-deformed near-complete succession of Fortescue Group volcanics and

sediments which range from the basal Mount Roe Basalt, which overlies Wyman Formation (potassic rhyolites) unconformably, to the Hardey Sandstone (arkosic sandstone and conglomerate), Kylena Basalt (amygdaloidal K-rich basalts), Tumbiana Formation (stromatolitic carbonates), Nymerina Basalt and Kuruna Siltstone. The basal unconformity of the Mount Roe Basalt rests in sharp relief on the rhyolites, characterised by high 5/7 BRs. The basalt shows very low radiometric counts, as distinct from the layered high K-Th-U units of the Hardey Sandstone, which display layer-controlled variations in the relative abundances of the three elements (Fig. 9.2). The Kylena Basalt displays significantly higher radioactive counts than the Mount Roe Basalt, in accord with its higher potassium levels, which may reach about 3 percent (Glikson and Hickman, 1981). Carbonate banks of the Tumbiana Formation overlie a basaltic unit of very low radiometric counts and display a marked clay-like high 5/7 BR signatures. At the core of the syncline occurs an outlier of Nymerina Basalt showing high 5/4 BR (Fig. 9.3).

9.2 Mingar Dome-Robe River area, west Pilbara

The Fortescue Group and Hamersley Group are well exposed along the southern flanks of the Mingar Dome, centred about 116°29'52.42"E; 21°23'14.15"S), display consistent lithological and stratigraphical correlations (Fig. 9.2; Appendix 5). Combination of Landsat-5-TM images and gamma ray spectrometric data allow discriminations between several units within the Kylena Basalt and Maddina Basalt, offering stratigraphic controls not readily achieved in the field:

Kylena Basalt. consists of the lower Kylena Basalt with low to very low radiometric counts, corresponding to an assemblage of high-Mg andesite and minor trachyandesite. The upper part of the Kylena Basalt shows very high counts, reflecting the predominance of intermediate and felsic rocks (trachyandesite, dacite and rhyolite); basalts occur locally. K2O values as high as 5% have been recorded in basalts of the Kylena Basalt in the Pinderi Hills 1:100 000 sheet area, by analogy to very high values in this formation the east Pilbara (Glikson and Hickman, 1986), .

Tumbiana Formation consists of siltstone and stromatolitic carbonate intercalated between the Kylena Basalt and Maddina Basalt, showing high total reflectance expressed by combined bands 1+7, representing the high albedo of the carbonates. Moderate to high radiometric counts are typical of these sediments.

Maddina Basalt consists of a low unit characterised by interlayered high and low radiometric zones, consisting of shoshonite with minor basalt and high-Mg basalt. The middle Maddina Basalt comprises a lower rhyolite/dacite member (high radiometric response) overlain by a sequence of trachyandesite, basalt and shoshonite (low to moderate radiometric response). The upper Maddina Basalt (high radiometric response) consists of dacite with minor interbedded basalt. Typical of the Maddina Basalt is a shallow stratigraphically controlled ridge-and-valley morphology, with the depressions occupied by ferruginous mud rich in basaltic boulders. These surficial units are characterised by very strong iron oxide signature, ie. high band 5 and band 7 signatures, high 5/4 and 3/2 band ratios, high band 6 thermal infrared radiance and very low gamma ray spectometric counts.

Warrie Shale. Overlying the Maddina Basalt is a unit of shale, chert, jaspilite and dolomite, which stands out on the images due to its very high total reflectance in the visible light bands, high 5/7 band ratio. The combined total reflectance is attributed to the combined effects of a mixture of all the lithological types. Intermediate to low thermal response in band 6 applies.

Nallanaring Volcanic Member. This unit, intercalated within the Warrie Shale, consists of pillow basalts and minor felsic volcanics, and shows moderately high 5/4 and 3/2 band ratios and a slightly lower thermal signature as compared to the enveloping sediments of the Warrie Shale.

Banded iron formations and pisolitic ironstones. Banded ironstones and derived terraces of pisolitic iron deposits, with a type area around Pannawonica, are characterised by strong iron oxide signatures, ie. high bands 5 and 7, high 5/4 band ratio and 3/2 band ratio, and very high thermal infrared band 6 emittance, representing the "black body" thermal infrared radiation of these rocks which strongly absorb shorter wavelength solar radiation. Terraces of retransported pisolite along Robe River stand out with similar features as the older terraces.

Wittenoom Formation carbonates. The plateau-forming carbonates of the Wittenoom Formation shows marked reflectance in the visible range (bands 1, 2, 3) and short wave near-infrared band (band 4) - which appears to be a unique spectral characteristic allowing the identification of carbonates. The 5/7 band ratio and thermal band 6 radiation are low, whereas directed principal components pc2[4/3; 5/7] shows high digital numbers for the carbonate. The carbonates show high correlations in PC1 and in particular PC4, and negative correlations in PC2, PC5 and PC6. Numerous linear gullies cut through the Wittenoom Formation have been excavated into the Marra Mamba Iron Formation, showing typical iron oxide-rich signatures. The carbonates are best distinguished from shale-dominated units by principal component analysis, showing marked contrasts in PC4 and PC5.

Principal component analysis. PC1 - Banded iron formations (Marra Mamba BIF Member and Brockman Iron formation) show distinct low correlations, siltstones and carbonates show high correlations, and mafic volcanics intermediate values. Thus, the Nallanaring Volcanic Member of the upper Fortescue Group yields a strong PC1 signature. The signature of green vegetation is subdued to eliminated, consequently gum-fringed creeks stand out on the image. PC2 - Mafic magnetite-bearing (iron oxide-rich weathered surfaces) rocks (dolerite, gabbro) and banded iron formations display uniquely high correlations; green vegetation (creeks) shows very low correlations; shales, carbonates and granites show low correlations. Fireburn areas display high correlations. PC3 - Banded ironstones and mafic intrusives show high correlations, whereas granitoids display low correlations. PC4 - Granitic rocks and green vegetation display high correlations whereas iron oxide-rich surfaces display very low correlations. Carbonates display very high correlations, ie. Wittenoom Formation, whereas shales display low correlations - providing a method for distinguishing carbonates from clays; PC5 - Green vegetation (band ratio 4/3) and carbonates display very low correlations, which allows this image to be used for identification of drainage patterns accompanied by gums and calcrete. The image yields palimpsest outlines of the domal structure of the Mingar Dome, due to alternations between zones high in clay (higher correlations) and low in clay (lower correlations). PC6 - Dotted image representing vague fireburn outlines.

Directed principal components of band ratios. A directed principal component image RGB pc2[4/3;5/7]:5/4:1+7 (Fig. 9.2) allows estimates of the clay : iron-oxide : quartz ratios in the weathering surfaces, and through them correlation with the original rock, as well as the expression of the drainage system by a green vegetation removal effect (Glikson, 1997, 1998). This image as well as band ratio 5/7 and 5/4 images suggest patchy surface alteration of parts of the Kylena Basalt to clay-rich materials, dominance of clays in the weathering surfaces of the lower part of the Maddina Basalt, and of iron oxides in the upper part of the Maddina Basalt. The Maddina Basalts contains strike-parallel zones consisting of basaltic gravel and boulders set in iron oxide-rich soil which display in apple green (high 5/4 band ratios). The directed principal component of ratios image allows detailed discrimination of the stratigraphy of the upper Fortescue Group and the Hamersley Group south of the Mingar Dome, including fine-scale separation of units of a wide range of sedimentary and volcanic units.

Chapter 10. Conclusions

Under the arid to semi-arid conditions prevailing in the Pilbara province and similar regions of central and western Australia, enhanced Landsat-5-TM data allow effective discrimination of a wide range of superficial deposits and weathered rock surfaces, and through the latter of the underlying fresh rock types. Combinations of band ratios, log residuals, principal components and directed principal components, aided by radiometric K-Th-U data, allow identification of (1) clay and/or other hydro silicates (OH molecule - high 5/7 band ratio response); (2) iron oxide-rich weathering crusts of mafic igneous rocks (high 5/4 and 3/2 band ratios response); (3) laterites (high 5/4 and high 3/2 band ratios); (4) plutonic quartz and derived abraded alluvial sediments (high total bands 1+7 reflectance); (5) green vegetation (high 4/3 band ratios). Chert, silcrete and carbonates are identified by their contained water inclusions and thereby high 5/7 response, but can be discriminated from clays using within-image (and in some instances between-image relationships). For example (1) the 1st principal component often assigns higher correlation values to carbonates as compared to clays and other hydro silicates; (2) the 3rd principal component allows discrimination between iron oxide-rich mafic igneous rocks and laterites. The Landsat-5-TM thermal infrared band 6 radiation allows identification of banded iron formation thanks to their common high black body radiation, particularly where enhanced as log residual images.

Directed principal components (PC) of band ratios enhance direct lithological discriminations between common natural materials. The 2nd PC of the combined band ratio file [4/3;5/7] selects clay, hydro silicates and carbonates and deselects green vegetation, due to the low correlation of 4/3-5/7 band ratios in clays and the high correlation of 4/3-5/7 band ratios in green vegetation. This results in negative expression of gum-fringed areas, which appear as dark features which outline drainage patterns, allowing effective use of images as topographic guides. The 5/4 band ratio is shown to uniquely express iron oxides. The combinations of bands 1+7 offers a semi-quantitative estimate of total radiance (albedo), in particular the expression of plutonic quartz in granitoids and quartz-bearing alluvial deposits, as distinct from materials which show high reflectance at the low end (clays) or the high end (iron oxide) of the spectrum. These features, combined in the algorithm RGB pc2(4/3;5/7):5/4:1+7, facilitates identification of field targets, interpolations and extrapolations of ground observations, location and ground navigation. A set of 1:100 000 image maps according to this algorithm has been prepared for general use (Glikson, 1997a,b). Combination of the above methods allow discrimination between several rock types characteristic of different stratigraphic units. Examples include:

1. Deformed tectonised early to mid-Archaean tholeiitic to high-Mg basalts (Warrawoona Group and Gorge Creek Group) display ferruginous weathering crusts (higher 5/4 band ratios) but little clay alteration. By contrast, little-deformed outliers of late Archaean (Fortescue Group) basalts - which include high-K basalts (Kylena Basalt) - show clay alteration (higher 5/7 band ratios) and correspondingly higher K-Th-U radiometric counts.
3. Carbonatisation of tholeiitic to high-Mg basalts of the upper Warrawoona Group is shown through increase in the 5/7 band ratios and in radiometric K-Th-U counts. Clay alteration patterns of andesitic volcanics associated with Cu-Zn sulphide mineralisation in the Strelley area are clearly discernible on Landsat-5-TM imagery, allowing alteration mapping.
4. Progressive increase in the importance of K-rich rhyolites with higher stratigraphic levels in the Duffer Formation is manifest by the increase in K radiometric counts.
5. Post-tectonic granitoids (Moolyella Granite, Cooglegong Granite, southern Corruna Downs batholith) display higher clay weathering (high 5/7) and have clay-coated quartz (low 1+7 reflectance) as compared to syntectonic granodioritic to adamellite gneisses. The higher K-feldspar and derived clay levels result in higher K-Th-U counts over these intrusions. Concentric variations between admaellite zones and granodiorite gneiss zones, manifest within batholiths by K-Th-U variations, are difficult to correlate with Landsat-5-TM data.
6. A link is observed between increases in surface clay contents (5/7 band ratios) and green vegetation (4/3 band ratios), related to moisture contents of the clay.
7. The little-deformed late Archaean Fortescue Group and early Proterozoic Hamersley Group volcanic and sedimentary rocks of the Hamersley Basin and its outliers over the north Pilbara Craton are particularly amenable to spectral characterisation. These sequences, which unlike the older greenstones are of mostly pumpelyite-prehnite metamorphic facies and are less affected by the shearing and attendant silicification and carbonatisation which resulted in various degrees of lithological homogenisation of the older greenstones, can be mapped in great detail with the aid of enhanced Landsat-5-TM images. In view of the poor accessibility of large parts of the Hamersley Basin, this method allows rapid and accurate interpolation and extrapolation of field traverses.

It is recommended that enhanced Landsat-5-TM imagery coupled with airborne gamma ray spectrometric and magnetic images should be routinely available to all AGSO's field mapping programs in arid Australian terrains.

Acknowledgments

I am grateful to John Creasey, supervisor of AGSO's Remote Sensing laboratory, for long term advice and assistance with image processing, and to John Vickers for an excellent field season in the Pilbara. I thank Phil Bierwirth, Taro Macias, Matt Peljo and Peter Wellman for their assistance with processing and interpretation of Landsat and geophysical data and with the preparation of this report, and Richard Blewett, John Creasey, Taro Macias and Peter Wellman for their comments on the manuscript. I wish to thank Terry Brown for drafting the line figures.

References

Bierwirth, P.N., 1990. Mineral Mapping and vegetation removal via data-calibrated pixel unmixing, using multispectral images. International Journal Remote Sensing, 11, 1999-2017.

Buick, R., Thornett, J.R., McNaughton, N.J., Smith, J.B., Barley, M.E. & Savage, M., 1995. Record of emergent continental crust ~3.5 billion years ago in the Pilbara craton of Australia. Nature, 375, 574-577.

Cheney, E.S., 1996. Sequence stratigraphy and plate tectonic significance of the Transvaal succession of southern Africa and its equivalents in Western Australia. Precambrian Research, 79, 3-24.

Feeken, E., 1991. Environmental mapping in BMR: Cainozoic deposits, landforms and vegetation in the Tomkinson Ranges. Australia Bureau Mineral Resources Geology Geophysics Research Newsletter, 14, 7-8.

Feeken, E., 1992. Notes on the 1:100 000 environmental map of the Tomkinson Ranges, Western Musgrave Block, central Australia. Australia Geological Survey Organisation Record, 92/34.

Forster, B.C., 1984. Derivation of atmospheric correction procedures for Landsat-5-MSS with particular reference to urban data. International Journal Remote Sensing, 5, 799-817.

Fraser, S.J. and Green, A.A., 1987. A software defoliant for geological analysis of band ratios. International Journal Remote Sensing, 8, 525-532.

Glikson, A.Y., 1997a. Directed principal components/band ratio correlations of Landsat-5-TM spectral data and NGMA 1:100 000 scale mapping, north Pilbara Craton, Western Australia. Australia Geological Survey Organisation Research Newsletter, 26, 1-4.

Glikson, A.Y., 1997b. Explanatory notes for a Landsat-5-TM image series processed according to an RGB directed principal components/band ratio formula, northern Pilbara Craton, Western Australia. Australia Geological Survey Organisation, Record 1997/20.

Glikson, A.Y. & Hickman, A.H., 1981. Geochemistry of Archaean volcanic sequences, eastern Pilbara Block, Western Australia. Australia Bureau Mineral Resources Geology Geophysics, Record 81/36.

Glikson, A.Y. & Hickman, A.H., 1981. Geochemical stratigraphy of Archaean mafic-ultramafic volcanic successions, eastern Pilbara Block, Western Australia. in: Archaean Geology [eds. J.E. Glover & D.I. Groves], Geological Society Australia Publication, 7, 287- 300.

Glikson, A.Y. and Creasey, J.W., 1995. Landsat-5-TM and Geoscan MKI correlations of the Giles Complex and associated granulites, Tomkinson Ranges, central Australia. Australia Geological Survey Organisation Journal, 16/1&2, 173-193.

Green, A.A. and Craig, M.D., 1985. Analysis of aircraft spectrometer data with logarithmic residuals. Jet Propulsion Laboratory Publication, 85-41, pp. 111-119.

Hickman, A.H., 1983. Geology of the Pilbara Block and its environs. Geological Survey of Western Australia Bulletin, 127.

Hickman, A.H., 1997. Dampier 1:100 000 Geological Map Series, Geological Survey of Western Australia.

Honey, F.R. and Daniels, J.L., 1986. Rock discrimination and alteration mapping for mineral exploration using the Carr Boyd/Geoscan airborne multispectral scanner. In: 5th Thematic Conference on Remote Sensing for Exploration Geology, Reno, Nevada.

Honey, F.R. and Daniels, J.L., 1987. Application of Carr Boyd Minerals Limited airborne multispectral scanner to spectral discrimination of hydrothermally altered areas. In: 4th Thematic Conference on Remote Sensing for Exploration Geology, San Francisco, California.

McNaughton, N.J., Compston, W. & Barley, M.E., 1993. Constraints on the age of the Warrawoona Group, eastern Pilbara Block, Western Australia. Precambrian Research, 60, 69-98.

Nelson, D.R., 1997. Compilation of SHRIMP U-Pb zircon geochronological data, 1995. Geological Survey of Western Australia Report 1996/5.

Pidgeon, R.T., 1984. Geochronological constraints on early volcanic evolution of the Pilbara Block, Western Australia. Journal Geological Society Australia, 31, 237-242.

Richards, J.A., 1986. Remote Sensing Digital Image Analysis. Springer Verlag, Berlin, 281 pp.

Simpson, C.J., 1978, LANDSAT-5: developing techniques and applications in mineral and petroleum exploration. Australia Bureau Mineral Resources Geology Geophysics, 3, 181-191.

Smithies, R.H., 1997. Sherlock 1:100 000 Geological Map Series, Geological Survey of Western Australia.

Thorpe, R.I., Hickman, A.H., Davis, D.W., Mortensen, J., Trendall, A.F., 1992. U-Pb zircon geochronology on Archaean felsic units in the Marble Bar region, Pilbara Craton, Western Australia. Precambrian Research, 56, 169-189.

Van Kranendonk, M.J., 1997. Results of field mapping, 1994-1996, in the North Shaw and Tambourah 1:100 000 shet areas, eastern Pilbara Craton, northwestern

Australia. Australia Geological Survey Organisation Record, 1997/23.

Williams, I.S. & Collins, W.J., 1990. Granite-greenstone terrains in the Pilbara, Australia, as coeval volcano-plutonic complexes: evidence from U-Pb zircon dating of the Mount Edgar batholith. Earth Planetary Science Letter, 97, 41-53.

Zegers, T.E., 1997. Structural, kinematic and metallogenic evolution of selected domains of the Pilbara granitoid-greenstone terrain. Geologica Ultratectina, 146.

Appendix 1 - Spectral bands of Landsat-TM data correlated with Geoscan Mark-I airborne scanner data

Landsat -TM band	*Geoscan band*	*spectral channel (microns)*	*spectral channel (microns)*
1	.45-.52	1 vis (blue)	0.45-0.5
2	.52-.60	2 vis (green)	0.55-0.6
3	.63-.69	3 vis (red)	0.65-0.7
4	.76-.90	4 near-infrared	0.83-0.87
		5 "	0.93-0.97
5	1.55-1.75		
		6 sw-infrared	1.98-2.08
7	2.08-2.35		
		7 sw-infrared	2.16-2.19
		8 "	2.205-2.235
		9 "	2.3-2.4
		10 thermal infrared	8.5-8.9
		11 "	9.7-10.1
6	10.4-12.5		
		12 "	10.8-11.2
		13 "	11.5-12.0

Appendix 2 - Average reflectance values (DN - Digital Number) and band ratios for Landsat-5-TM of lithologically relatively uniform sub-image test areas, Pilbara Craton.

North Star Basalt

	NSB McPhee		*NSB Coongan belt*	
	15.3	11.5	26.4	22.2
band 2	14.9	11.75	20.9	18.3
band 3	30.4	23	31.8	28.4
band 4	33	26	31.1	27.4
band 5	89.8	72.5	75.6	74.9
band 6	17.1	14	14.4	15.3
band 7	57.6	46.2	49.6	54.6
bands1+7	72.9	57.7	76	76.8
5/7	1.55	1.56	1.52	1.37
5/4	2.72	3.03	2.43	2.73
3/2	2.04	1.95	1.52	1.55
4/3	1.08	1.13	0.98	0.96

Mount Ada Basalt

	MAB Coongan belt		MAB north Coongan belt	
band 1	44.7	25.2	22.7	15.9
band 2	33.1	18.8	21.6	14.1
band 3	46.1	28.5	42.4	27.9
band 4	45.9	28.6	46.7	31
band 5	100.6	70.1	81.4	82.8
band 6	14.7	13.9	17.3	17.9
band 7	63.9	43	43.8	51.5
bands1+7	108.6	68.2	66.5	67.4
5/7	1.57	1.63	1.85	1.61
5/4	2.19	2.45	1.73	2.67
3/2	1.39	1.51	1.96	1.98
4/3	0.99	1	1.1	1.11

Apex Basalt and altered basalts

	Apex Basalt, Coongan belt		*carbonated basalts, Salgash SG, Chinaman Creek*		*carbonated basalts, Warrawoona belt*	
band 1	20.9	18.7	30.1	26.9	21.9	21.6
band 2	16.8	16	26.6	25.8	17	17.4
band 3	25.8	26.1	45.6	44	25.6	27.4
band 4	26.8	26.9	53.4	52.5	29.3	32.8
band 5	80.7	84.1	84.4	104.1	59.8	68.8
band 6	18	17.8	14.8	18.4	14	14.6
band 7	58.3	60	40.6	49.1	34.2	39.2
bands1+7	79.2	78.7	70.7	76	56.1	60.8
5/7	1.38	1.4	2.08	2.12	1.75	1.75
5/4	3.86	3.12	1.58	1.98	2.04	2.09
3/2	1.53	1.63	1.71	1.7	1.5	1.57
4/3	1.03	1.03	1.17	1.19	1.14	1.19

Altered basalts

	Sulphur Springs, Clay-altered basalt		*Sulphur Springs, Fe-altered basalts*	
band 1	25	21.4	16.3	14.7
band 2	21.4	16.1	15.6	13.1
band 3	38.4	27.2	34.2	27.3
band 4	47.4	36.7	36.8	30.8
band 5	102.9	70	99.7	76.1
band 6	13	16.3	18.7	20
band 7	52.4	35.8	55.2	45.4
bands1+7	77.4	57.2	71.5	60.1
5/7	1.96	1.95	1.8	1.68
5/4	2.17	1.9	2.71	2.47
3/2	1.79	1.69	2.19	2.08
4/3	1.23	1.34	1.07	1.13

Fortescue Group basalts

	Mount Roe Basalt, W of Chinaman Ck		*Mount Roe Basalt, S of Panorama Ridge*		*Mount Roe Basalt E of Soanesville Syncline*	
band 1	18.6	19.2	19.9	21.4	21	21.3
band 2	15.7	15.9	16.3	18.3	17.6	18.3
band 3	28.2	28.5	26.4	30.2	32.1	34.9
band 4	33.9	33.9	31.7	35.1	33.4	36.8
band 5	71.3	73.1	65	69.7	77.3	85.9
band 6	12.7	17.7	12.4	13.3	13.9	11.9
band 7	41.4	42.8	37	40.5	45.2	49.6
bands1+7	60	62	56.9	61.9	66.2	70.9
5/7	1.72	1.71	1.75	1.72	1.71	1.73
5/4	2.1	2.15	2.05	1.98	2.31	2.33
3/2	1.8	1.79	1.62	1.65	1.82	1.91
4/3	1.2	1.19	1.2	1.16	1.04	1.05

Kylena, Nymerina and Maddina basalts

	Kylena Basalt, W of Chinaman Ck		*Kylena Basalt, Chichester Range*		*Nymerina Basalt, Chichester Range*		*Maddina Basalt, Chichester Range*	
band 1	22.9	23.6	12.3	11	16.6	15.8	14.2	12.1
band 2	18.2	18.1	12.1	11.1	16.2	15.6	12.8	12.9
band 3	28.7	29	25.1	24.5	33.6	30.8	25	27.9
band 4	34.5	34.1	28.1	27.6	36.6	32.4	28.9	31.4
band 5	77.6	75.2	85.7	77.9	93.3	83.6	83.8	86.5
band 6	15.4	15.2	8.6	9	10.7	10.5	8.1	9.7
band 7	43	41	51.3	48.3	55.8	51.4	50.2	52.2
bands1+7	65.9	64.6	63.6	59.3	72.4	67.2	64.4	64.3
5/7	1.8	1.83	1.67	1.61	1.67	1.62	1.67	1.65
5/4	2.25	2.2	3.04	2.82	2.55	2.58	2.89	2.75
3/2	1.57	1.6	2.07	2.2	2.07	1.97	1.95	2.16
4/3	1.2	1.17	1.12	1.13	1.09	1.05	1.16	1.12

Mafic sills and dykes

	Black Ridge dolerite		*gabbro sill, Sulphur Springs*			*gabbro, Soanesville sill*	
band 1	13.3	8.5	22	25	17	24.3	20.3
band 2	10.5	6.5	18	20	16	21.3	17.8
band 3	20	10.8	34	37	29	38.8	31.8
band 4	21.5	14.3	37	41	31	43	37.3
band 5	56.3	51.3	98	100	84	101.5	90.8
band 6	9	11	13	14	14	13	12
band 7	34.5	29	52	51	47	51.5	47
bands1+7	47.8	37.5	74	76	64	75.8	67.3
5/7	1.63	1.77	1.88	1.96	1.78	1.97	1.93
5/4	2.61	3.59	2.64	2.43	2.71	2.36	2.43
3/2	1.9	1.66	1.88	1.85	1.81	1.82	1.78
4/3	1.07	1.32	1.09	1.11	1.06	1.11	1.17

Felsic volcanics

	Duffer Formation, Marble Bar		*Duffer Formation north Coongan belt*		*Panorama Ridge*		*Wyman Formation, Brockman Hay Ck*	
band 1	25.4	18.7	22.7	22.3	23.8	28.4	29.7	24.2
band 2	24.6	18.5	21.6	20.4	22.5	25.1	27.3	21.2
band 3	47.8	33.5	42.4	36.2	41.2	44.1	48.3	35.7
band 4	54.6	39.5	46.7	42.6	49.2	50.2	55.1	43.3
band 5	97.6	72.2	81.4	78	90.1	81.8	104.9	79.8
band 6	15.7	14.2	17.3	16.9	13.8	14.5	14.5	13.3
band 7	43.4	32.7	43.8	40.4	43.3	40.8	54.3	38.6
bands1+7	68.8	51.4	66.5	62.7	67.2	69.2	84	62.8
5/7	2.24	2.2	1.85	1.93	2.08	2	1.93	2.06
5/4	1.88	1.82	1.74	1.83	1.83	1.63	1.9	1.84
3/2	1.94	1.81	1.96	1.77	1.83	1.75	1.77	1.68
4/3	1.14	1.18	1.1	1.18	1.19	1.14	1.14	1.21

Ultramafic intrusions

	Camel Creek peridotite		*Soanesville peridotite sill*		*altered um N of Tambina Granite*		*altered um, NW of Tambina Granite*	
band 1	20.2	21.8	22	24.5	19.5	22.8	33.9	22.5
band 2	17.3	16.9	17.3	17.5	17.6	20.1	29.1	19.7
band 3	30.6	26.6	30.3	27.3	31.4	35.7	47.9	35.5
band 4	36.1	31.3	30.8	29	34.4	39.7	48.1	39.3
band 5	87.8	77.5	46.8	50.8	50.4	60.8	72.2	74.6
band 6	16.9	13.9	11.5	13.5	6.9	11.8	10.7	9.7
band 7	47.5	40.6	24	27.5	27.9	32.3	36.2	38.2
bands1+7	67.7	62.4	46	52	47.4	55.1	70.1	60.7
5/7	1.84	1.9	1.95	1.84	1.8	1.88	1.99	1.95
5/4	2.43	2.47	1.52	1.84	1.46	1.53	1.5	1.11
3/2	1.77	1.57	1.75	1.56	1.78	1.77	1.65	1.8
4/3	1.18	1.18	1.02	1.06	1.09	1.11	1	1.11

Proterozoic felsic volcanics/pyroclastics/derived sediments

	tuff over Hardy SS, w. of Chinaman Ck.		*Jeerinah Formation, shale and sandstone*	
band 1	19.1	19	17.5	19.2
band 2	15.9	16.8	16.7	18.8
band 3	28.3	28.8	31.5	35.9
band 4	32	34.3	34.5	38.9
band 5	80.3	77.7	69.6	72.4
band 6	11.3	10	8.3	7.6
band 7	40.9	39.2	39.3	38.9
bands1+7	60	58.2	56.8	58.1
5/7	1.96	1.98	1.77	1.86
5/4	2.5	2.26	2.02	1.86
3/2	1.78	1.71	1.89	1.91
4/3	1.13	1.19	1.09	1.08

Granitoids

	Tambourah Ck, west Shaw banded gneiss		*granodiorite North Shaw*		*Tambina Granite*		*Cooglegong Granite*	
band 1	27.1	27.5	26.4	29	29.6	31.1	23.8	23.5
band 2	24.6	25.4	27.4	29.2	27.9	30.5	20.9	19
band 3	44.4	47	59.2	57.7	51.5	61	37.6	32
band 4	48	51.1	67.6	66.7	54.1	64.1	40.6	34.2
band 5	103.6	110.3	140.9	138.1	118.9	138.4	92.1	81.2
band 6	10.6	11.3	18.3	17.8	11.5	12.1	12.8	13.1
band 7	59.9	62.3	82.3	79.9	67.3	78.8	46.9	41.6
bands1+7	87	89.8	108.7	108.9	96.9	109.9	70.7	65.1
5/7	1.72	1.77	1.71	1.73	1.77	1.76	1.96	1.95
5/4	2.16	2.16	2.08	2.07	2.2	2.16	2.27	2.37
3/2	1.8	1.85	2.16	1.97	1.84	2	1.8	1.68
4/3	1.08	1.08	1.14	1.15	1.05	1.05	1.08	1.07

Strelley Granite

	external zone (A)		*intermediate zone (B)*		*external zone (C)*	
band 1	23.6	23.5	23.3	23.5	22.7	24.9
band 2	20.2	20.1	20.6	20.1	18.7	23.8
band 3	36.6	36.4	35.6	36.4	32.6	42.5
band 4	41.5	41.1	44.6	41.1	36.3	47.8
band 5	85.2	86.3	81.5	86.3	88	97.2
band 6	12.3	14.4	14	14.4	17.5	13.8
band 7	41.7	42.1	44.5	42.1	52	53
bands1+7	65.3	65.6	67.8	65.6	74.7	77.9
5/7	2.04	2.04	1.83	2.04	1.69	1.83
5/4	2.05	2.1	1.82	2.1	2.42	2.03
3/2	1.81	1.81	1.73	1.81	1.74	1.78
4/3	1.13	1.13	1.25	1.13	1.11	1.12

Alluvial (creek) sand

	Shaw River sand		*Fortescue River valley alluvium*	
band 1	33.3	39.3	13.4	14.6
band 2	30	33.3	15.2	17.1
band 3	49.3	54.3	38.3	43.6
band 4	49	53.5	43.5	48.7
band 5	125	121.8	89.3	96.7
band 6	21	19	18.2	16.5
band 7	77	76.8	60.4	63
bands1+7	110.3	116.1	73.8	77.6
5/7	1.62	1.58	1.48	1.53
5/4	2.55	2.27	2.05	1.98
3/2	1.64	1.63	2.52	2.54
4/3	0.99	0.98	1.13	1.11

Sandstones, Archaean

	Gorge Creek sandstone, Coongan belt		*sandstone below Soanesville sills*		*Llala Rookh SS, east of Sulphur Springs*	
band 1	25.6	17.8	30.8	20.6	24.4	26
band 2	21.6	16	26.7	17.3	18.9	24.2
band 3	35.2	29.8	48.2	28.8	31.3	45.8
band 4	39.1	35.2	51.8	32.4	36.1	52
band 5	77	71.7	93.4	53.7	62	79.8
band 6	13.4	13.7	13.2	6.8	16.3	16.9
band 7	39.7	34.9	48.7	27.3	30.6	40.4
bands1+7	65.3	52.7	79.5	47.9	55	66.4
5/7	1.93	2.05	1.92	1.96	2.02	1.97
5/4	1.97	2.18	1.8	1.66	1.71	1.72
3/2	1.63	1.86	1.8	1.66	1.65	1.65
4/3	1.11	1.18	1.07	1.12	1.15	1.13

Siltstones

	siltstone/mudstone, Sulphur Springs		*limestones, Carawine Dolomite*	
band 1	17.9	19.1	17.3	18.3
band 2	14.4	15.2	14.9	16.8
band 3	23.9	26.8	27	30.4
band 4	27	29.4	32.2	34.8
band 5	52.9	48.4	68.8	73.1
band 6	13	13.2	8.3	7.1
band 7	28	25.2	38.9	41
bands1+7	45.9	44.3	56.2	59.3
5/7	1.88	1.92	1.76	1.78
5/4	1.96	1.64	2.13	2.1
3/2	1.66	1.4	1.81	1.81
4/3	1.13	1.09	1.19	1.14

Sandstones, Proterozoic

	Hardy SS, north Shaw		*Hardy SS, east of Soanesville syncline*		*Hardy SS, e. of Tambina Granite*		*ss lens in Kylena Basalt*	
band 1	27.6	30.2	30.8	20.6	26.3	28.9	25.5	22.8
band 2	25.1	29.1	26.7	17.3	23.8	24.8	26.5	22.4
band 3	44.4	53.6	48.2	28.8	44.8	44.1	48.2	42.7
band 4	50.4	58	51.8	32.4	49.9	46.5	54.6	48
band 5	100	116.2	93.4	53.7	100.1	91.3	104.5	97.9
band 6	13.4	13.6	13.2	6.8	13.5	12.6	16.7	16.7
band 7	50.9	59.4	48.7	27.3	47.4	47	54.5	49.4
b1+7	78.5	89.6	79.5	47.9	73.7	75.9	80	72.2
5/7	1.96	1.95	1.92	1.96	2.11	1.94	1.92	1.98
5/4	1.98	2	1.8	1.65	2	1.96	1.91	2.04
3/2	1.76	1.84	1.8	1.66	1.88	1.78	1.82	1.91
4/3	1.13	1.08						

Banded iron stones

	Gorge Creek BIF, north Coongan belt		*Soanesville syncline, BIF*		*Marra Mamba BIF, Chichester Range*	
band 1	18.2	16.2	22	18.5	14.9	14.9
band 2	16.7	16.1	19.8	17.8	15.5	13.8
band 3	32	31.4	36.5	31.8	35.1	30
band 4	34.4	32.7	39.5	34.3	38.1	32.5
band 5	68.9	68.1	66	54.5	91.9	74.5
band 6	11	12	11	8	12.4	15
band 7	40.9	41.3	38	32.3	58.4	50.3
bands1+7	59.1	57.5	60	50.8	73.3	65.2
5/7	1.68	1.65	1.73	1.68	1.57	1.48
5/4	2	2.08	1.67	1.59	2.41	2.29
3/2	1.91	1.95	1.84	1.78	2.26	2.17
4/3	1.07	1.04	1.08	1.08	1.08	1.08

Chert

	Marble Bar chert		*Strelley chert*
band 1	24.5	16.5	35
band 2	23.2	16.25	26
band 3	39.5	27	41
band 4	40.7	25.2	46
band 5	49	11.5	64
band 6	15	10	14
band 7	32.7	11.5	33
bands1+7	57.2	28	68
5/7	1.5	1	1.94
5/4	1.2	0.45	1.39
3/2	1.7	1.66	1.57
4/3	1.03	0.93	1.12

Green vegetation

	gum trees, Coongan River		*creek, E of Sulphur Springs*	
band 1	22	20	18.3	21
band 2	17	17	14.3	14
band 3	25	23	19.5	18
band 4	39	36	37.3	32
band 5	64	64	56.5	64
band 6	18	19	15	15
band 7	38	38	30.3	32
bands1+7	60	58	48.6	53
5/7	1.68	1.68	1.86	2
5/4	1.64	1.77	1.51	2
3/2	1.47	1.35	1.36	1.28
4/3	1.56	1.56	1.91	1.77

Laterites

	laterite, N of Tambina granite		*laterite, above BIF, Strelley area*	
band 1	18.3	14.6	16.9	16.6
band 2	14.9	12.9	14.7	13.7
band 3	25.6	23.1	27.1	26.6
band 4	25.8	23.2	28.8	27.1
band 5	71.3	68.3	72.8	68.3
band 6	17.6	18.9	14.4	14.5
band 7	48	44.7	47.5	46.3
bands1+7	66.3	59.3	64.4	62.9
5/7	1.48	1.53	1.53	2.62
5/4	2.76	2.94	2.52	2.52
3/2	1.72	1.79	1.84	1.94
4/3	1	1	1.06	1.02

Appendix 3 - spectral values in digital numbers (DN) of mean log residual values for test pixel groups within the central Pilbara region.

A. Warrawoona Group basalts

	North Star Basalt				*Mount Ada Basalt*			
	McPhee Reward		*North Coongan belt*		*Coongan belt*		*north Coongan belt*	
band 1	52	46	67	69	105	90	70	54
band 2	72	70	81	82	116	100	86	71
band 3	110	101	93	98	118	111	108	104
band 4	88	84	74	76	87	82	85	85
band 5	150	157	141	141	128	137	142	153
band 6	35	38	49	38	24	35	40	42
band 7	180	184	187	195	149	154	167	173

B. Altered basalts

Apex Basalt and altered basalts

	Apex Basalt, Coongan belt	*Salgash Subgroup, carbonated basalts*		*carbonated basalts, Warrawoona belt*	
band 1	61	83	75	90	79
band 2	78	109	97	103	95
band 3	94	138	122	113	110
band 4	71	119	107	95	97
band 5	150	127	143	131	138
band 6	40	28	32	40	38
band 7	196	112	124	138	144

Sulphur Springs, Strelley basalts

	clay-altered basalt		*little-altered basalts*	
band 1	68	79	48	53
band 2	87	88	69	70
band 3	115	109	111	107
band 4	104	108	88	89
band 5	152	139	160	149
band 6	24	41	38	49
band 7	142	130	163	163

C. Fortescue Group basalts

Mount Roe Basalt

	west of Chinaman Ck		*south of Panorama Ridge*		*east of Soanesville syncline*	
band 1	69	67	78	76	71	67
band 2	86	82	95	97	89	86
band 3	113	108	113	118	120	121
band 4	101	97	100	101	92	94
band 5	143	143	138	135	143	147
band 6	32	42	33	33	32	26
band 7	152	152	144	144	153	157

Kylena, Nymerina and Maddina basalts

	Kylena Basalt, west of Chinaman Ck		*Kylena Basalt, Chichester Range*		*Nymerina Basalt, Chichester Range*		*Maddina Basalt Chichester Range*	
band 1	78	82	45	43	52	54	52	42
band 2	92	94	66	65	79	79	70	67
band 3	107	110	101	105	114	115	101	107
band 4	95	95	83	87	92	89	85	89
band 5	143	141	171	165	158	155	167	165
band 6	37	37	22	24	23	24	20	23
band 7	146	141	187	188	173	174	184	183

D. Mafic dykes and sills

	Black Ridge dolerite		*gabbro sill, Sulphur Springs*				*gabbro, Soanesville sill*
band 1	65	56	66	71	58	67	63
band 2	77	56	80	84	82	88	81
band 3	108	68	111	115	109	118	103
band 4	86	71	89	94	86	97	91
band 5	152	177	159	154	157	154	163
band 6	31	47	27	27	33	25	25
band 7	171	181	159	145	161	143	157

E. ultramafic intrusions

	Camel Creek peridotite		*Soanesville peridotite sill*		*altered um north of Tambina Granite*		*altered um NW of Tambina Granite*	
band 1	64	78	98	105	86	84	100	78
band 2	82	90	115	112	114	110	128	100
band 3	107	104	148	128	149	143	154	132
band 4	93	91	111	101	121	117	114	107
band 5	152	151	114	119	119	121	115	138
band 6	37	34	35	40	21	30	22	23
band 7	151	144	107	118	120	118	106	130

F. Felsic volcanics

Archaean felsic volcanics

	Duffer Formation, Marble Bar		*Duffer Formation north Coongan belt*		*Panorama Ridge*		*Wyman Rhyolite, Brockman Hay Creek*	
band 1	67	67	67	72	69	81	71	78
band 2	97	99	95	97	96	107	98	101
band 3	138	131	138	123	130	138	129	125
band 4	117	114	112	109	114	116	109	111
band 5	140	139	131	135	141	128	140	137
band 6	29	36	35	38	28	29	25	31
band 7	114	116	130	128	125	117	133	122

Fortescue Group volcanic/pyroclastics derived seiments

	Tuff above Hardy Sandstone		*Jeerinah Formation sediments & tuff*	
band 1	69	69	66	68
band 2	85	90	93	99
band 3	111	114	138	135
band 4	93	100	106	108
band 5	157	153	143	141
band 6	28	25	21	19
band 7	147	142	148	139

G. Granitoids

	Tambourah Ck, west Shaw banded gneiss		*granodiorite North Shaw*		*Tambina Granite*		*Cooglegong Granite*	
band 1	70	67	51	57	100	78	71	77
band 2	94	92	79	85	128	100	93	87
band 3	125	125	125	123	154	132	123	110
band 4	100	101	106	105	114	107	98	89
band 5	145	146	148	147	115	138	149	155
band 6	19	19	24	24	22	23	26	30
band 7	154	152	159	156	106	130	138	142

Strelley Granite

	external zone (A)		*intermediate zone (B)*		*external zone (C)*	
band 1	74	73	72	76	67	70
band 2	94	93	95	99	95	84
band 3	126	124	121	130	126	107
band 4	105	103	112	109	104	89
band 5	145	145	137	133	143	147
band 6	27	31	30	28	26	37
band 7	130	130	137	132	143	158

H. Sandstones

Archaean sandstones (deformed)

	Gorge Creek sandstone, Coongan belt		*sandstone below Soanesville sills*		*Llala Rookh sandstone, E. of Sulphur Springs*	
band 1	83	67	73	80	91	74
band 2	105	89	100	100	105	103
band 3	125	122	134	127	128	144
band 4	103	106	108	100	109	120
band 5	136	145	137	140	126	124
band 6	31	36	25	28	42	33
band 7	128	129	132	131	113	115

Proterozoic sandstones

	Hardy SS, north Shaw		*Hardy sandstone, E. of Soanesville syncline*		*Hardy sandstone, E.. of Tambina Granite*		*lens of sandstone in Kylena Basalt*	
band 1	72	69	80	90	70	80	63	62
band 2	98	98	104	112	95	102	97	91
band 3	127	133	138	138	131	134	131	127
band 4	107	106	109	115	108	104	109	106
band 5	143	143	133	128	145	138	140	145
band 6	24	21	24	20	25	24	28	31
band 7	133	134	127	119	126	130	135	134

I. Recent alluvial sediments

	Shaw River sand		*Fortescue River valley alluvium*	*Coongan River sand*	
band 1	70	80	40	80	76
band 2	95	101	69	100	97
band 3	114	122	130	120	118
band 4	84	89	107	89	94
band 5	144	136	143	136	136
band 6	31	27	31	33	32
band 7	163	157	171	151	151

J. Siltstones

	siltstone/mudstone, Sulphur Springs	
band 1	83	88
band 2	99	104
band 3	121	135
band 4	101	109
band 5	133	122
band 6	41	42
band 7	129	116

K. Limestones

	Carawine Dolomite	
band 1	65	67
band 2	86	92
band 3	117	125
band 4	103	104
band 5	148	147
band 6	22	18
band 7	155	149

L. Banded iron formations and chert

	Gorge Creek BIF, Coongan belt		north Soanesville syncline, BIF		Marra Mamba BIF, Chichester Range		Marble Bar chert		Strelley chert	
band 1	67	59	77	84	45	54	89	115	110	106
band 2	91	88	103	105	70	74	126	171	122	125
band 3	129	122	141	126	118	118	157	203	142	157
band 4	103	102	112	107	94	92	119	138	117	118
band 5	138	141	125	132	153	142	95	41	110	104
band 6	28	30	26	24	26	37	41	55	30	35
band 7	150	159	133	137	180	177	117	72	104	95

M. Laterites

	laterite, N of Tambina Granite		*laterite, above BIF, Strelley area*	
band 1	67	58	62	63
band 2	81	76	80	78
band 3	103	101	109	112
band 4	77	74	86	84
band 5	144	148	146	143
band 6	45	52	36	38
band 7	177	177	174	177

N. Green vegetation

	Creek, E of Sulphur Springs	
band 1	78	87
band 2	91	87
band 3	92	82
band 4	128	108
band 5	132	145
band 6	44	43
band 7	129	133

Appendix 4 - Pilbara Craton, Western Australia - stratigraphy and ages of supracrustal sequences and plutonic units.

U-Pb zircon ages [Ga]	Stratigraphy and sub province	Supracrustal lithological assemblages	Plutonic units
c.3.51	Cooterunah Sequence. north Strelley Block	Bimodal mafic/felsic volcanics	-Older crustal environments include sialic crustal sectors (c.3.725 Ga relic zircons in acid volcanics of the Panorama Formation); -3.712±98 Ga Sm-Nd isochron precursor age of mafic-ultramafic volcanics; -(3.574±4 Ga anorthosite enclaves in the Shaw Batholith).
unconformity			
c.3.48-3.43	Warrawoona Supergroup (North Star Basalt; Mount Ada Basalt; Duffer Formation; Apex Basalt; Panorama Formation; Euro Basalt. eastern and central Pilbara; probably Wodgina and Pilbara Well greenstone belts (central west Pilbara)	Tholeiites, high-Mg basalts, andesite, Na-dacite, K-rhyolites, chert, minor banded iron formation. Volcanic centres migrated laterally with time and persisted to at least 3.43 Ga in southern greenstone belts (McPhee dome; Kelly belt).	Coeval c.3.47-3.45 Ga tonalite-granodiorite-adamellite plutonic suites including parts of the Mount Edgar, Corunna Downs, Shaw, Yule and Carlindie batholiths - an area at least 10^4 km^2 large.
probable unconformity (not observed)			
c.3.3	Wyman Formation. eastern Pilbara	Potassic rhyolites	Coeval plutonic felsic activity in the Mount Edgar and Shaw batholiths. interpreted as the time of vertical movement, remobilisation and emplacement of the composite batholiths into supracrustal sequences, resulting in elevation and exposure of batholiths and formation of inter-batholithic supracrustal synclinoria - ie. greenstone belts.
c.3.27-3.25	Honey Eater Basalt (Strelley volcanics)	Basalts and dacites; chert	Central Pilbara - Strelley granite sill; granitic phases in the Yule batholith. western Pilbara (north of Sholl shear zone - basalts of the Regal Formations (Roebourne Group)
c.3.12	Whundo Group, west Pilbara, south of the Sholl shear zone.	Felsic and mafic volcanics	Granitoids in the Chirata-Sholl block, south of the Sholl shear zone
unconformity (observed in the Shay Gap area, NE Pilbara)			
c.3.095			Caines Well granitoid complex
c.3.014	Gorge Creek Group, Corboy Quartzite; Cleaverville Formation (west Pilbara - 3014±6 Ga); Paddy Market Formation, (central and eastern Pilbara)	Pilbara-wide deposition of banded ironstone/silica - shale formations	
unconformity (Pilbara-wide)			
>3.0	De Grey Group, consisting of the Constantine (Llala Rookh sandstone and conglomerate	Rifting and deposition of coarse grained clastic sediments and conglomerates (including granite clasts).	

U-Pb zircon ages [Ga]	Stratigraphy and sub province	Supracrustal lithological assemblages	Plutonic units
c.3.01-2.99	Whim Creek Group, including: Warrambie Basalt; Mons Cupri Volcanics (inc. Mount Brown Rhyolite); Cistern Formation; Rushall Slate		Pilbara-wide isotopic resetting of Rb-Sr and Pb-Pb systematics
c.3.0-2.925	Louden Volcanics; Mount Negri Volcanics	Tholeiitic and high-Mg basalts, amygdaloidal basalts	
<3.0	Mallina Formation and Mosquito Creek Formation	Siltstone and greywacke	
c.2.95			*West Pilbara* Peawah Granodiorite; Toweranna Porphyry
c.2.925-2.860			*West Pilbara* Munny Munny layered intrusion and equivalents (Millindina Complex); Bookingarra Granite
c.2.85			Moolyella and Cooglegong granites - high-K tin granites within the older batholiths.
c.2.765			*West Pilbara*: leucogranite
major unconformity			
c.2.76-2.69	Fortescue Group (Pilbara-wide): Mount Roe Basalt; Hardy Sandstone; Kylena Basalt; Tumbiana Formation (>2.715 Ga); Nymerina Basalt; Kuruna Siltstone; Maddina Basalts.	Massive and amygdaloidal basalts, minor pillowed basalts, pyroclastics, sandstone/conglomerate lenses	*West Pilbara* Cooya Pooya dolerite;
unconformity			
c.2.68-2.67	Jeerinah Formation	Shale, tuff, greywacke; containing a unit of *spherulitic microkrystite* at its upper part.	
c.2.63	Hamersley Group: Marra Mamba Formation	Banded ironstones and shale	
c.2.6			Dampier gabbro/granophyre lopolith complex
c.2.603 c.2.56	Wittenoom Formation /Carawine Dolomite; Mt Sylvia Formation; McRae Shale.	Sedimentary carbonates and clastics, containing a unit of stratigraphically consistent *spherulitic microkrystite* (2.603 Ga)	
c.2.47	Brockman Iron Formation; Weeli Wolli Iron Formation; Wongarra volcanics; Boolgeeda Iron Formation	Banded ironstones-tuff-shale, including a unit of *spherulitic microkrystite* in the Dales Gorge Member; felsic volcanics.	

Appendix 5 - summary of remotely sensed characteristics* of stratigraphic/lithological units of the Fortescue Group and Hamersley Group associated with the Mingar Dome.

Unit	Lithology	Remotely Sensed characteristics
Hardy Sandstone	sandstone, pebbly sandstone, conglomerate	high 5/7 band ratios, high radiometric counts.
Kylena Basalt	lower: high-Mg andesite and minor trachyandesite; upper: trachyandesite, dacite and rhyolite, local basalts; high K2O levels (<5%).	low to very low radiometric counts. very high radiometric counts.
Tumbiana Formation	siltstone and stromatolitic carbonate	high combined bands 1+7 reflectance; moderate to high radiometric counts.
Maddina Basalt	lower: shoshonite, minor basalt, high-Mg basalt; middle: rhyolite/dacite; trachyandesite, basalt and shoshonite; upper: dacite, minor basalt; surficial units: ferruginous mud with basalt boulders	-interlayered high and low radiometric zones; -high radiometric response; low to moderate radiometric response; -high radiometric response; -very strong iron oxide signature (high bands 5 and band 7 signatures), high 5/4 and 3/2 band ratios, high band 6 thermal radiance, very low radiometric counts.
Warrie Shale	shale, chert, jaspilite, dolomite	high reflectance in the VIS and high 5/7 band ratios; low PC2 and PC4 correlations.
Nallanaring Volcanic Member	pillow basalt, minor felsic volcanics	moderately high 5/4 and 3/2 band ratios; high PC1 correlation.
Marra Mamba and Hamersley Iron Formations	banded ironstones and pisolitic iron deposits	high bands 5 and 7, high 5/4 and 3/2 band ratios, strong thermal band 6 radiance; low PC1 and PC4 correlation; high PC2 and PC3 correlation.
Wittenoom Formation	carbonates	strong VIS, band 4 reflectance; low band 6, moderately high 5/7 band ratio and high total 1+7 band combination; high PC1 and PC4 correlation; low PC2 and PC5 correlations. The carbonates are best distinguished from shales by PC4 and PC5 differences.

* note - principal component (PC) signatures can be reversed as a function of the statistics of the Landsat scene or sub-scene used in the analysis.

A

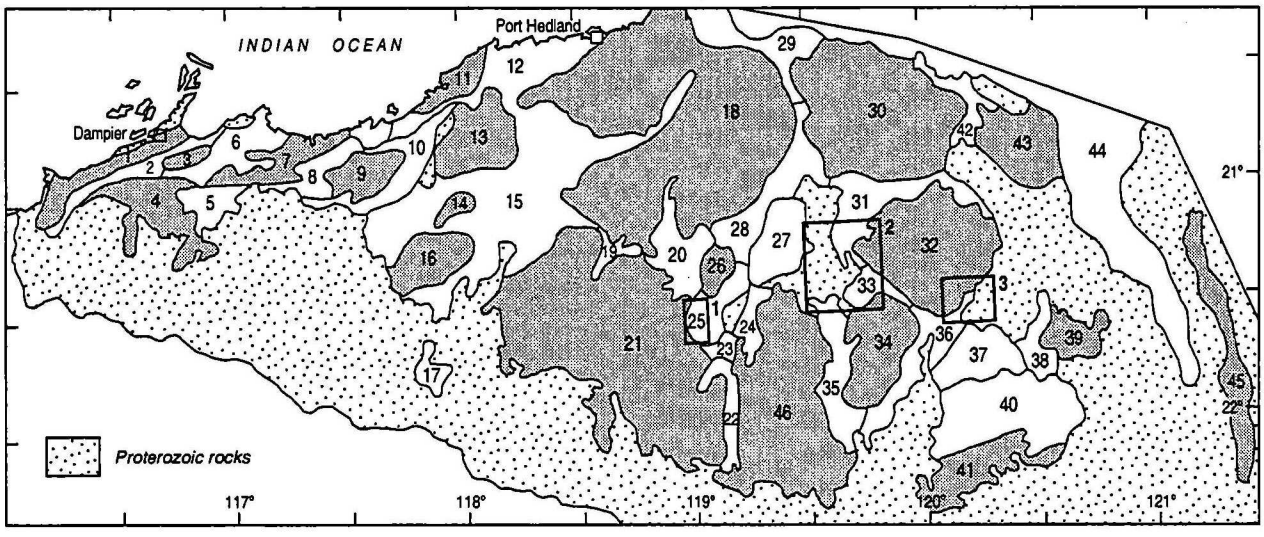

1 Dampier Batholith
2 Regal Belt
3 Karratha Granite
4 Chiratta Batholith
5 Sholl Belt
6 Roebourne Syncline
7 Harding Granite
8 Sherlock Belt
9 Caines Well Granite
10 Whim Creek Belt
11 Balla Balla Granite
12 Boodarie Belt
13 Portree Granite
14 Peawah Granodiorite
15 Mallina Synclinorium
16 Satirist Granite
17 Nunyerry Inlier
18 Carlindi Batholith
19 Wodgina Belt
20 Pilgangoora Syncline
21 Yule Batholith
22 Western Shaw Belt
23 Tambina Complex
24 North Shaw Belt
25 Soanesville Belt
26 Strelley Granite
27 North Pole Dome
28 Lalla Rookh Syncline
29 Goldsworthy Syncline
30 Muccan Batholith
31 Marble Bar Belt
32 Mount Edgar Batholith
33 Warrawoona Syncline
34 Corunna Downs Batholith
35 Coongan Syncline
36 Kelly Belt
37 McPhee Dome
38 Mount Elsie Belt
39 Yilgalong Granite
40 Mosquito Creek Synclinorium
41 Kurrana Batholith
42 Shay Gap Syncline
43 Warrawagine Batholith
44 Canning Basin
45 Gregory Granitic Complex
46 Shaw Batholith

1 SOANSVILLE - TAMBORAH AREA
2 MARBLE BAR - CAMEL CREEK
3 MEETHENA SYNCLINE

B

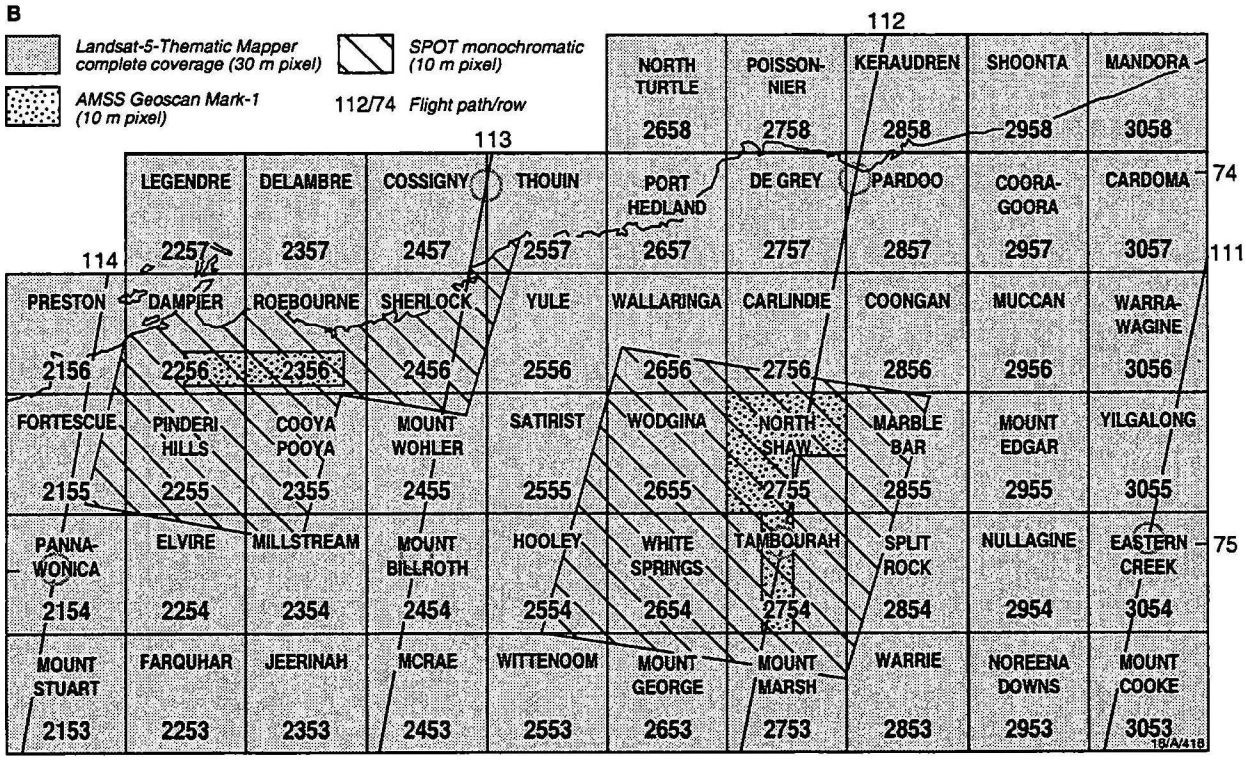

Figure 1.1 - Geological and location maps of the Pilbara Craton; A geological sketch map showing principal supracrustal and plutonic units (numbered, after Hickman, 1984), and the location of type areas for the Landsat correlation: 1 - Soanesville area (Fig. 8.1); 2 - Marble Bar area (Fig. 8.4); 3 - Meentheena area (Fig. 9.1).B - Distribution of Landsat-5-TM, Spot and Airborne Multispectral Scanner (AMSS) Geoscan imagery.

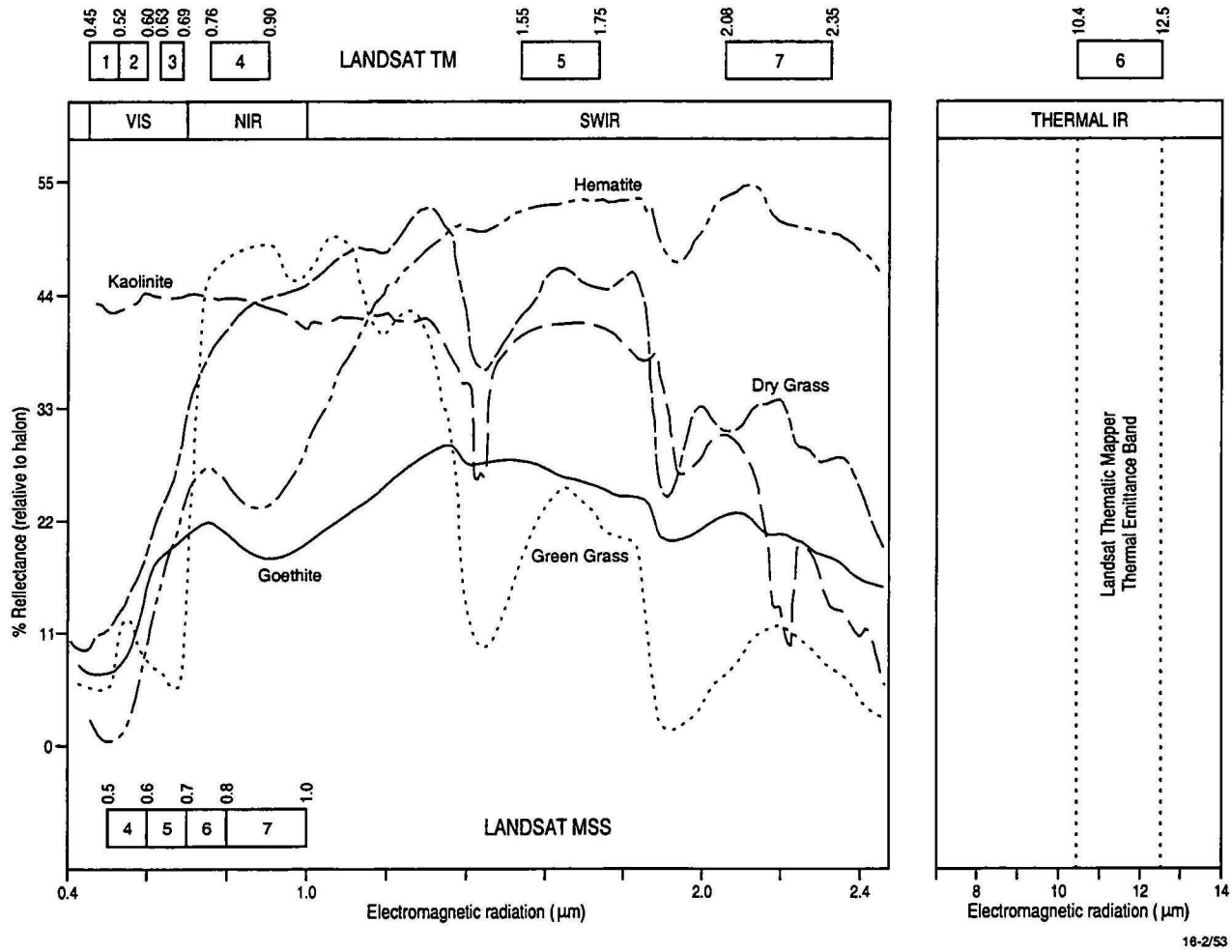

Figure 2.1 - Spectral %Reflectance features (relative to halon) of clay (kaolinite), hematite, goethite, green vegetation and dry vegetation.

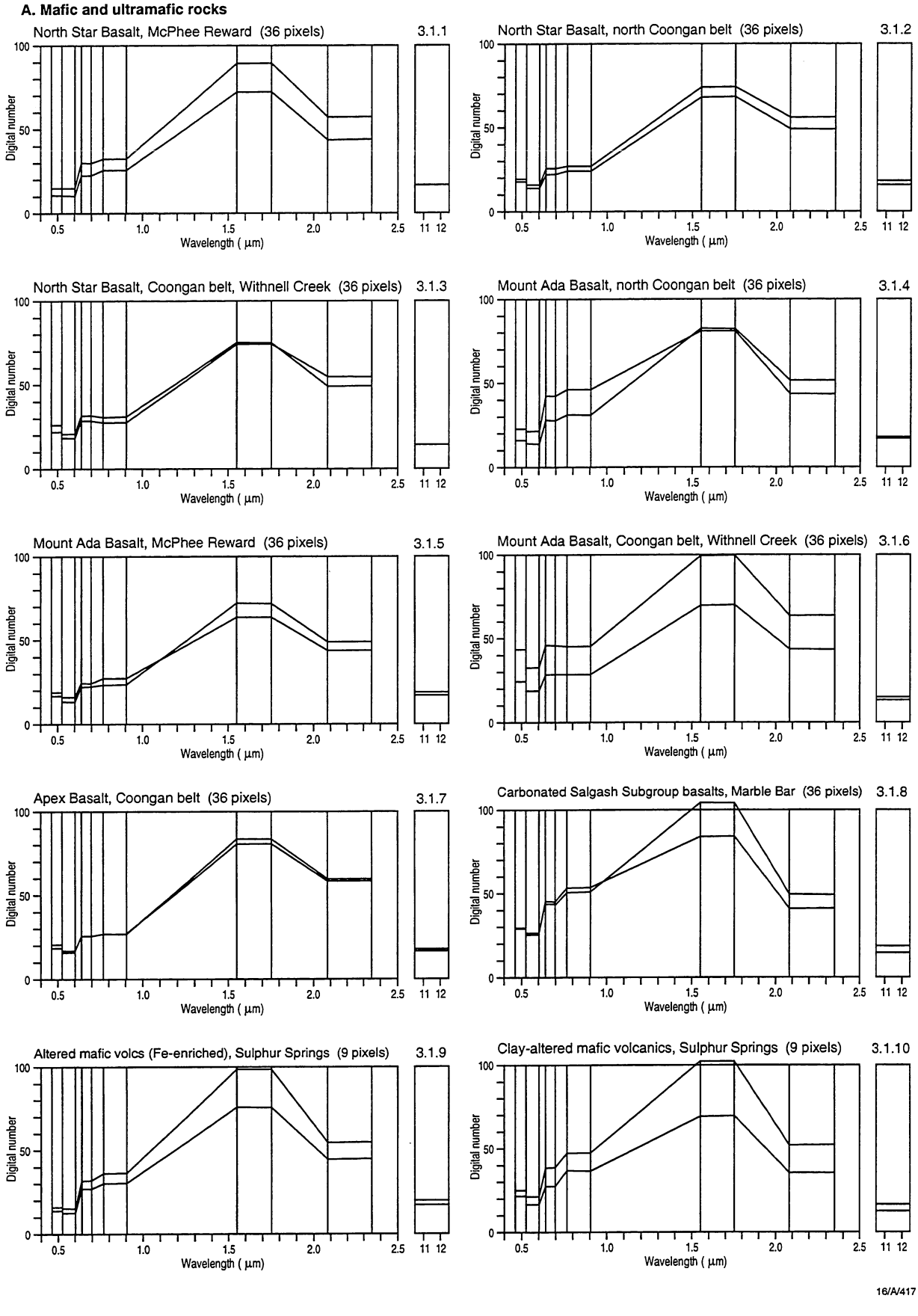

Figure 3.1 Mean reflectance values in DN (Digital Number) for Landsat-5-TM lithologically relatively uniform sub-image test areas within the Marble Bar and Nullagine 1:250 000 sheet areas, Pilbara Craton.

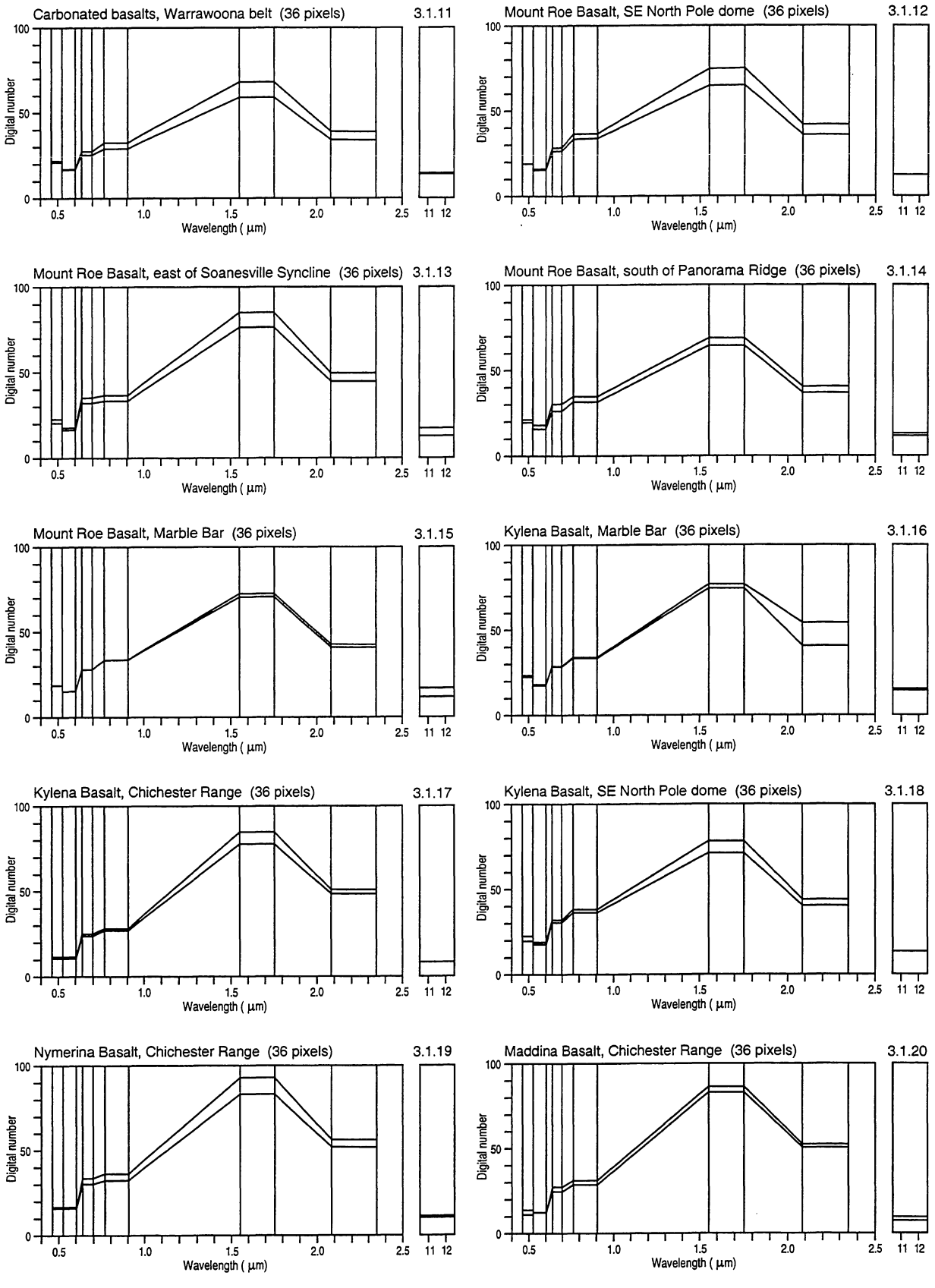

Figure 3.1 continued

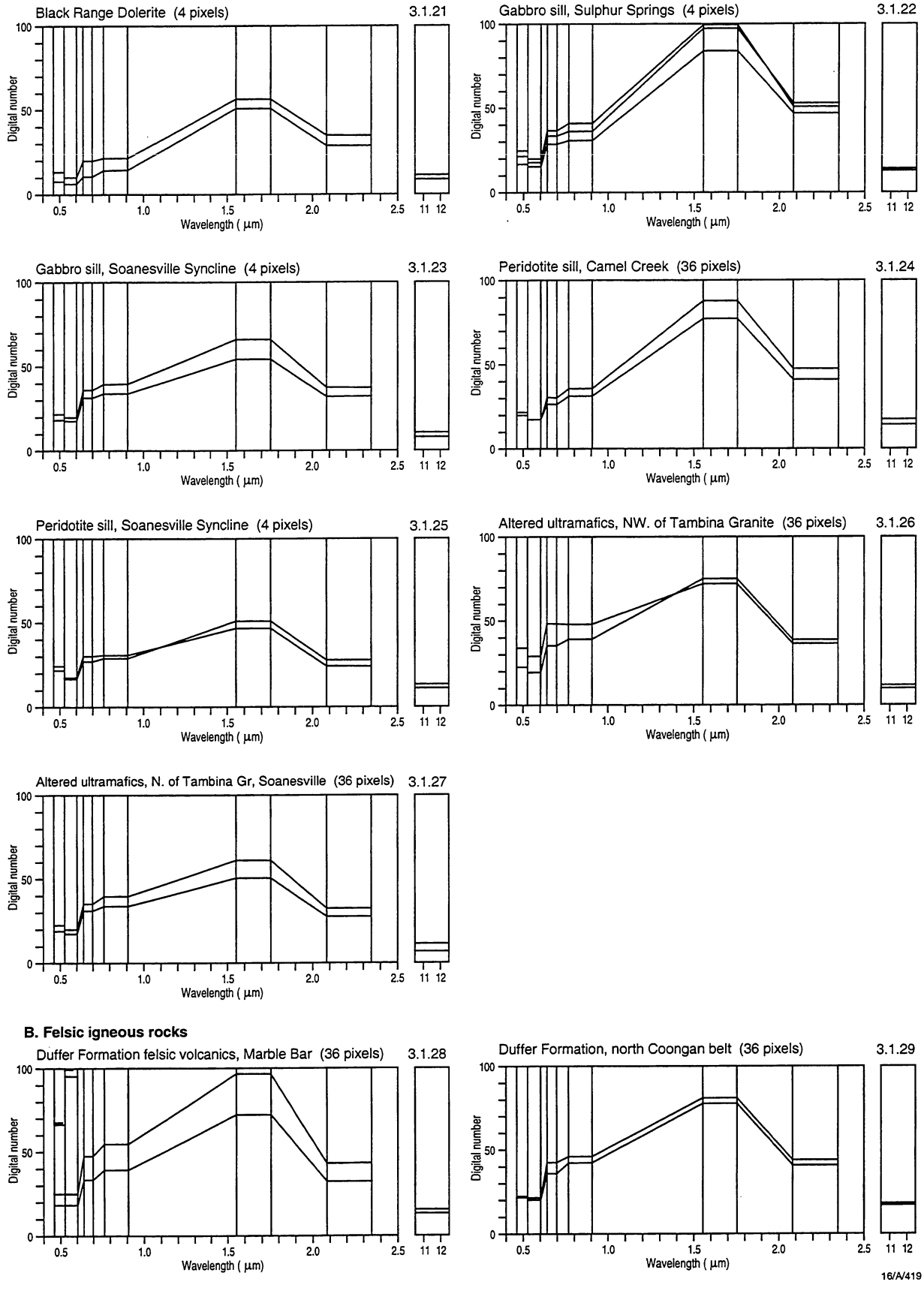

Figure 3.1 continued

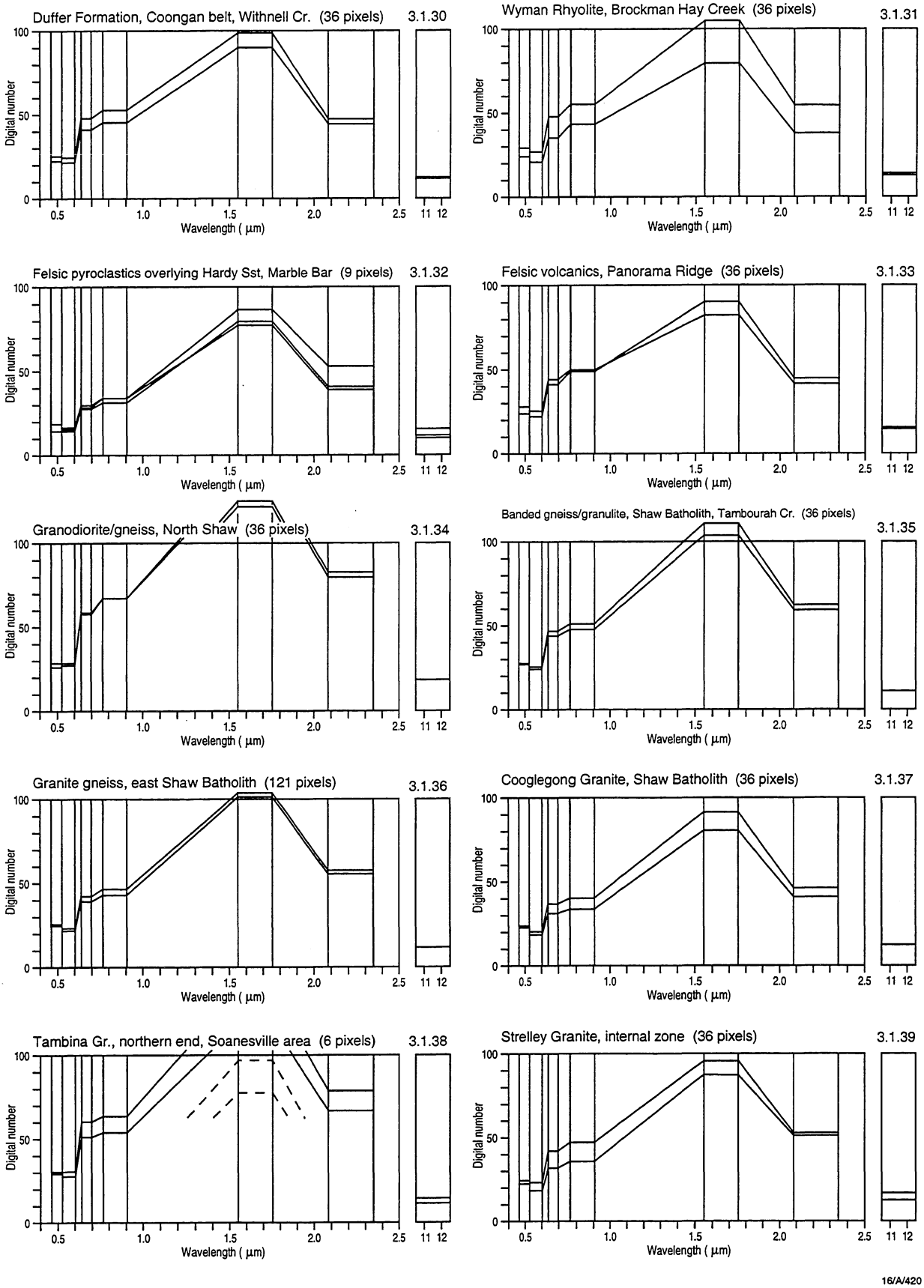

Figure 3.1 continued

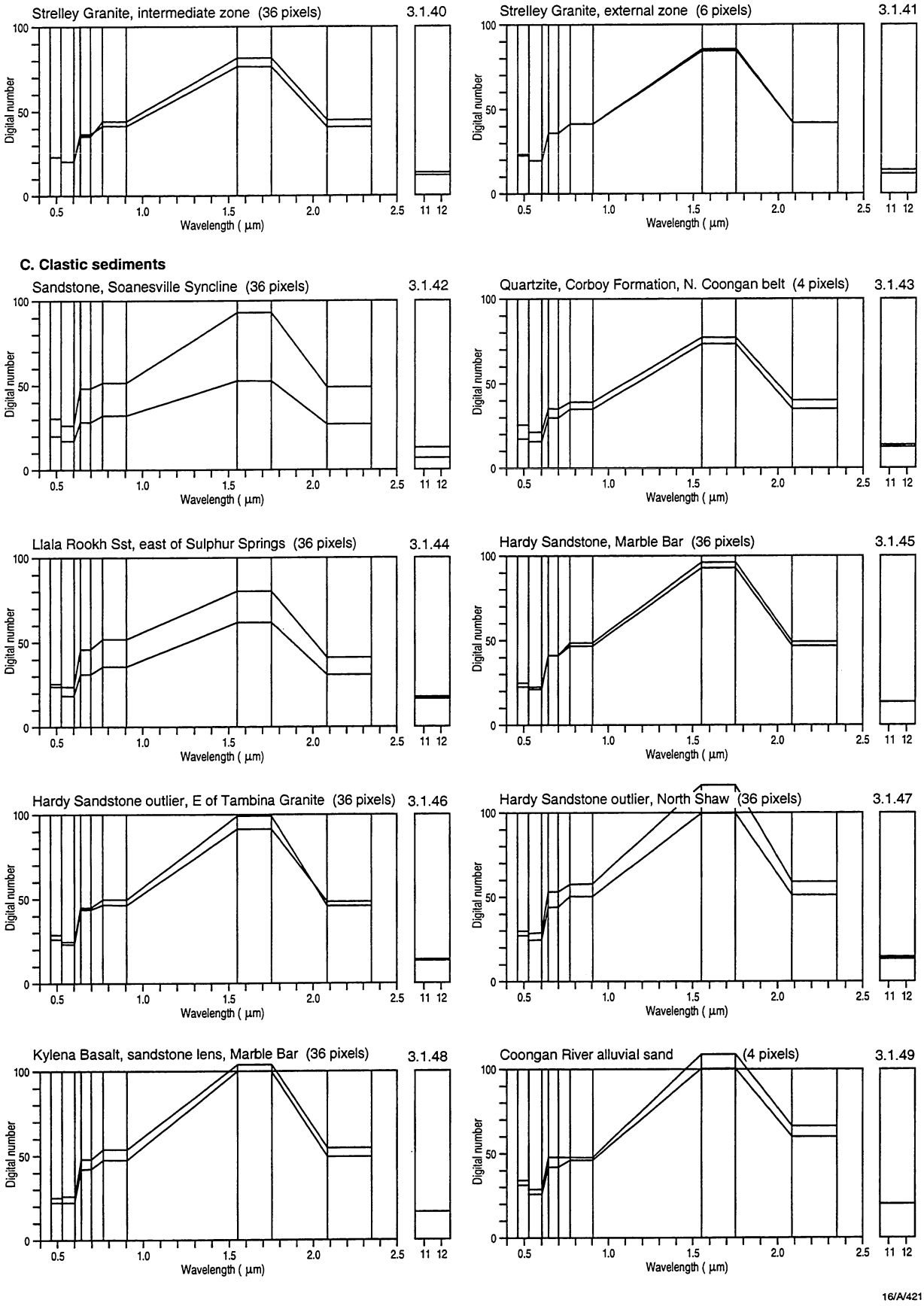

Figure 3.1 continued

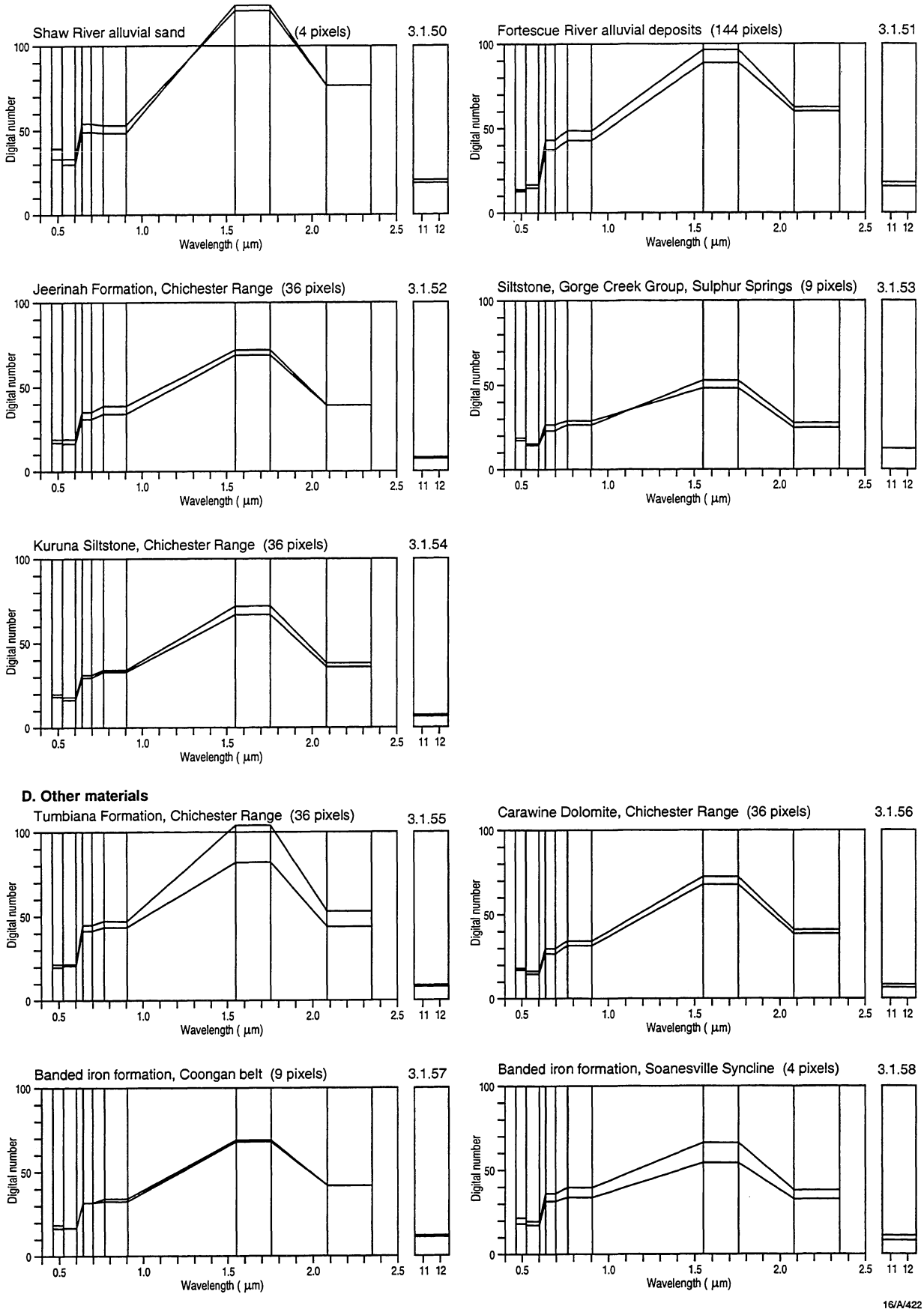

Figure 3.1 continued

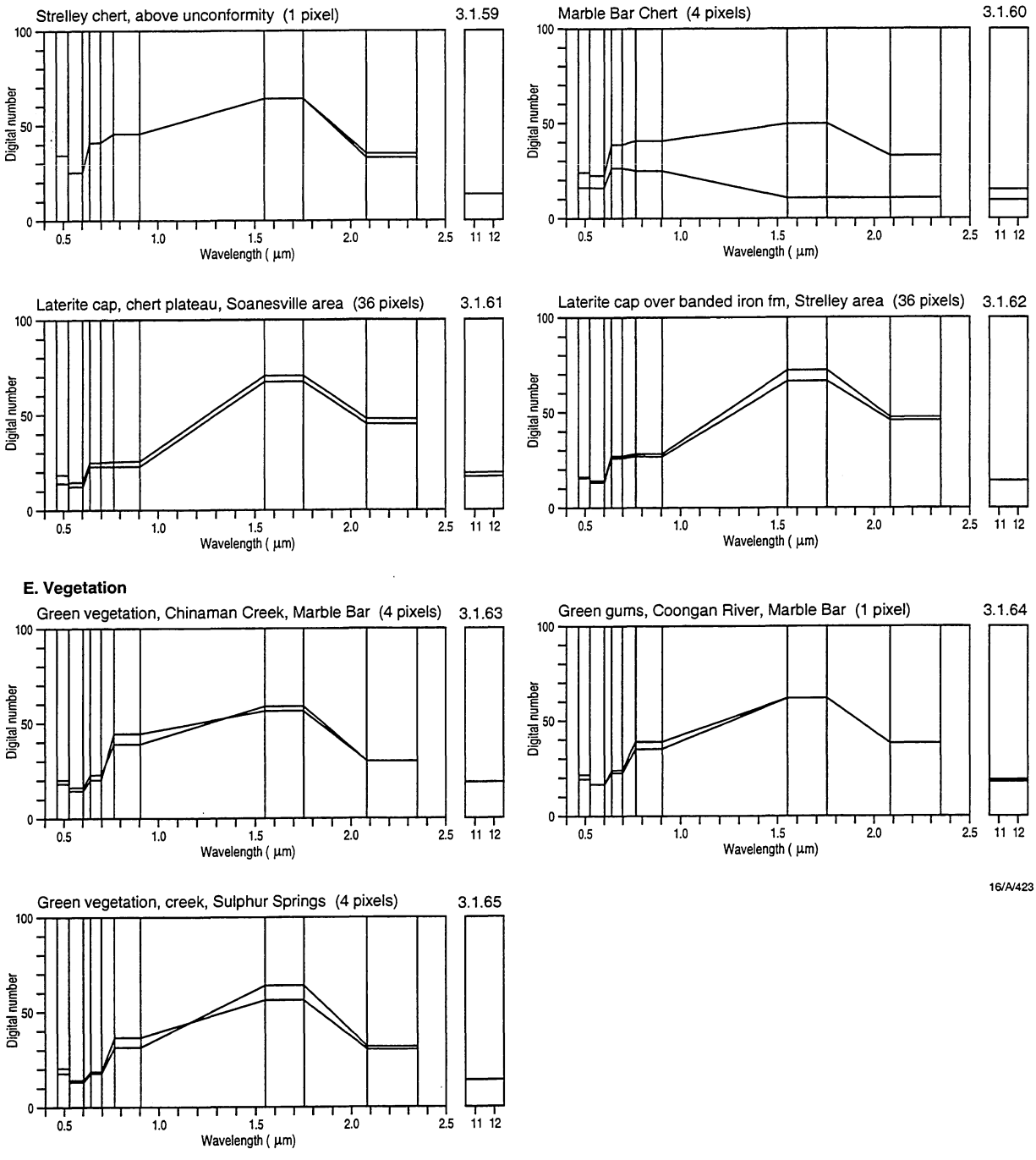

Figure 3.1 continued

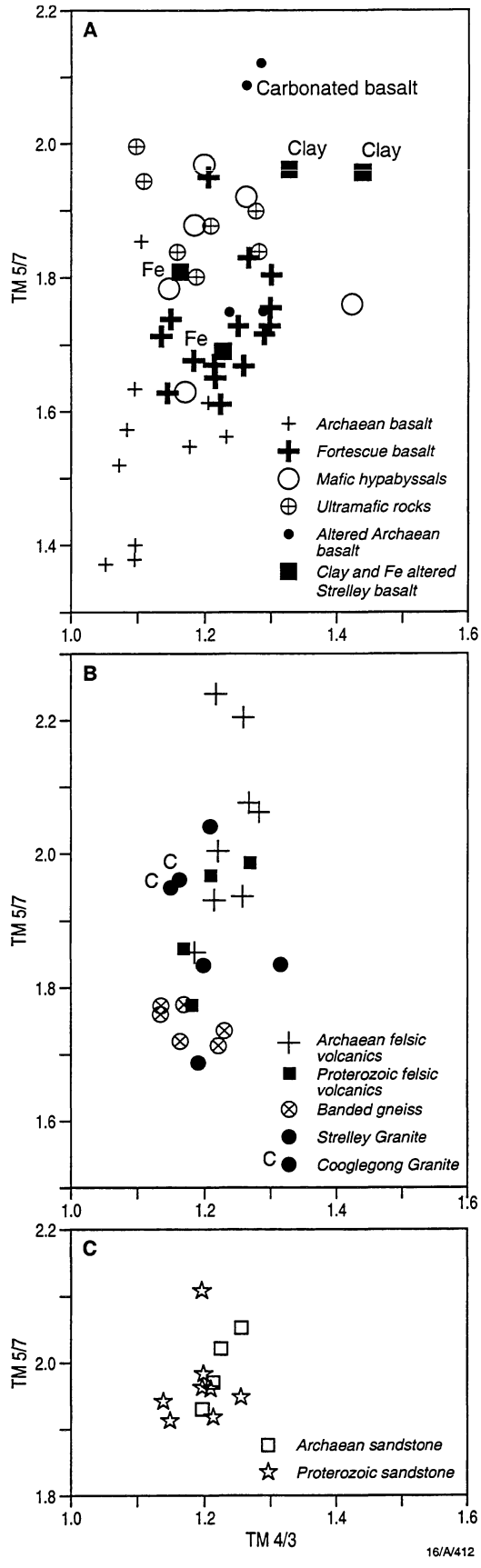

Figure 3.2 - Band ratio 5/7 vs 4/3 plots for mean spectra of test pixel groups in the Marble Bar region. A. mafic and ultramafic rocks; B. felsic igneous rocks; C. sediments.

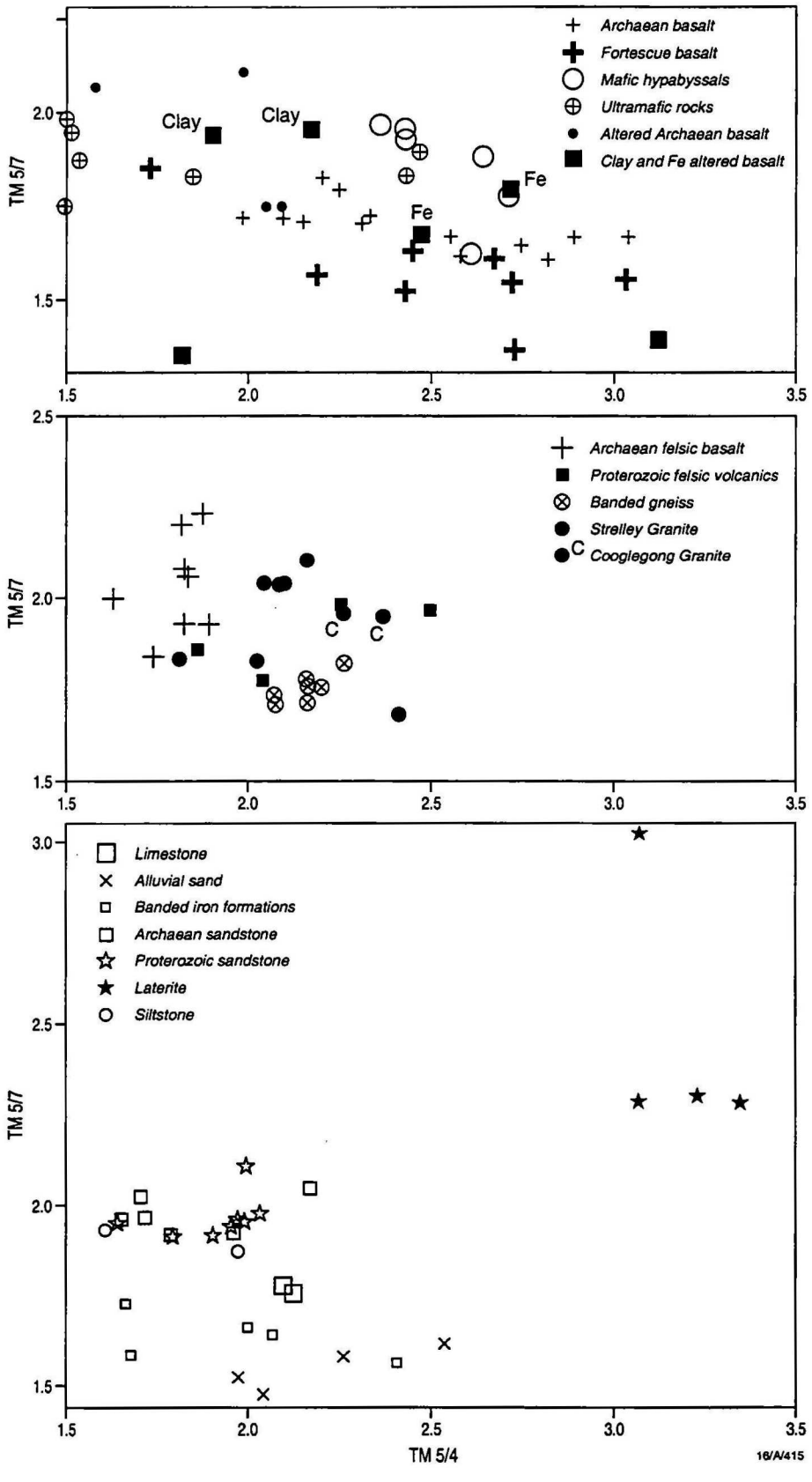

Figure 3.3 - Band ratio 5/7 vs 5/4 plots for mean spectra of test pixel groups in the Marble Bar block. A. mafic and ultramafic rocks; B. felsic igneous rocks; C. sediments.

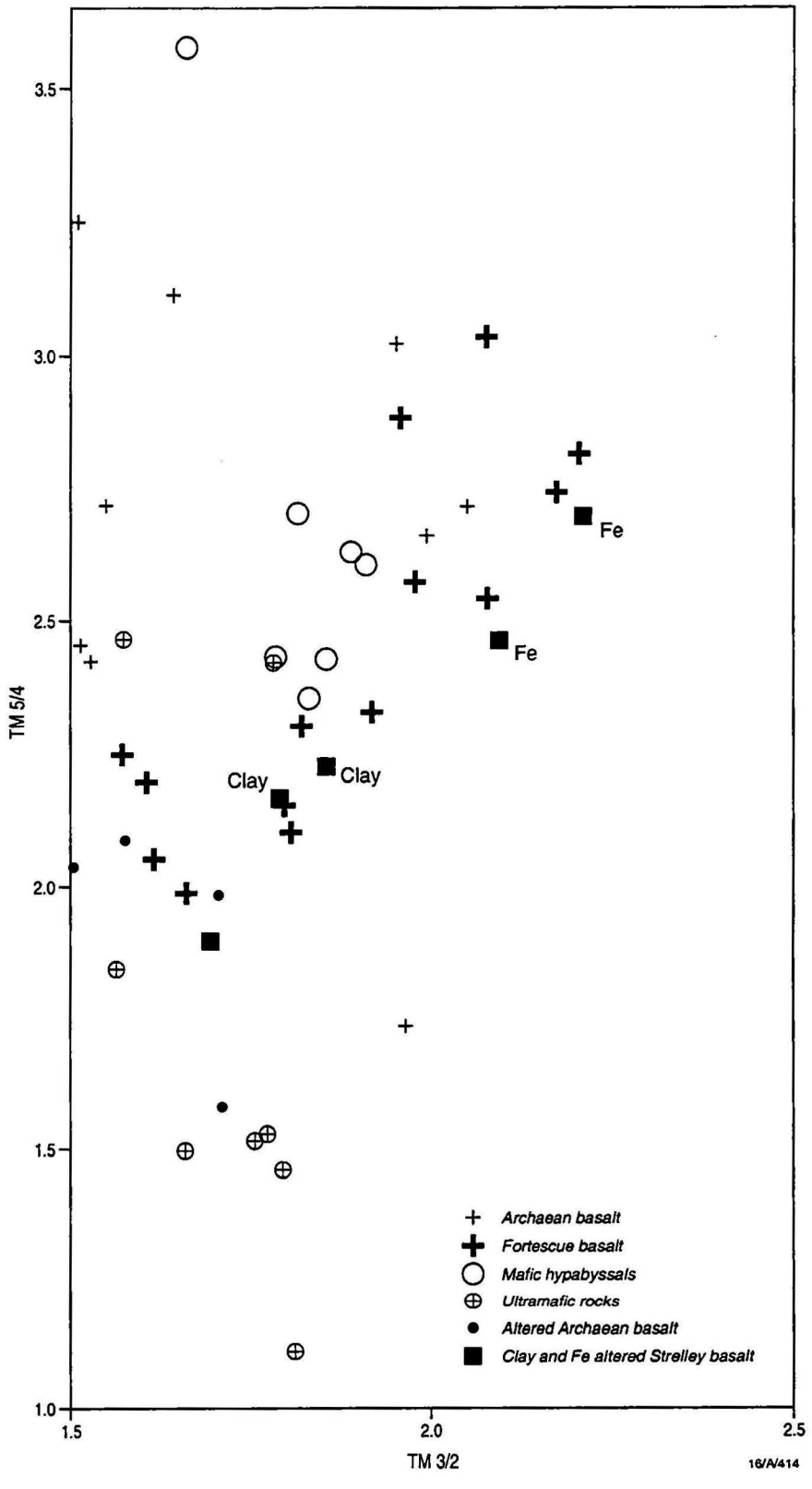

Figure 3.4 - Band ratio 5/4 vs 3/2 plots for mean spectra of test pixel groups for mafic igneous rocks in the Marble Bar block.

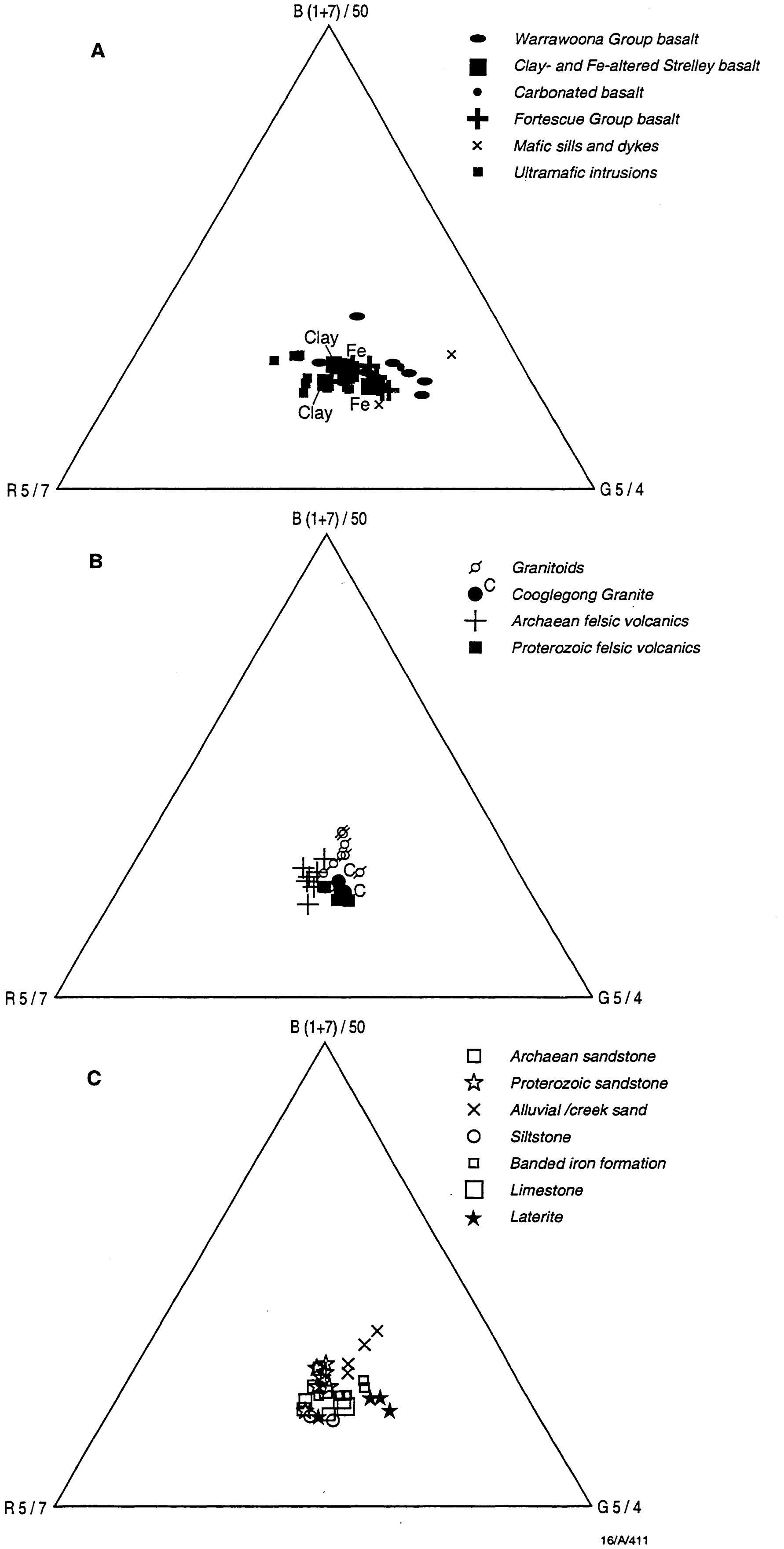

Figure 3.5 - A triangular plot showing the relationships between bands 1+7 (mainly signifying plutonic quartz and derived alluvial sediments), band ratio 5/7 (mainly representing hydrosilicates, clay, carbonate, dry vegetation) and band ratio 5/4 (mainly representing iron oxides). A. mafic and ultramafic rocks; B. felsic igneous rocks; C. sediments.

Fig. 3.6

Figure 3.6 A band 6 (thermal infrared) image for the Soanesville-Tambourah area, showing the high radiance of ferruginous material, in particular laterite. For legend of symbols see Fig. 5.1A.

Fig. 3.7

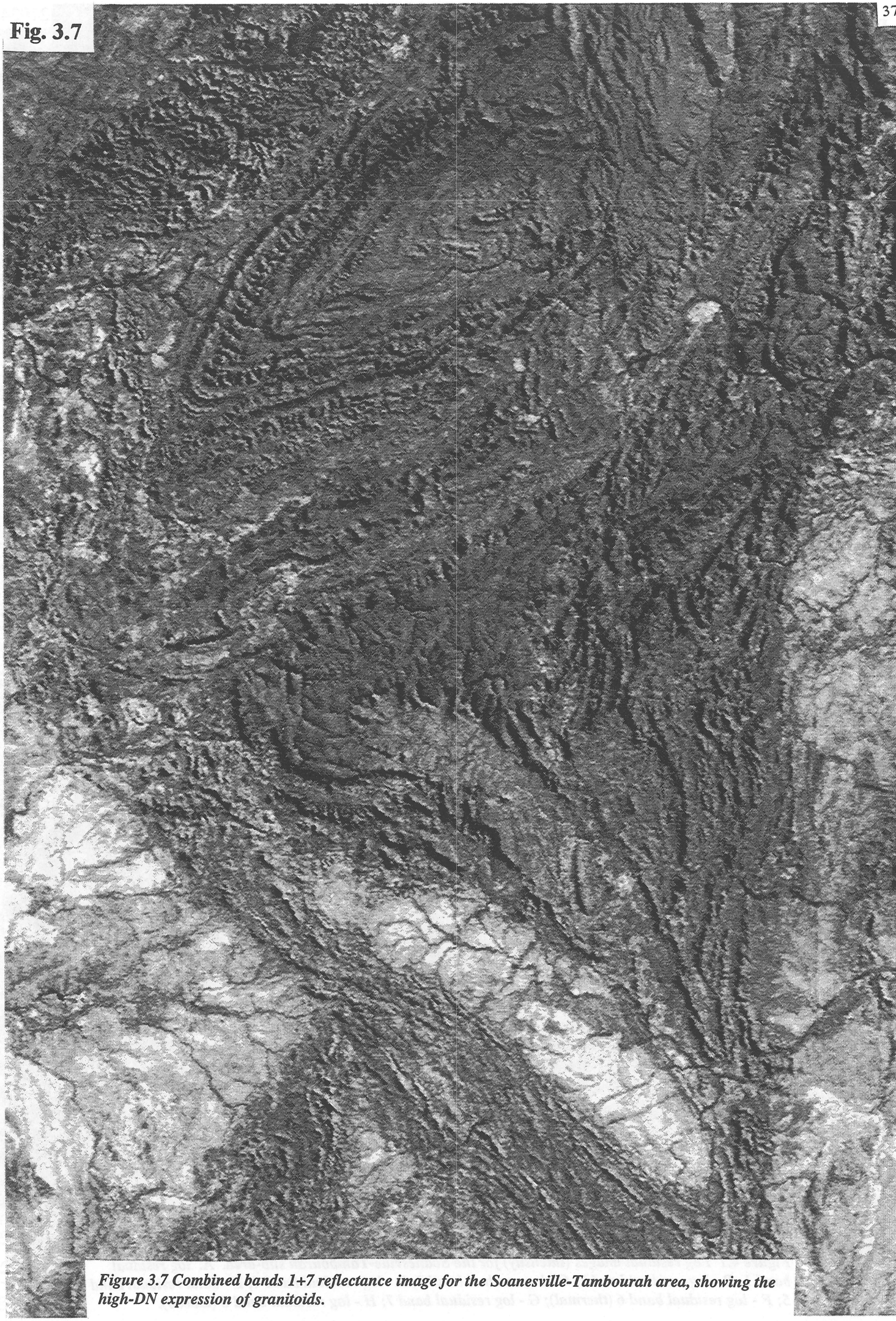

Figure 3.7 Combined bands 1+7 reflectance image for the Soanesville-Tambourah area, showing the high-DN expression of granitoids.

Fig. 4.1A Soanesville-Tambourah area

Figure 4.1 Log residual images (intensity) for the Soanesville-Tambourah sub-area. A. log residual band 1; B - log residual band 2; C - log residual band 3; D - log residual band 4; E - band residual band 5; F - log residual band 6 (thermal); G - log residual band 7; H - log residual band 8 (albedo).

Fig. 4.1B

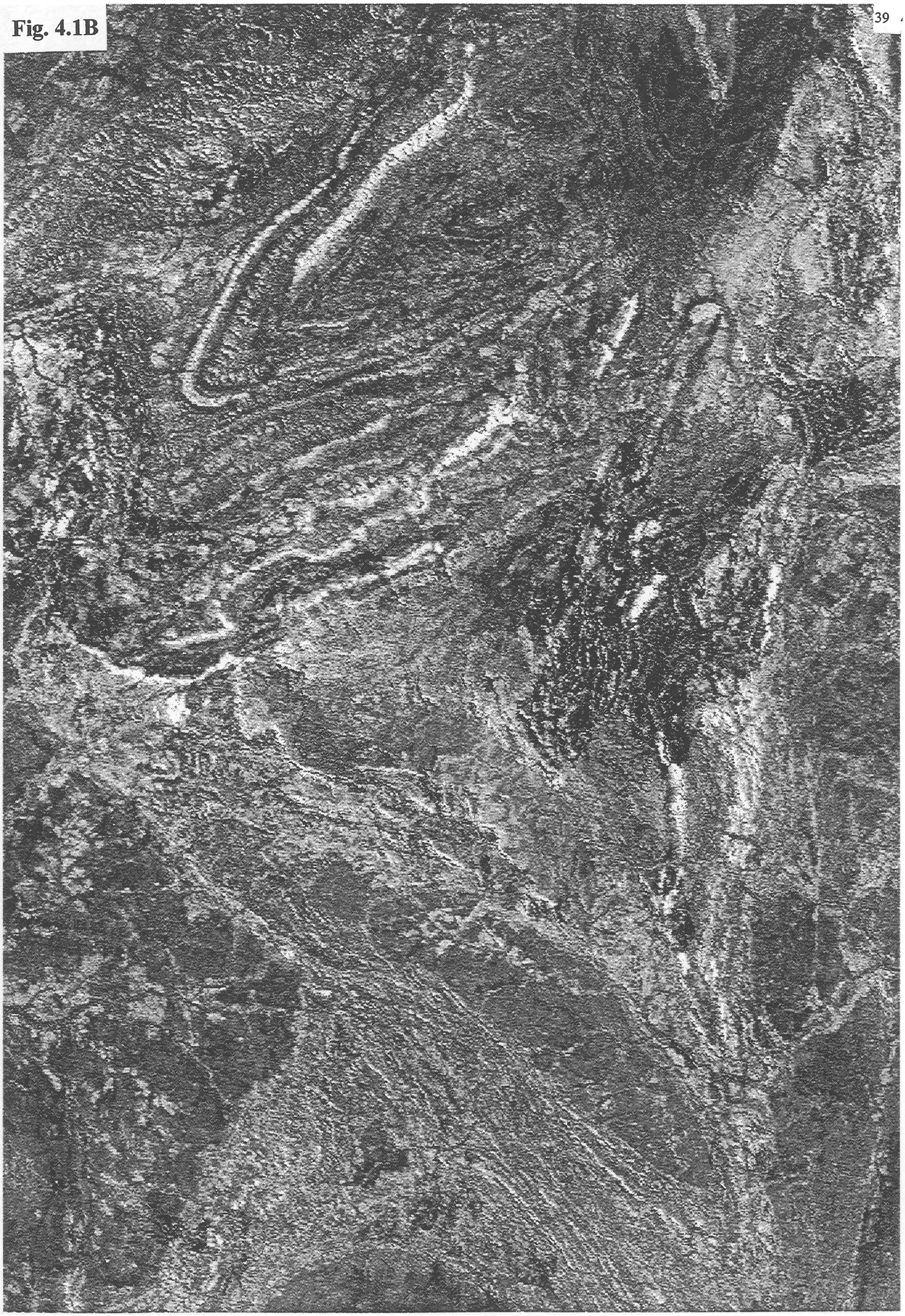

Fig. 4.1C

Fig. 4.1D

Fig. 4.1E

Fig. 4.1F

Fig. 4.1G

Fig. 4.1H

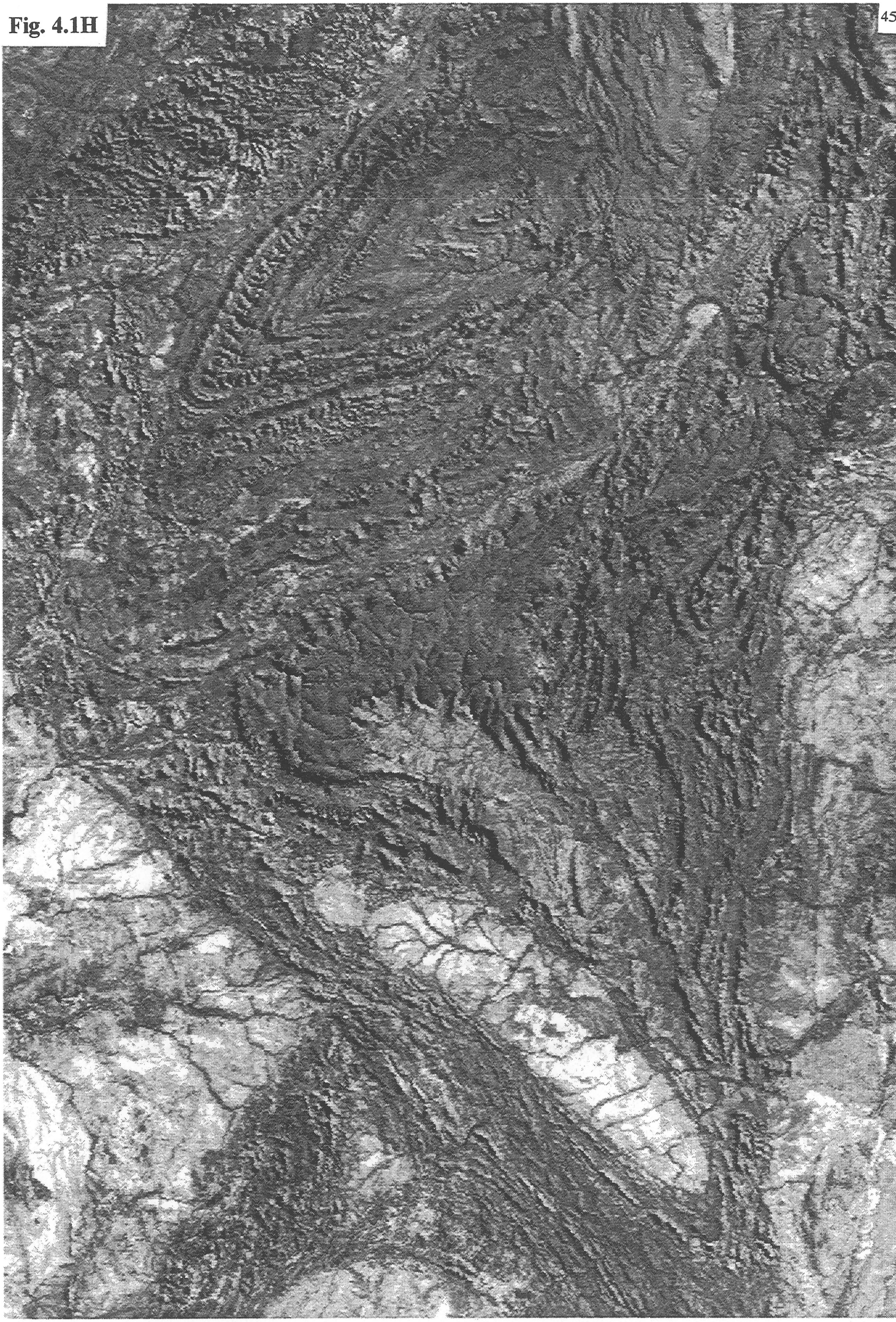

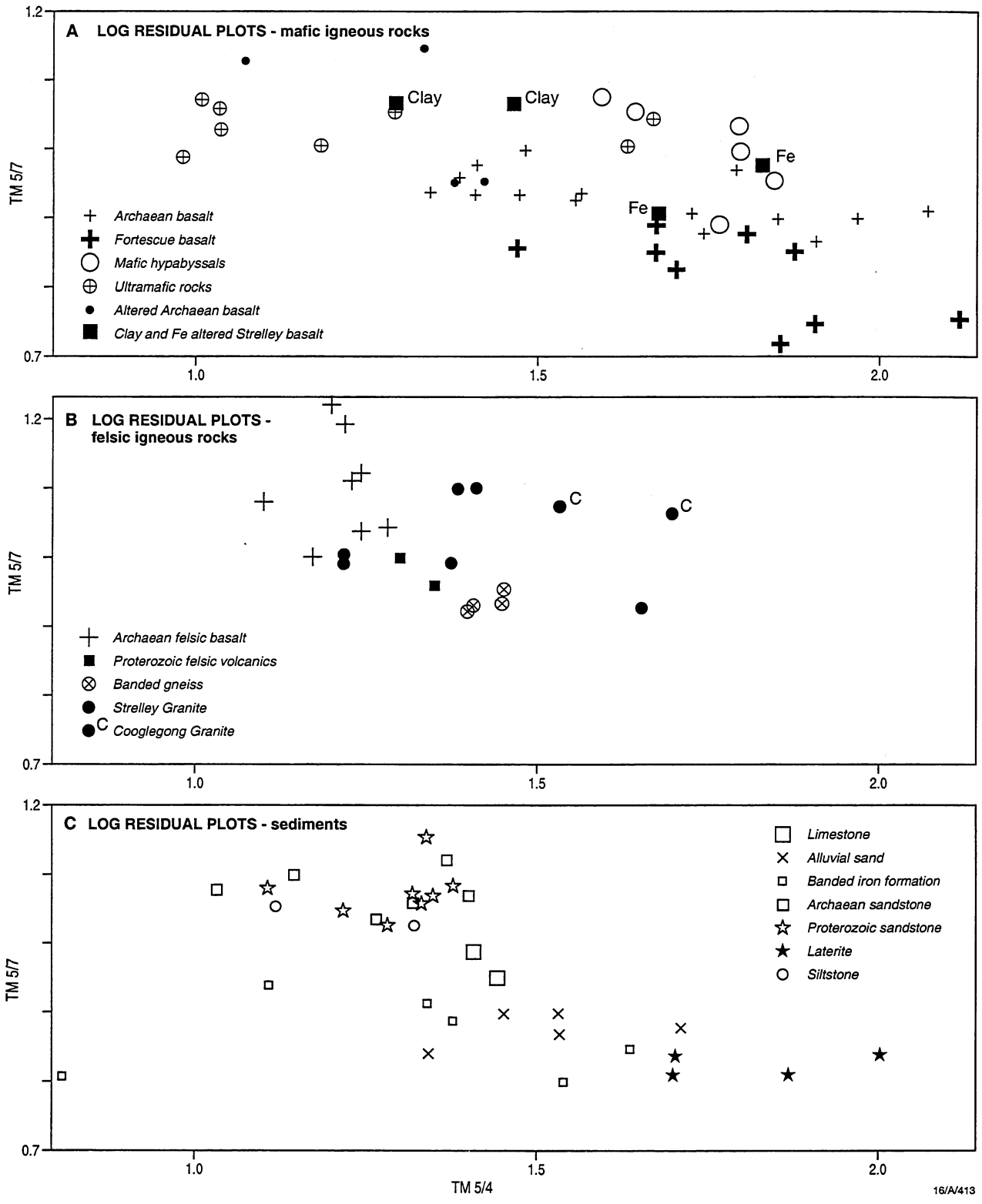

Figure 4.2 - Plots of log residual band ratios 5/7 versus log residual band ratios 5/4 for mean spectra of test pixel groups in the Marble Bar region. A. mafic and ultramafic rocks; B. felsic igneous rocks; C. sediments.

Fig. 5.1A

Figure 5.1 Landsat-5-TM band ratio and band combination images (intensity) for the Soanesville-Tambourah test area (119°02'-119°13'E; 21°24'-21°33'S)(Fig. 8.1); A - 5/7 band ratio; B - 5/4 band ratio; C - 3/2 band ratio; D - 4/3 band ratio.

Fig. 5.1B

Fig. 5.1C

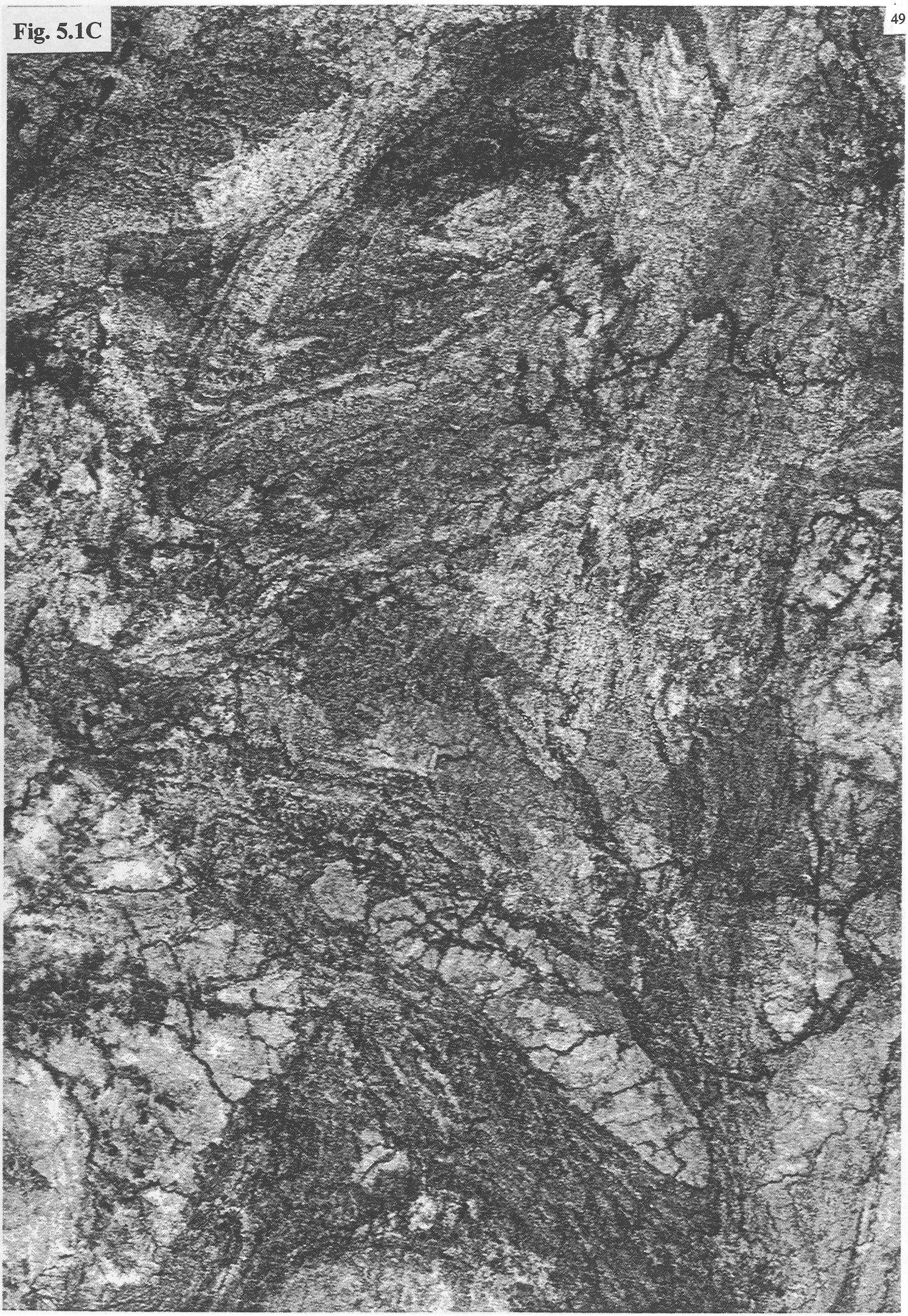

Fig. 5.1D

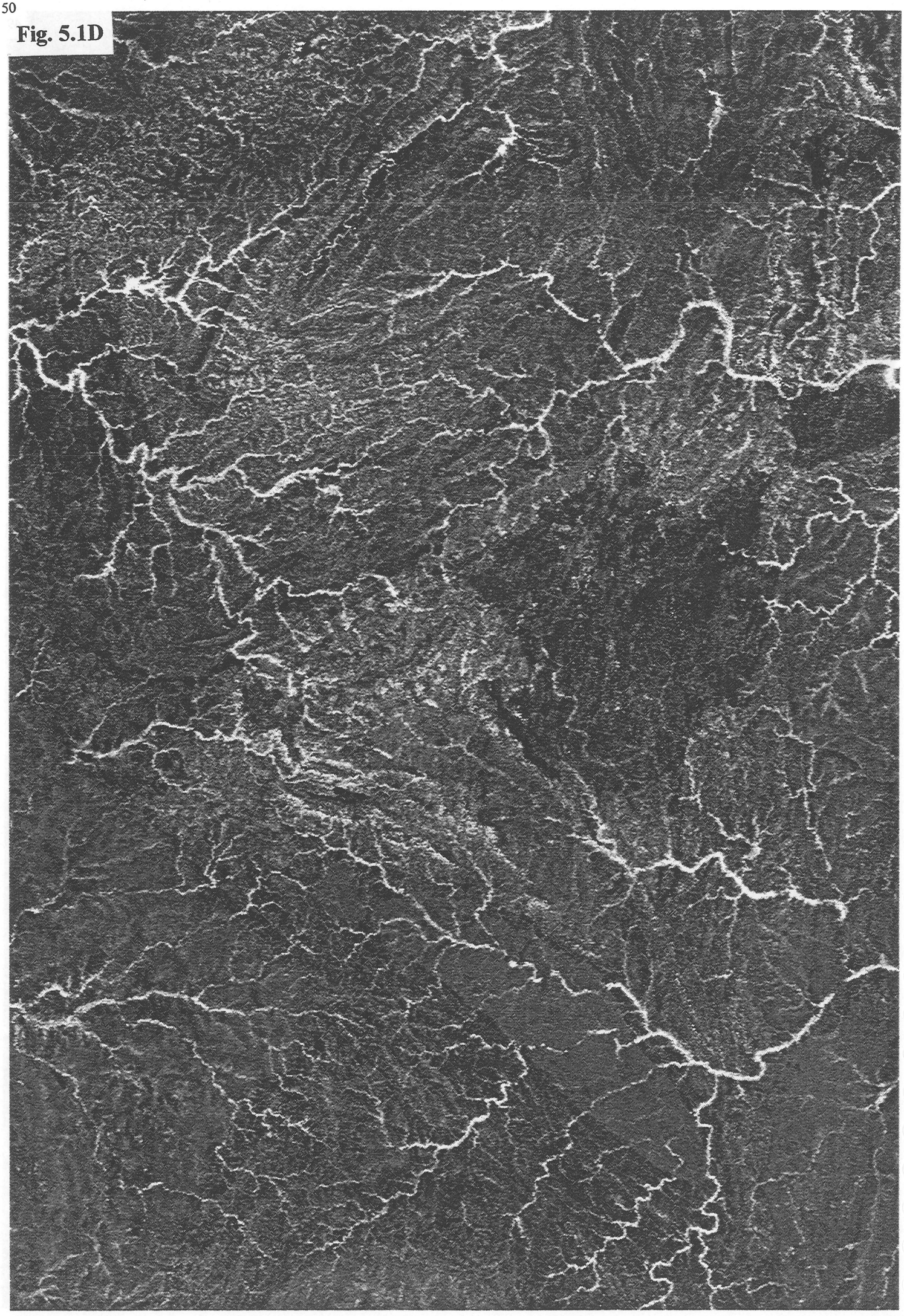

Fig. 6.1A

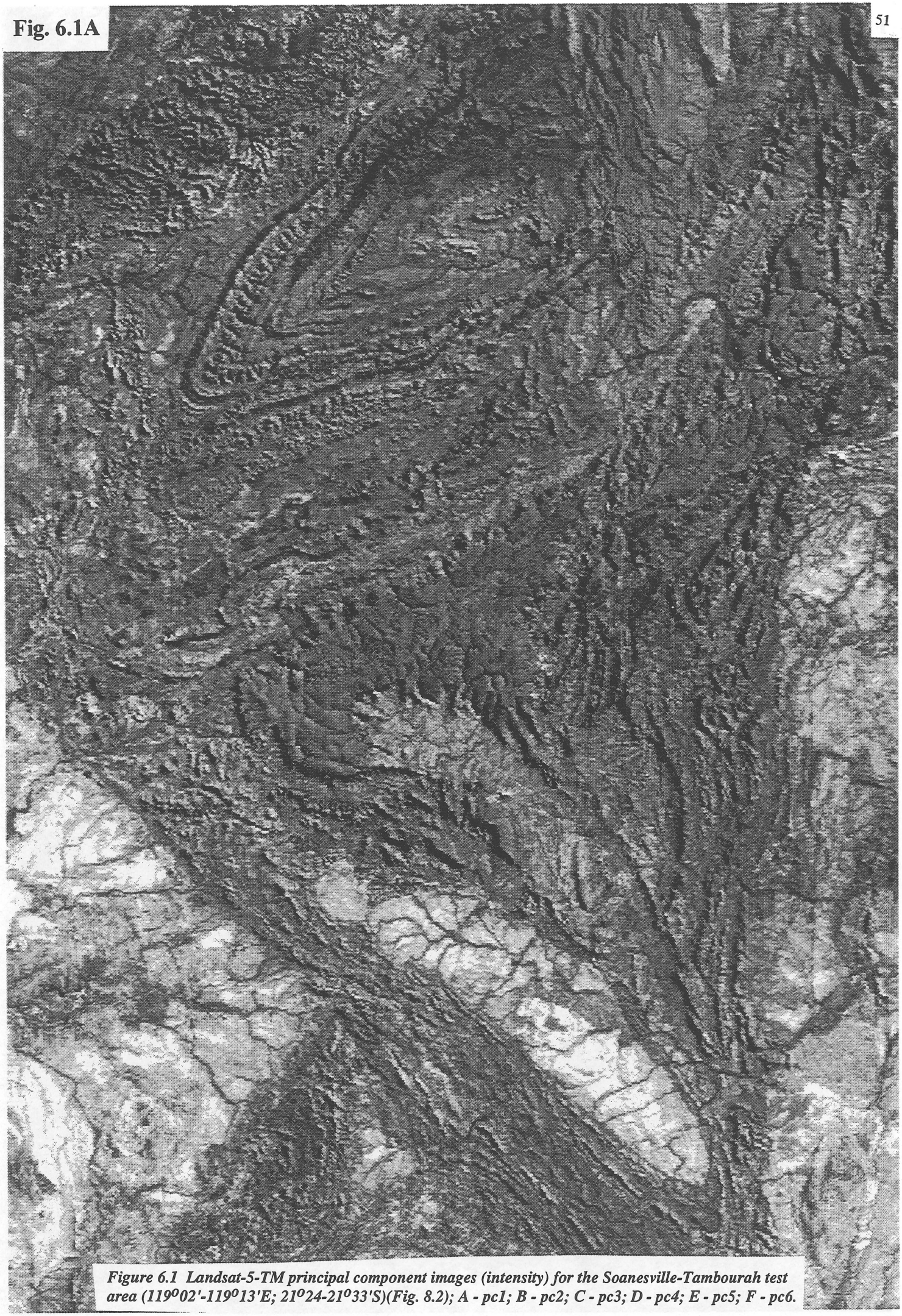

Figure 6.1 Landsat-5-TM principal component images (intensity) for the Soanesville-Tambourah test area (119°02'-119°13'E; 21°24-21°33'S)(Fig. 8.2); A - pc1; B - pc2; C - pc3; D - pc4; E - pc5; F - pc6.

Fig. 6.1B

Fig. 6.1C

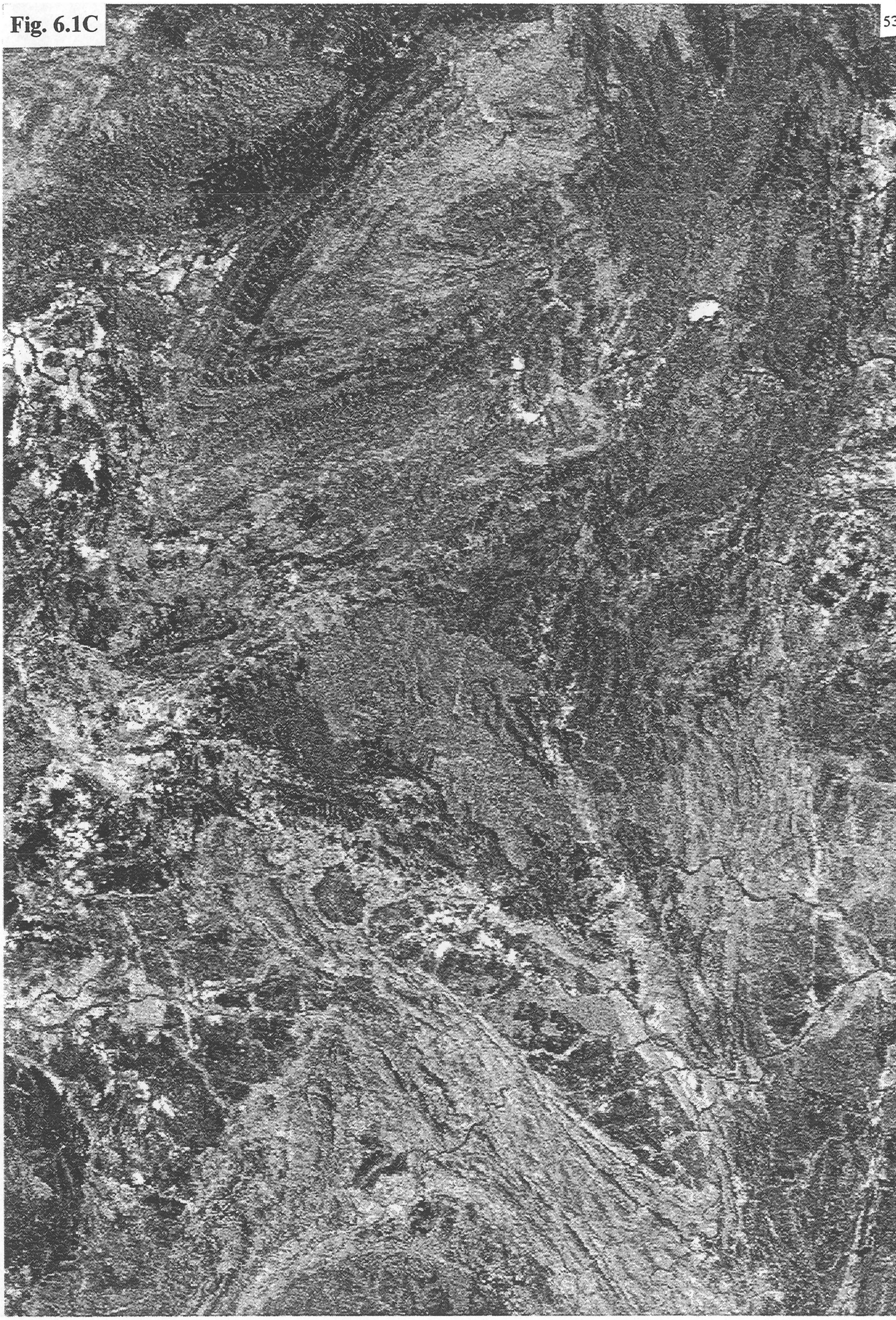

Fig. 6.1D

Fig. 6.1E

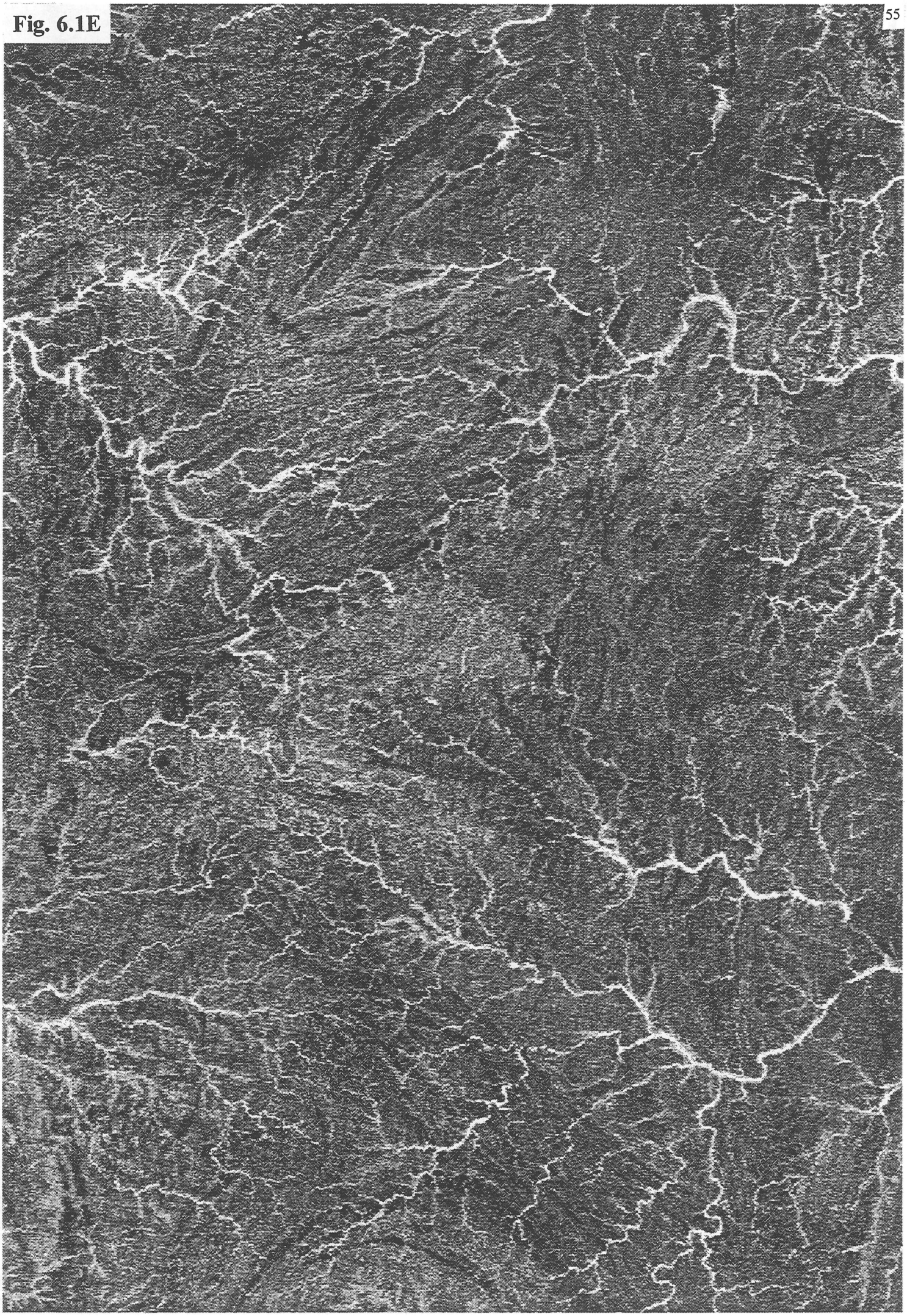

Fig. 6.1F

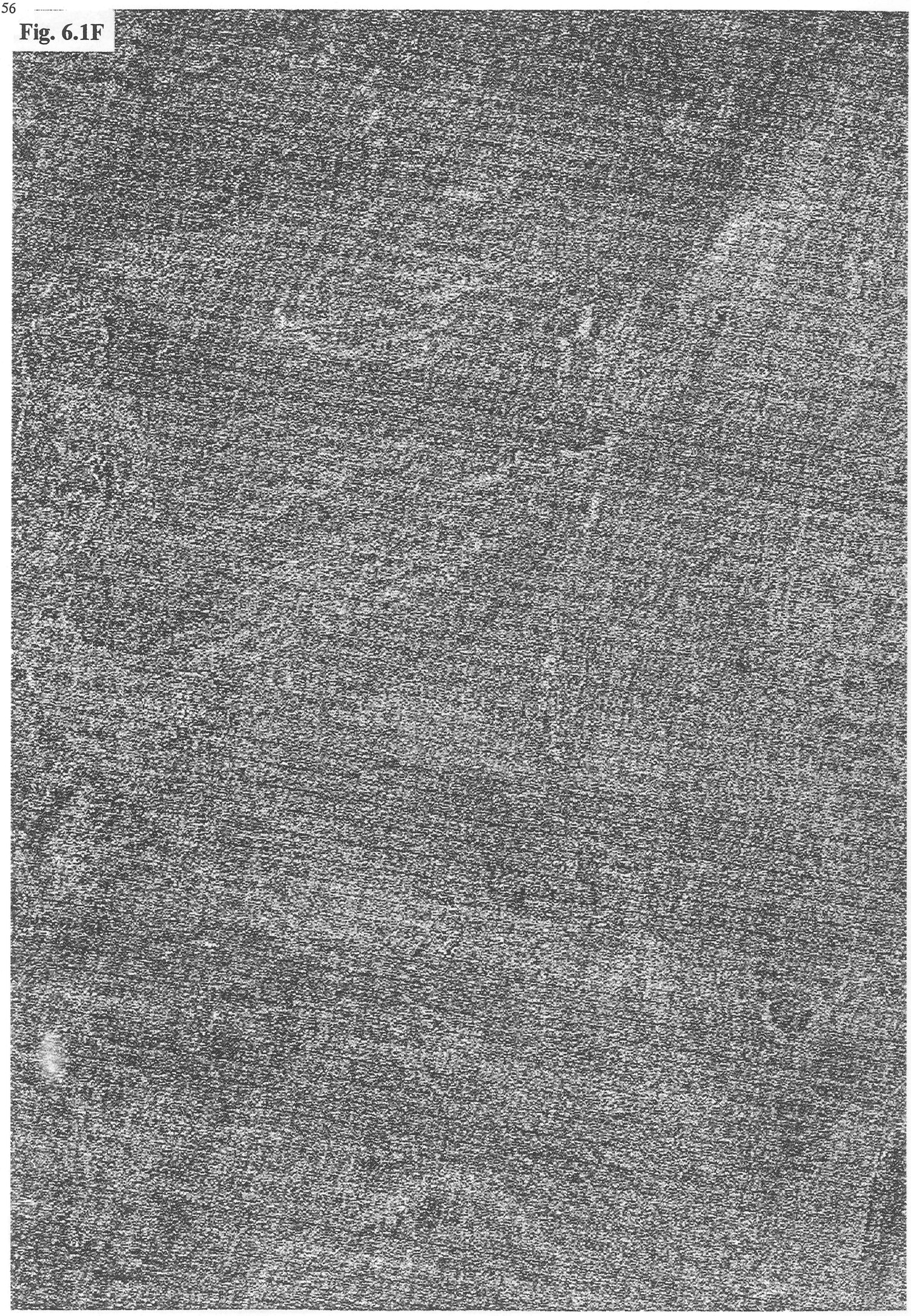

Fig. 7.1

Figure 7.1 K-Th-U gamma ray spectrometric image of the Mount Edgar and Corruna Downs batholiths, Marble Bar and Nullagine 1:250 000 sheet areas.

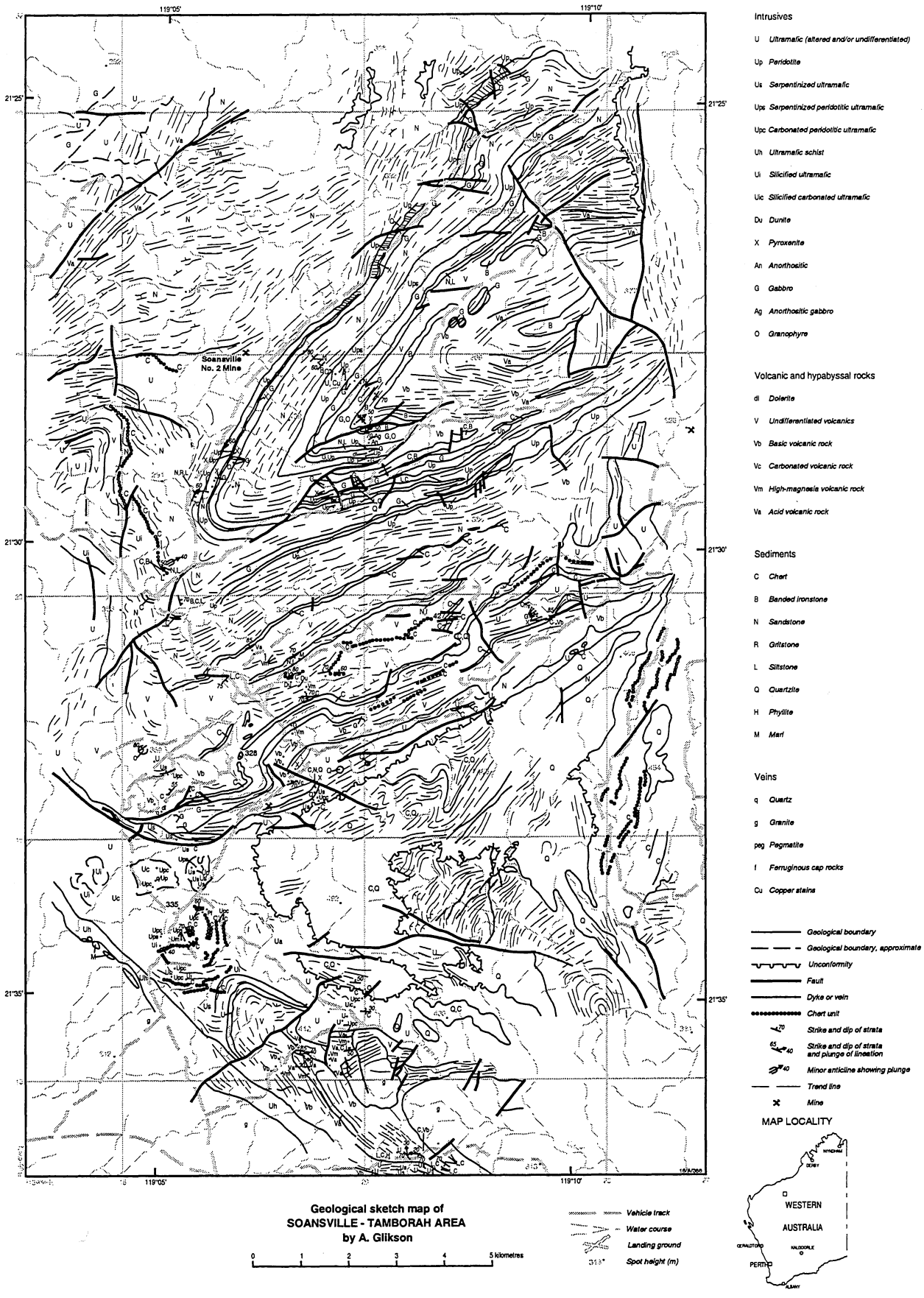

Figure 8.1 - A Geological sketch map of the Soanesville-Tambourah area (21°24-21°33'S;119°2'-119°13'E), Marble Bar 1:250 000 Sheet area.

Fig. 8.2

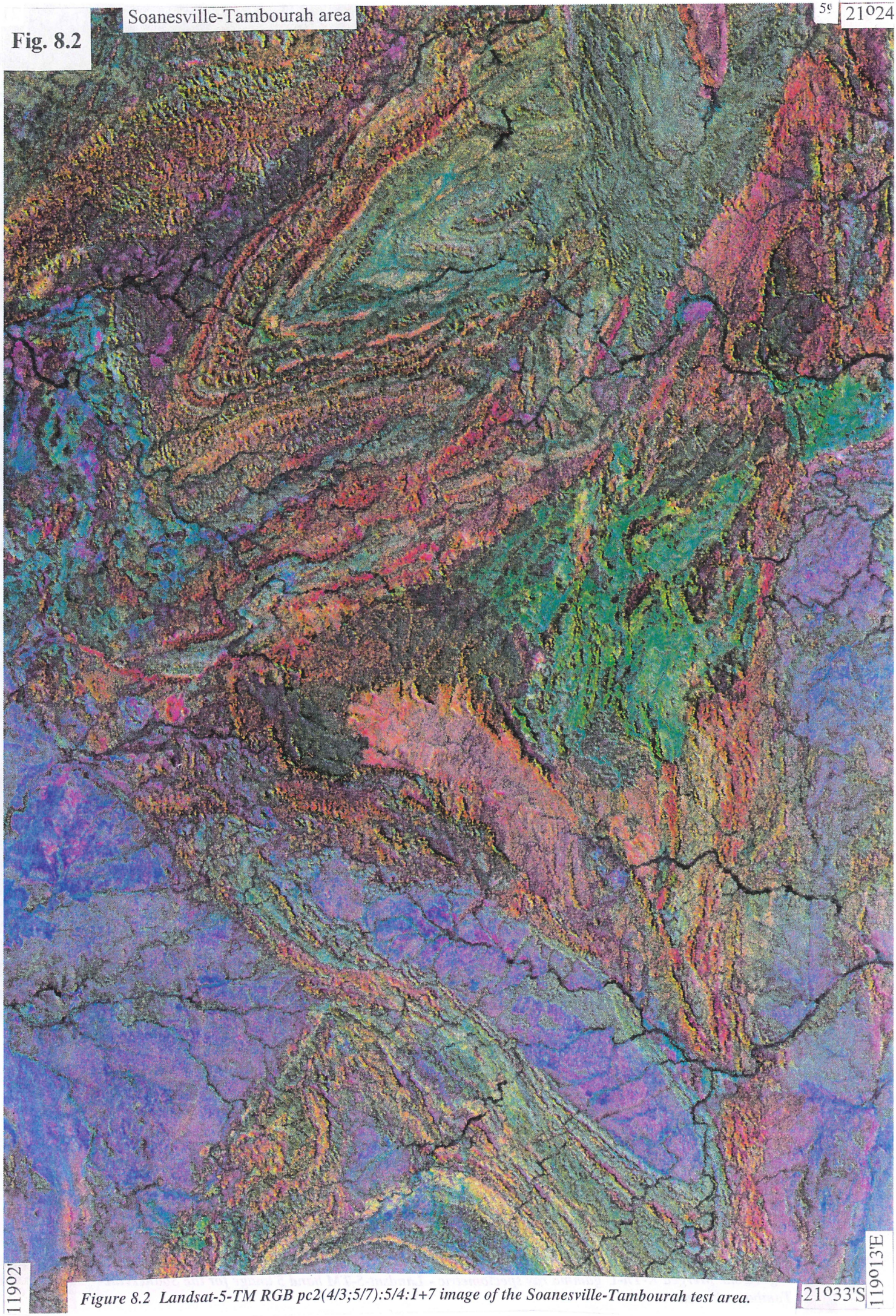

Figure 8.2 Landsat-5-TM RGB pc2(4/3;5/7):5/4:1+7 image of the Soanesville-Tambourah test area.

Fig. 8.3

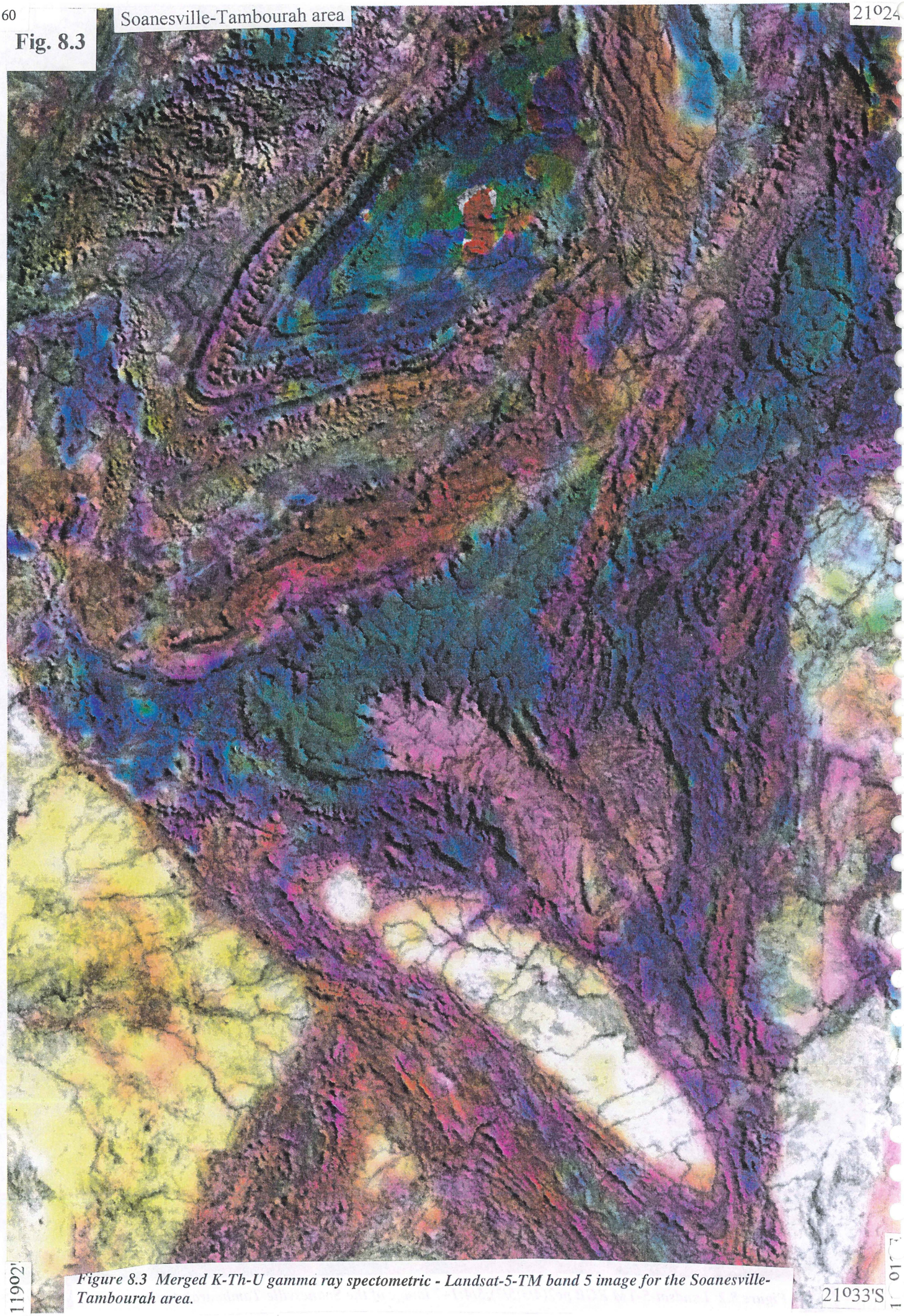

Figure 8.3 Merged K-Th-U gamma ray spectometric - Landsat-5-TM band 5 image for the Soanesville-Tambourah area.

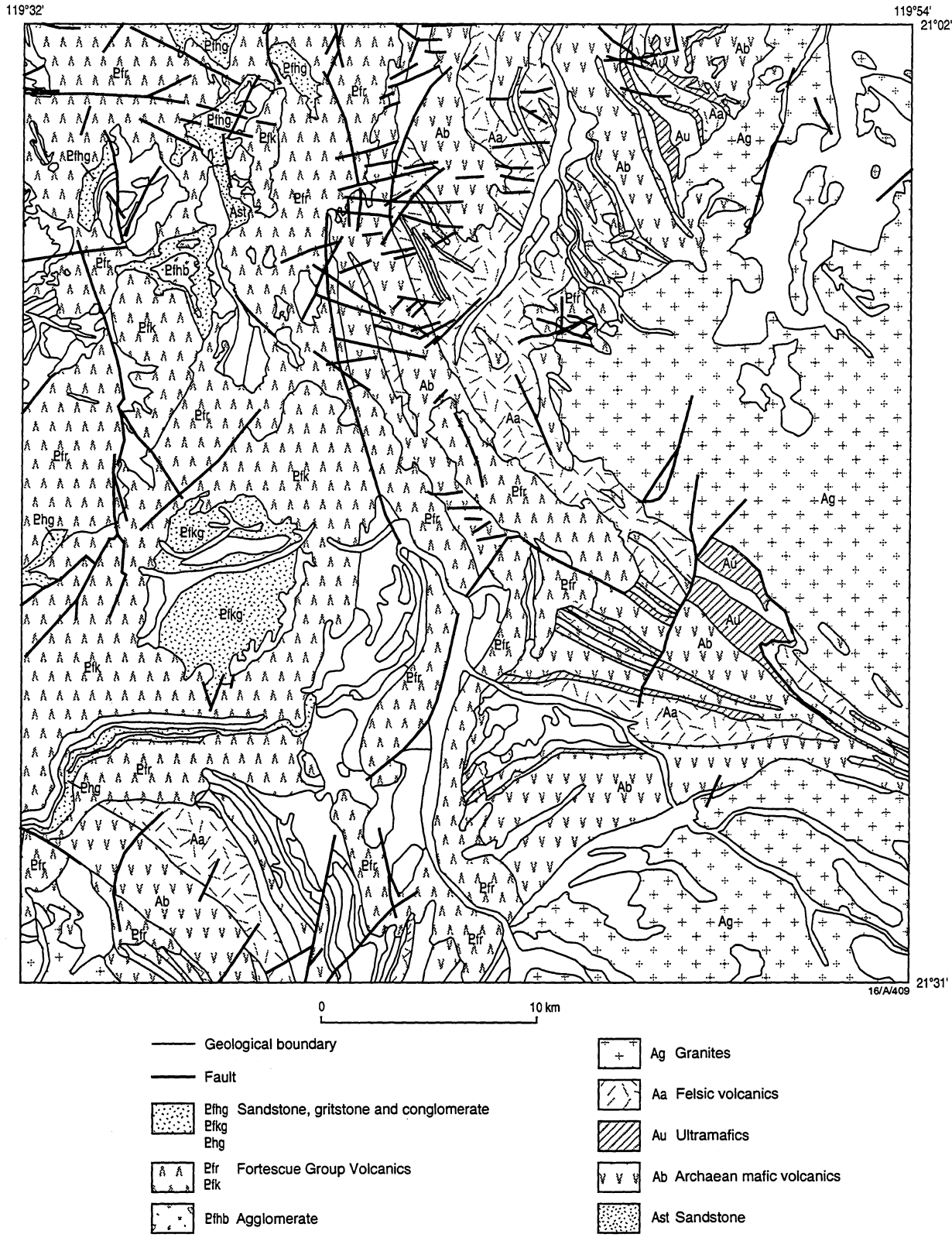

Figure 8.4 - Geological sketch map of the Marble Bar-Camel Creek area (21°02'-21°26'S; 119°32'-119° 54'E), Marble Bar 1:250 000 sheet area.

Fig. 8.5

Figure 8.5 Landsat-5-TM RGB pc2(4/3;5/7):5/4:1+7 image of the Marble Bar-Camel Creek area.

Fig. 8.6

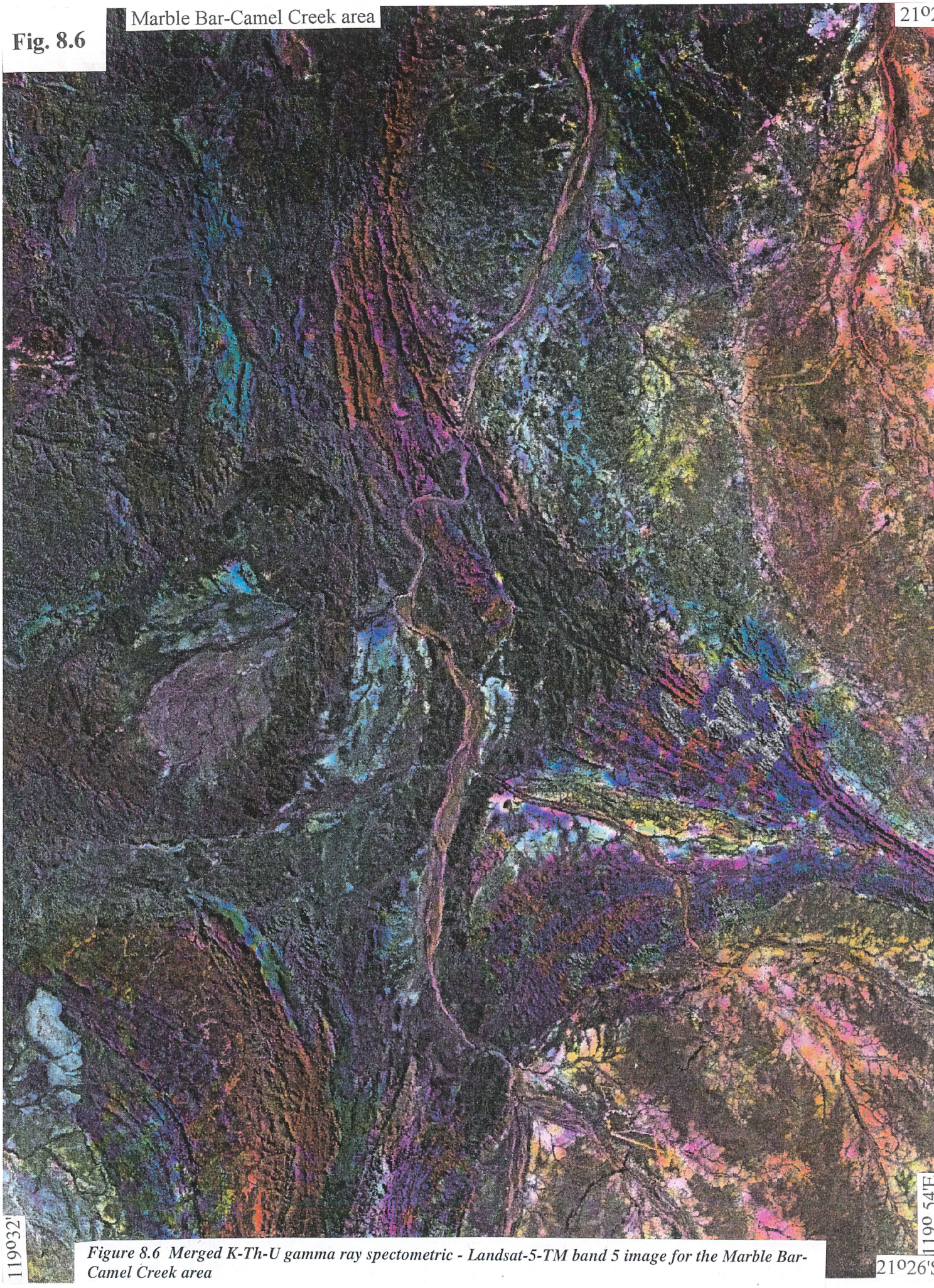

Figure 8.6 Merged K-Th-U gamma ray spectometric - Landsat-5-TM band 5 image for the Marble Bar-Camel Creek area

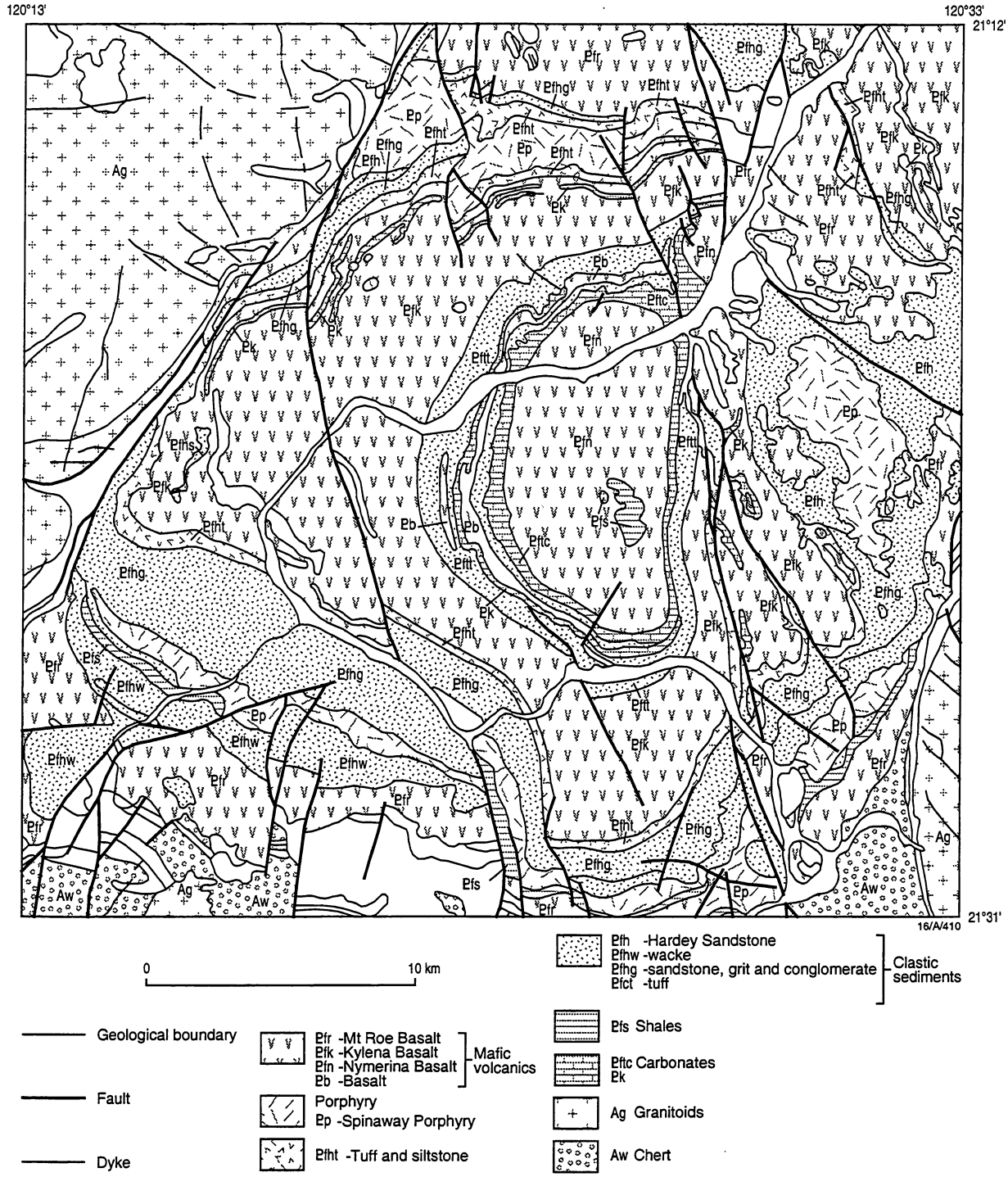

Figure 9.1 - Geological sketch map of the Meentheena syncline area (21°12-21°31'S;120°13'-120°33'E), Nullagine 1:250 000 Sheet area.

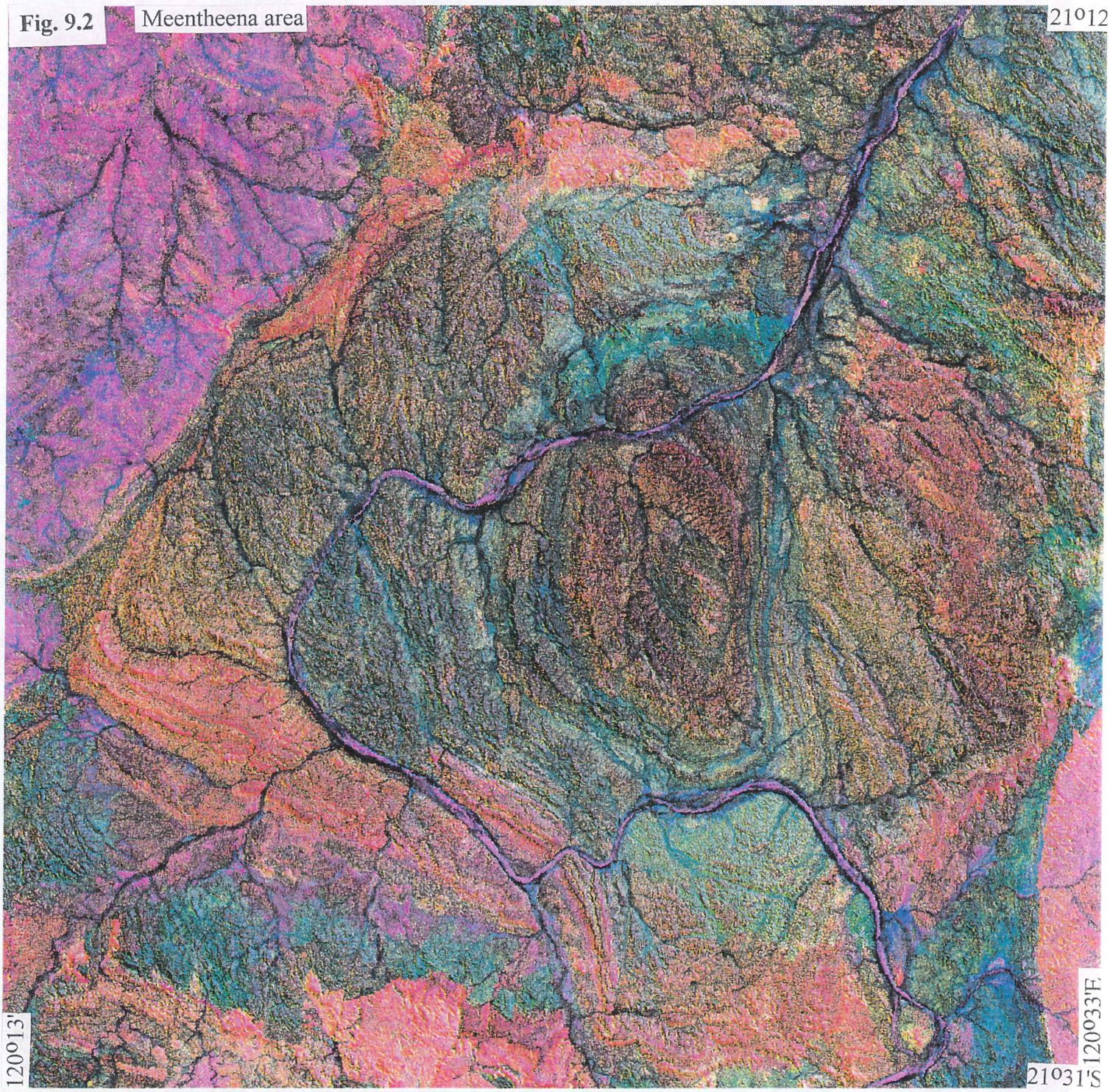

Figure 9.2 Landsat-5-TM RGB pc2(4/3;5/7):5/4:1+7 image of the Meentheena syncline area.

Fig. 9.3

Figure 9.3 Merged K-Th-U gamma ray spectometric - Landsat-5-TM band 5 image for the Meentheena syncline area.

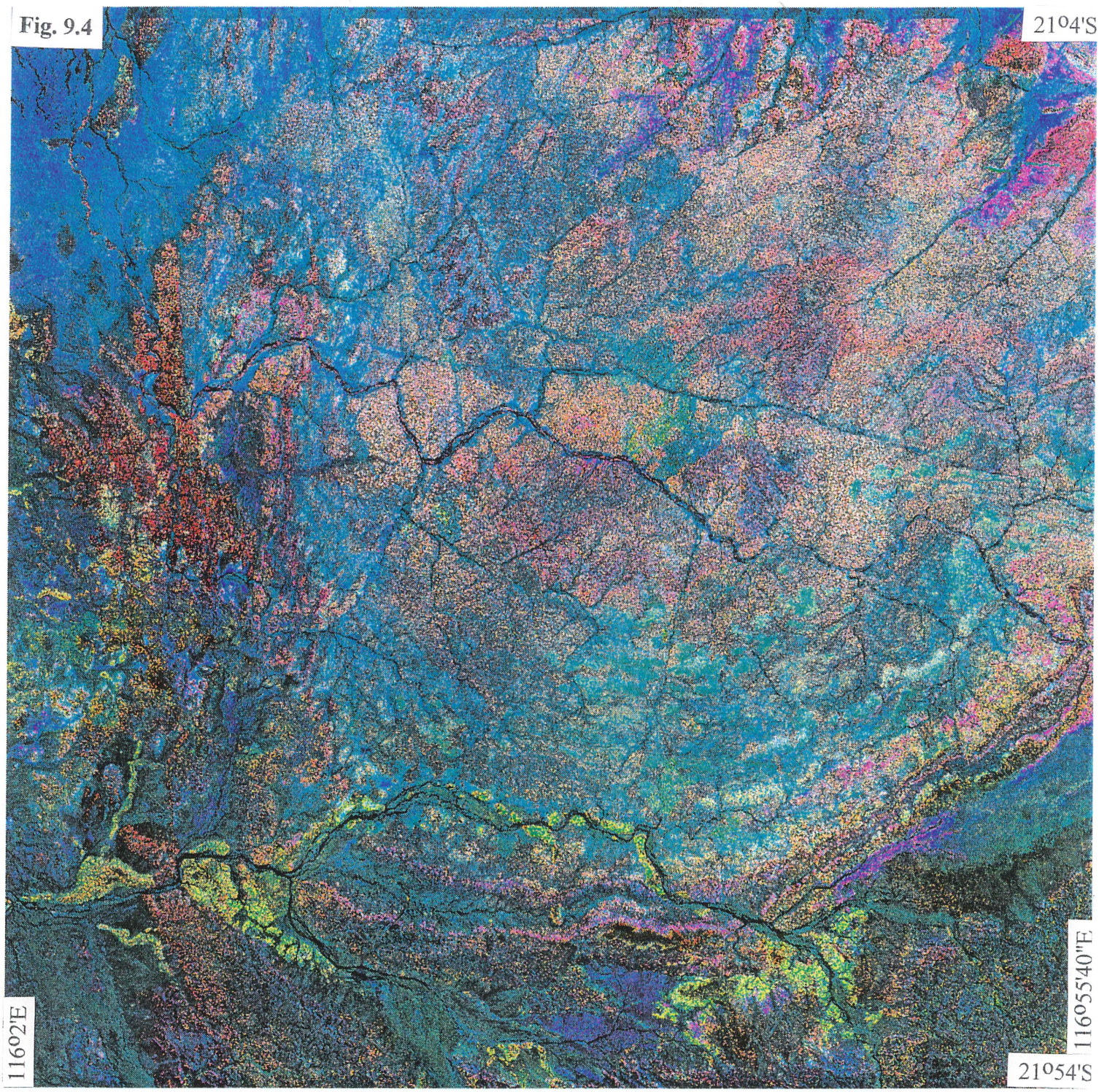

Figure 9.4 Landsat-5-TM RGB pc2(4/3;5/7):5/4:1+7 image of the Mingar Dome-Robe River area.